National Library of Canada
Acquisitions and Bibliographic Services Branch
395 Wellington Street
Ottawa, Ontario
K1A 0N4

Bibliothèque nationale du Canada
Direction des acquisitions et des services bibliographiques
395, rue Wellington
Ottawa (Ontario)
K1A 0N4

Your file Votre référence

Our file Notre référence

NOTICE

The quality of this microform is heavily dependent upon the quality of the original thesis submitted for microfilming. Every effort has been made to ensure the highest quality of reproduction possible.

If pages are missing, contact the university which granted the degree.

Some pages may have indistinct print especially if the original pages were typed with a poor typewriter ribbon or if the university sent us an inferior photocopy.

AVIS

La qualité de cette microforme dépend grandement de la qualité de la thèse soumise au microfilmage. Nous avons tout fait pour assurer une qualité supérieure de reproduction.

S'il manque des pages, veuillez communiquer avec l'université qui a conféré le grade.

La qualité d'impression de certaines pages peut laisser à désirer, surtout si les pages originales ont été dactylographiées à l'aide d'un ruban usé ou si l'université nous a fait parvenir une photocopie de qualité inférieure.

Canada

Broadband Indoor Wireless Communications Using Infrared

by

Mohammad Reza Pakravan, B.Sc.

A thesis submitted to
the School of Graduate Studies and Research
University of Ottawa
in partial fulfillment of the requirements
for the degree of

Master of Applied Science

Ottawa-Carleton Institute for Electrical Engineering
Department of Electrical Engineering
Faculty of Engineering
University of Ottawa
Ottawa, Ontario, Canada

August 1994

ISBN 0-612-00592-5

UNIVERSITÉ D'OTTAWA
ÉCOLE DES ÉTUDES SUPÉRIEURES ET DE LA RECHERCHE

UNIVERSITY OF OTTAWA
SCHOOL OF GRADUATE STUDIES AND RESEARCH

PERMISSION DE REPRODUIRE ET DE DISTRIBUER LA THÈSE - *PERMISSION TO REPRODUCE AND DISTRIBUTE THE THESIS*

NOM DE L'AUTEUR*-*NAME OF AUTHOR*

PAKRAVAN, Mohammad Reza

ADRESSE POSTALE-*MAILING ADDRESS*

207-290 Nelson, Ottawa, Ontario K1N 7S3

GRADE-*DEGREE*

M.A.Sc.(Electrical Engineering)

ANNÉE D'OBTENTION-*YEAR GRANTED*

TITRE DE LA THÈSE-*TITLE OF THESIS*

BROADBAND INDOOR WIRELESS COMMUNICATIONS USING INFRARED

L'AUTEUR PERMET, PAR LA PRÉSENTE, LA CONSULTATION ET LE PRÊT DE CETTE THÈSE EN CONFORMITÉ AVEC LES RÈGLEMENTS ÉTABLIS PAR LE BIBLIOTHÉCAIRE EN CHEF DE L'UNIVERSITÉ D'OTTAWA. L'AUTEUR AUTORISE AUSSI L'UNIVERSITÉ D'OTTAWA, SES SUCCESSEURS ET CESSIONNAIRES, À REPRODUIRE CET EXEMPLAIRE PAR PHOTOGRAPHIE OU PHOTOCOPIE POUR FINS DE PRÊT OU DE VENTE AU PRIX COÛTANT AUX BIBLIOTHÈQUES OU AUX CHERCHEURS QUI EN FERONT LA DEMANDE.

LES DROITS DE PUBLICATION PAR TOUT AUTRE MOYEN ET POUR VENTE AU PUBLIC DEMEURERONT LA PROPRIÉTÉ DE L'AUTEUR DE LA THÈSE SOUS RÉSERVE DES RÈGLEMENTS DE L'UNIVERSITÉ D'OTTAWA EN MATIÈRE DE PUBLICATION DE THÈSES.

THE AUTHOR HEREBY PERMITS THE CONSULTATION AND THE LENDING OF THIS THESIS PURSUANT TO THE REGULATIONS ESTABLISHED BY THE CHIEF LIBRARIAN OF THE UNIVERSITY OF OTTAWA. THE AUTHOR ALSO AUTHORIZES THE UNIVERSITY OF OTTAWA, ITS SUCCESSORS AND ASSIGNEES, TO MAKE REPRODUCTIONS OF THIS COPY BY PHOTOGRAPHIC MEANS OR BY PHOTOCOPYING AND TO LEND OR SELL SUCH REPRODUCTIONS AT COST TO LIBRARIES AND TO SCHOLARS REQUESTING THEM.

THE RIGHT TO PUBLISH THE THESIS BY OTHER MEANS AND TO SELL IT TO THE PUBLIC IS RESERVED TO THE AUTHOR, SUBJECT TO THE REGULATIONS OF THE UNIVERSITY OF OTTAWA GOVERNING THE PUBLICATION OF THESES.

04/10/94
DATE

M.R. Pakravan
(AUTEUR) SIGNATURE (AUTHOR)

* NB. LE MASCULIN COMPREND ÉGALEMENT LE FÉMININ

FS10-AS25 86/12

UNIVERSITÉ D'OTTAWA
UNIVERSITY OF OTTAWA

Abstract

In this thesis, we discuss the issue of using infrared light as a carrier for broadband indoor wireless networks. We discuss the infrared channel and show how it differs from conventional radio frequency channel. Noise sources for this environment and the practical ways of reducing their harmful effects are discussed. We determine the safety levels for the radiated power of an IR transmitter and we show how the system should be designed to operate within the safety limits. We introduce a computer simulation algorithm to find the impulse response of an indoor infrared channel and discuss several implementation issues for the algorithm. Using the simulation software, we investigate temporal and spatial distributions of the channel e.g., the delay spread of impulse response and the total received optical power. We use the results of the simulations to investigate the effects of receiver rotation on the channel properties. We propose an angular diversity as a mean for performance improvement in an infrared receiver. Simulating the noise sources and signal sources in a typical indoor environment, we see how diversity improves the signal-to-noise ratio in a receiver with the angular diversity reception.

Acknowledgments

Thanks God to whom I owe all I have. I wish to express my sincere gratitude to my thesis supervisor, Dr. Mohsen Kavehrad, for his constant support and encouragement during the course of my M.A.Sc. program.

I would like to thank Dr. J. Barry, Dr. D. Falconer, Dr. H. Hashemi, Dr. Q. Jiang, Dr. L. Strawczynski and Dr. G. Yun for all the useful information they provided me and inspiring discussions that we had during my research.

My dear wife showed constant understanding and was extremely supportive. A mere acknowledgment by no means compensate the hardship she had to go through on the account of this thesis.

Special thanks to my parents who always supported me in the wonderful world of science and encouraged me in getting over all the difficulties.

I would like to thank the Islamic Republic of IRAN for the financial support during my M.A.Sc. program at University of Ottawa. Also thanks to the Canadian Institute for Telecommunications Research (CITR) for supporting the infrastructure of this project.

Contents

List of Figures

Acronyms

AWGN	Additive White Guassian Noise
BER	Bit Error Rate
CCI	Co-Channel Interference
CDF	Cumulative Distribution Function
CPC	Compound Parabolic Concentrator
DD	Direct Detection
EMI	Electromagnetic Interference
FOV	Field-Of-View
HPBW	Half-Power Emission Angle of a diffused source.
IM	Intensity Modulation
ISI	Intersymbol Interference
IR	Infrared
Kbps	kilo bit per second
L-PPM	L-pulse position modulation
LAN	Local Area Network
LED	Light Emitting Diode
LOS	Line-Of-Sight (In this thesis, this word was used for non-directed LOS configuration of an indoor infrared link)
LP	The ratio between the power in the LOS impulse response to the received power from the reflected rays.
LTI	Linear Time Invariant
Mbps	Mega bit per second
MRC	Maximal Ratio Combining
MPE	Maximum Permissible exposure
OOK	On-Off Keying modulation
PDF	Probability Distribution Function
PSD	Power Spectral Density
RF	Radio Frequency
Rx	Receiver
SNR	Signal-to-Noise Ratio
Tx	Transmitter

Chapter 1

Introduction

Using infrared (IR) light for indoor wireless communications is a promising technique with its own advantages compared to radio frequency waves (RF) [1][2][3][4]. At infrared, there is an abundance of bandwidth which is free from regulations, as yet. Infrared light does not pass through walls and therefore is confined to the same room in which it originates. Hence, each room is a separate cell without mutual interference with its neighbors. This is a major advantage for IR compared to RF because it allows many neighboring cells in a large building to operate independent IR links without interference problem. IR devices are immune to electromagnetic interferences (EMI) and this makes them an interesting choice for environments with high levels of EMI such as factories [5][6]. Infrared devices are compact, consume little power and due to high volume production of commercial devices operating in this wavelength region such as Compact Disks and remote controls, are very inexpensive.

Using IR for indoor communications has its own disadvantages, too. Due to the limited range of optical signals and their blockage by solid objects, a transmitter or base station is needed for each room. This increases the wiring cost of a wireless IR based network compared to its RF counterpart. Optical transmission is also very sensitive to shadowing by objects. Although there are techniques to reduce this sensitivity, there is no way an optical device can compete with an RF device in its tolerance to shadowing and blockage.

Recently, there has been a growing interest in using IR technology for wireless communications. Computer networking seems to be an interesting application for IR technology [7][8][9][10][11]. A major interest is in using IR as a mean of wireless transportation of signals for the existing LANs using IEEE 802 standards. Allowing wireless connection to a backbone cabled LAN without the need for changing the LAN protocols is a major interest for commercial applications [12][13][14][15][16]. Currently, there are some commercial products available for this purpose which operates on Ethernet™ or Token ring™ networks

[17][18][19][20]. IEEE 802.11 group has been formed to standardize wireless access to existing cabled LANs through IR and RF carriers. There have also been some works in using IR for transferring signals with IEEE 488 and RS-232/RS-423/RS-422 format [21][22] and also some attempts in using IR for commercial applications. A remote TV controller is a typical example. Other recent works have used IR for transmission of audio signals to handheld receivers [23][24][25][26] or to theater stereo speakers [27][28].

There is also a rapidly growing interest in using IR for broadband indoor wireless communications [29][30][31]. Future portable computers need wide band connections to the cabled backbone LANs to transfer high data rates in multimedia communications. Data rates on the order of more than 100 Mbps needed for true multimedia communications in the future portables. Speaking of this range of data rates, there are major technological limitations ahead of both RF and IR technology. Noting that a portable terminal has a limited battery power and has to be inexpensive, light-weight and small, the challenge of providing such a service is an important research area for scientific community.

Pioneer work on characterization of IR channel started by Gfeller, *et al.* and was continued by other researchers [32][33]. A general computer simulation method for IR channel characterization was presented by Barry [34]. Experimental measurements of indoor IR channel was performed at University of Ottawa [35] over a 40 MHz band. Later, Krause, *et al.* [36][37] measured IR channel over a 150 MHz 3-dB band. The results show a good agreement with results of the simulation algorithm presented by Barry.

Theoretical work on communications aspect of a broadband indoor IR system was done by many researchers [38][39][40][41]. Studies on different modulation techniques were reported by Barry [42]. Among different modulation techniques, On-Off Keying (OOK) and L-Pulse Position Modulation (L-PPM) seems to be more attractive for IR communications. Chen [43] has a published work on the use of OOK, and L-PPM was studied in detail by Kahn and Audeh in [44][45]. Use of decision feedback equalizers to compensate for multipath distortions were reported by Audeh, *et al.* [46][47][48].

1.1. Optical configurations

Indoor unguided optical communications can be implemented in several different ways. Fig. 1.1 [42] shows different possible configurations for an optical link. A

directed LOS configuration, illustrated in Fig. 1.1.a, uses a collimated beam from the transmitter to the receiver and a narrow Field-Of-View (FOV) receiver. Alignment between the receiver and transmitter is essential in this configuration. Such a configuration is suitable for one-to-one communications and for each additional receiver, there is a need for an additional transmitter looking into that direction. In this configuration, light signal is confined to a narrow beam and the receiver with a limited FOV detects only the light signals from the transmitter direction. There are almost no reflections of light by other objects detected by the receiver and therefore there is no multipath problem in this configuration. Confinement of light to a limited direction also allows more efficient use of optical energy in carrying information. Power levels can be increased up to the safety limits, increasing the resulting SNR for this configuration. Hence, it is possible to achieve very high data rates using this configuration.

Yen and Crawford [49] presented a wireless link using narrow beam IR transmitters with a beamwidth of 3° in the base station and 2° in the portables. They reported a bit rate of 1 Mbps over a 50 m range using 165 mW from the base station to the portable and 5 mW from the portable to the base station. Chu and Gans [50] proposed a system using several 1° pencil beams each carrying 1 mW optical power. They achieved a data rate of 50 Mbps over a range of 30m. There are also commercial products on the market using this configuration. BICC communication is marketing a product that can achieve a range of 24 m at a rate of 4 Mbps. A.T.S. Comm. Co. [17] is selling Ethernet compatible devices using narrow 6° beam transceivers to transfer LAN traffic at a rate of 10 Mbps in a ring configuration. There are reports of very high data rate commercial devices as well. For example, a bit rate of 125 Mbps was achieved by using a transmitter beamwidth of 1° and a receiver FOV of 6° over a 30 m range by JDL 889-LS transceivers built by JOLT, Ltd.[51]. Recently, McCullagh, *et al.* [52] proposed a directed LOS link for bit rates of about 1 Gbps. Their proposed system also includes a tracking mechanism in the base station that follows the position of the portable and sends optical signals in a narrow beam to the proper direction.

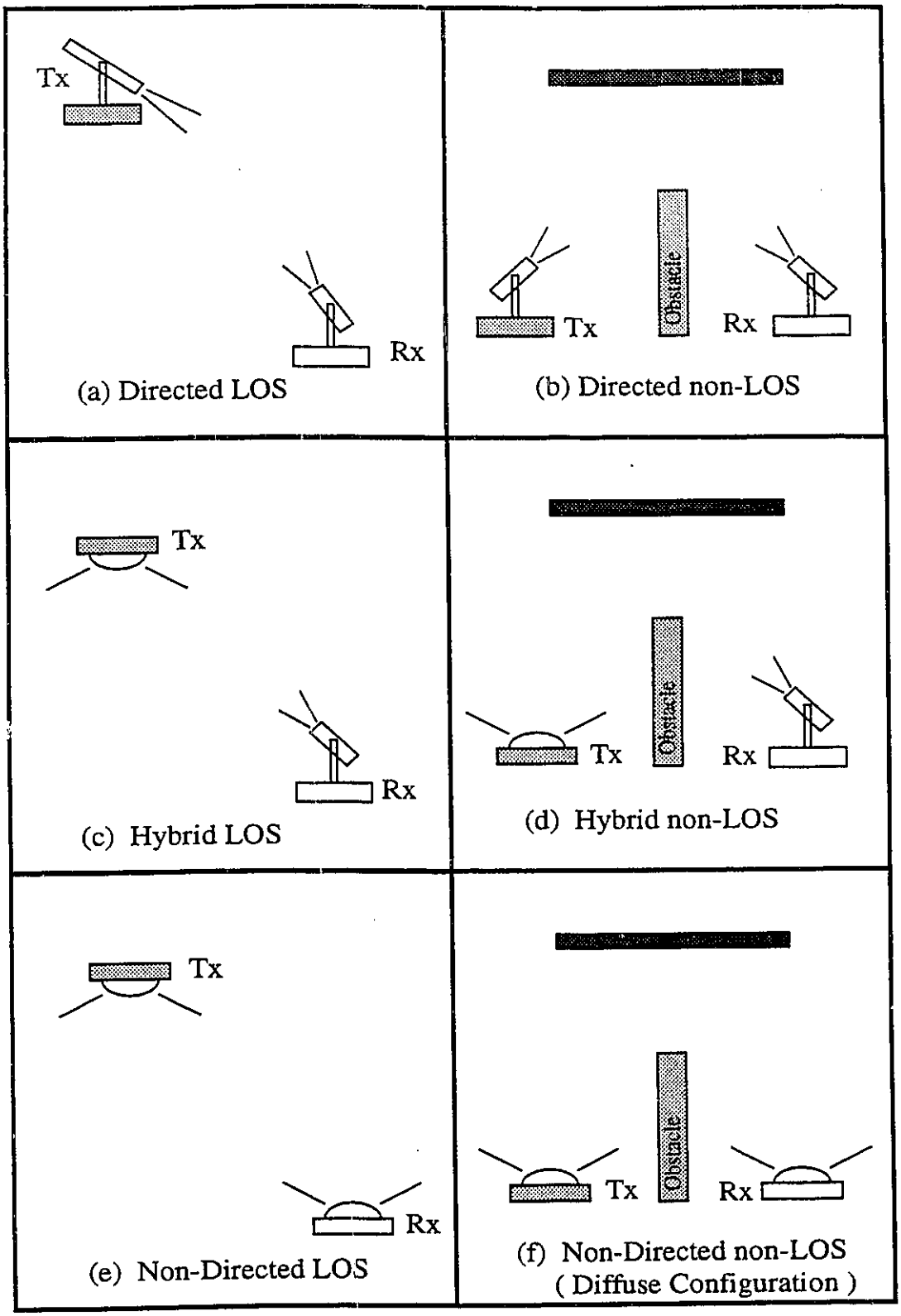

Figure 1.1 Configurations for optical wireless links (from [42])

Directed LOS configuration is not capable of handling many-to-one and one-to-many communications links. A directed non-LOS configuration shown in Fig. 1.1.b may solve this problem. A common point is used for all the transmitters and all the receivers to look at for proper reception of optical energy. Narrow beam transmitters and narrow FOV receivers are used in this configuration. The common point on the ceiling reflects the incoming beam according to a Lambertian pattern, making it possible for all terminals across the room looking toward the common point to receive a portion of the optical energy from that point. Such a configuration was proposed by Minami, *et al.* [53] for peer-to-peer communications of their wireless modem operating at 19.2 Kbps. A product by Photonics group developed in 1985 used this configuration to achieve a bit rate of 230 Kbps over a 22 meters range. Similar ideas was also proposed in [54] and [57] using directed beams toward some diffusing spots on the ceiling to provide diversity against shadowing.

A hybrid LOS configuration is made by putting a repeater or a base station on the ceiling and transmitting up-link signals using a wide beamwidth. A narrow FOV receiver then picks up the optical energy by looking in the transmitter direction. Minami, *et al.* [53] used this configurations for base to portable communications of their optical modem operating at 19.2 Kbps. A similar work reported by Nakata, *et al.* [55] used this configuration to achieve a bit rate of 1 Mbps over a range of 5 m by transmitting 300 mW in a wide beam of 120° in the downlink and a 10° beam in the uplink.

Hybrid non-LOS system is made by allowing a transmitter to transmit optical energy in a wide beam, illuminating all the ceiling of a room. Then using a narrow FOV receiver to collect the light from the ceiling or a proper direction. This configuration is shown in Fig. 1.1.d.

None of the mentioned configurations are suitable for portable wireless communications. A portable communication system, needs to operate without any alignment requirement. Therefore, the only possible choices are non-directed configurations, either LOS or non-LOS known as a diffuse configuration throughout this thesis.

A non-directed non-LOS configuration was first proposed by Gfeller, *et al.*[56]. In this configuration, transmitter illuminates the ceiling with a wide beam and a wide FOV receiver detects the signal energy from the reflected rays. Such an arrangement does not require alignment between a transmitter and a receiver.

Gfeller showed that the ratio of the light reflected from the surface of typical office materials are in the range of 40% to 90% in IR wavelength region. He also showed that in most cases, the pattern of reflected light can be described by a Lambertian pattern. This shows that reflections do not weaken the signals too much and a receiver would be capable of receiving energy from the reflected rays. In a diffuse configuration, the ceiling acts as a distributed source of optical energy. Therefore, this configuration is much more tolerant to shadowing than its counterparts, because it is difficult to block the wide FOV receiver from seeing the ceiling. It is obvious that in a diffuse configuration, the receiver should detect a signal from a sum of delayed and attenuated pulses that arrive at the receiver after multiple reflections. Multipath distortion, a result of this process is the major drawback of this configuration that limits transmission at high data rates with this configuration.

A non-directed LOS configuration is illustrated in Fig. 1.1.f. In this configuration, the path between transmitter and receiver should be kept unobstructed. This configuration, uses optical energy more efficiently and results in a much less distortion due to multipath. The direct path between transmitter and receiver carries most of the received energy, forcing the multipath effect to be quite negligible compared to that in the diffuse configuration. Importance of LOS path makes this system more sensitive to shadowing compared to diffuse configuration. It is possible to use several passive reflectors to provide multi-LOS coverage for an indoor environment [57]. Such a system relies on a LOS but due to the existing multiple LOS the system is more tolerant to shadowing. More details about this configuration is presented in chapter 3.Throughout the rest of this thesis we will consider both LOS and diffuse configurations and compare them considering various design criterion.

There are other important aspects in the design of an optical wireless communication system. Background radiation of other optical sources such as sun-light and fluorescent and incandescent lamps produce a strong noise component in the signal detected by a photodetector [58]. Therefore, narrow-band optical bandpass filters should be used to reduce the amount of detected background radiation. In a non-directed configuration, this filter should have a wide FOV to be able to detect the incoming beams from all directions. This makes the design of such a filter a challenging problem [42][59][60][61][62]. Another important aspect of optical design of a system is the radiation pattern of a transmitter and the transmission area. Eye safety limits restrict the power emitted from IR point

sources [63][64]. For high power transmission of IR beams, we have to increase the radiation area. For efficient use of transmitted optical power we have to shape the radiation pattern of a source. New holographical techniques have been proposed by Smyth, *et al.* for these purposes [65][66][67][68]. Other recent works includes a study by Gfeller, *et al.* [69] on planning cell size and coverage area in an indoor environment, and a simulation study by Lomba, *et al.* [73] on indoor IR channel.

1.2. Thesis Overview

In chapter 2 of the thesis, we will introduce the baseband channel model for free space non-directed optical communications. This channel is compared to conventional RF channels. A major concern in IR wireless systems is the safety issues and the health hazards considerations. Operation wavelength of IR systems are usually chosen around 800 nm because of the inexpensive components available for this band. The eye is transparent to this wavelength. Therefore, this limits the radiation levels of an IR transmitter. We will study terms and conditions regulated by standard bodies in chapter-2 and give some numerical examples for the maximum permissible radiated power from a transmitter.

A computer simulation algorithm for an indoor IR channel is presented in chapter-3. Following [34], we present models used for sources, receivers and reflectors and describe the algorithm used for simulation. Some features of this simulation program are discussed in the same chapter. The simulation program will then be used to compute power profiles and delay spread profiles for various rooms. We also use these results to investigate effects of room size, reflection coefficient, receiver and transmitter FOV on the detected impulse response. The results give us a more detailed knowledge about an indoor IR channel.

Chapter-4 is devoted to investigation of diversity techniques in IR receivers. Since detection of optical signals is very sensitive to the direction of reception, we discuss the effects of receiver rotation on the detected impulse response. We use these results to conclude some points that are useful in designing receivers with angular diversity techniques. Later in this chapter we investigate the effects of noise on the diversity combining techniques and compare Maximal Ratio Combining (MRC) with selection diversity combining. Noise sources are simulated in this chapter as real lamps used in an office and the effect of directionality of noise is observed on the results. To illustrate the advantages of

angular diversity techniques we also compare the results with the case of a single photodiode receiver and show the improvements made by using diversity techniques.

Chapter-5 presents a summary and the conclusions of this work.

Chapter 2

Non-directed Infrared Optical Channel

2.1. Introduction

In this chapter, we present a model for non-directed IR channel and compare this channel with conventional RF channels. This gives us a more accurate view on the theoretical side of the system design for IR wireless communications. Effect of ambient light as a major source of noise in such system will be discussed in section 2.3. One of the major concerns in the design of IR communications devices is safety considerations. In the last section of this chapter we will discuss different aspects of safety limits based on currently available standards. Numerical values derived in this section are helpful examples for system design.

2.2. Channel model

Consider a non-directed IR transmission system. This system contains an optical source that converts electrical signals into optical intensity, a photodiode receiver that detects the optical signal and converts it to an electrical signal. Generated optical signal passes through the media between the transmitter and the receiver which has some effects on it. In this section, we discuss the model for this system. We will discuss systems employing a wide FOV photodetector that collects the light from all directions converting the optical intensity of the received signal to an electrical current, a process called Direct Detection (DD). Also, the optical source in this discussion, modulates the intensity of the transmitted optical signal to carry information. Considering today's technological limits, intensity modulation at the transmitter and direct detection at the receiver, (IM/DD), is the most feasible choice for non-directed optical communications [42].

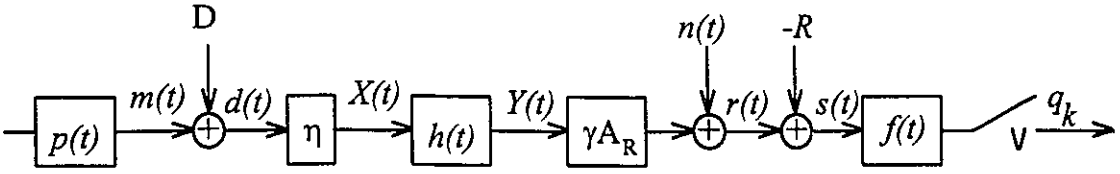

Figure 2.1. Block diagram of an IR transmission system (from [36])

Transmission of a digital stream from the transmitter to the receiver is summarized in Fig. 2.1 [36]. An analog signal, $m(t)$, is generated by applying a proper modulation scheme, $p(t)$, on an incoming stream of digital information. This modulation can be any kind of digital modulation[1]. This signal, is used to modulate the current of an optical signal generator device such as a laser Diode (LD) or a Light Emitting Diode (LED). These devices should be driven with a positive current to generate an optical signal. To insure this, a proper dc. bias, D, should be added to the signal before modulating the optical device with it. Changing the driving current of the optical device changes the intensity of the generated optical signal, with a conversion ratio, η. So $X(t)$, intensity of the optical signal is related to $d(t)$, driving current, by: $X(t)=\eta d(t)$.

It can be shown [37] that a non-directed optical transmission system employing IM/DD, is modeled as a Linear system[2]. Such a system can be described by its impulse response, $h(t,\tau)$. In most applications, the rate of change in channel impulse response is much slower than the duration of $h(t,\tau)$, so we can assume this channel to be a linear time invariant (LTI) system. An LTI system is completely characterized by its impulse response $h(t)$. Therefore, optical signal at the receiver, $Y(t)$, is the convolution of the transmitted signal and the channel impulse response, $Y(t)=X(t)\otimes h(t)$.

A photodiode converts the received optical signal to an electrical signal (current) with a conversion ratio γ. Amplitude of the generated current is also proportional to the area of the photodetector, A_R. Background light is also detected by the photodiode and generates a dc current plus an additive white noise, $n(t)$.

[1]Some possible examples are Pulse Amplitude Modulation (PAM), Frequency Modulation (FSK), Multiple Subcarrier Modulation, or Pulse Position Modulation (PPM). One of the simplest modulation techniques used in IR systems is 2-level PAM also known as On-Off-Keying (OOK). For more details refer to [42].
[2]Refer to [37] for the proof.

The dc component of the photodiode is removed (Subtracting R from $r(t)$) and the result is passed through the receiver matched filter $f(t)$. Decision is made based on the samples of the output of this filter.

2.3. IR channel and RF channel: A comparison

There are some major differences between an infrared (IR) channel and a conventional Radio Frequency (RF) channel. In RF channels, the wavelength of the carrier is in the order of millimeter (GHz range of frequencies) or centimeters (UHF range) while in the IR, the wavelength is in the 700-900 nm range. Also in IM/DD systems, the intensity of optical signal carries information while in radio, the amplitude and phase of radio-wave carry the information. Consequently, multipath effects in radio channels are different from optical channels. In radio, carrier signal cancellation due to multipath induces fading in the received signal. These fades occur in space, time or frequency and can potentially cause deep nulls in the frequency response of the received signal or huge reduction in the level of received signal.

In an optical channel, the size of photodiode is in the mm-range, thousands of times larger than the IR wavelength. There is a built-in averaging process in the photodiode which adds up the peaks and nulls due to cancellation in the optical carrier frequency range. Therefore, the output of the photodiode will never go to zero because of the fades due to multipath. An illustration of this phenomenon is presented in Fig. 2.2. This is why an IR channel is a baseband channel. Note that, the averaging process, averages out space-domain nulls while there are still frequency-domain nulls due to multipath effect in IR channels. In other words, regardless of the dimension of the detector, the frequency response of an IR channel may have nulls and peaks. In chapter three, we will see some samples of the frequency response of IR channels having nulls and peaks. These nulls and peaks are a result of multipath dispersion caused by reflection of optical signals from reflectors. We will discuss this issue in more detail.

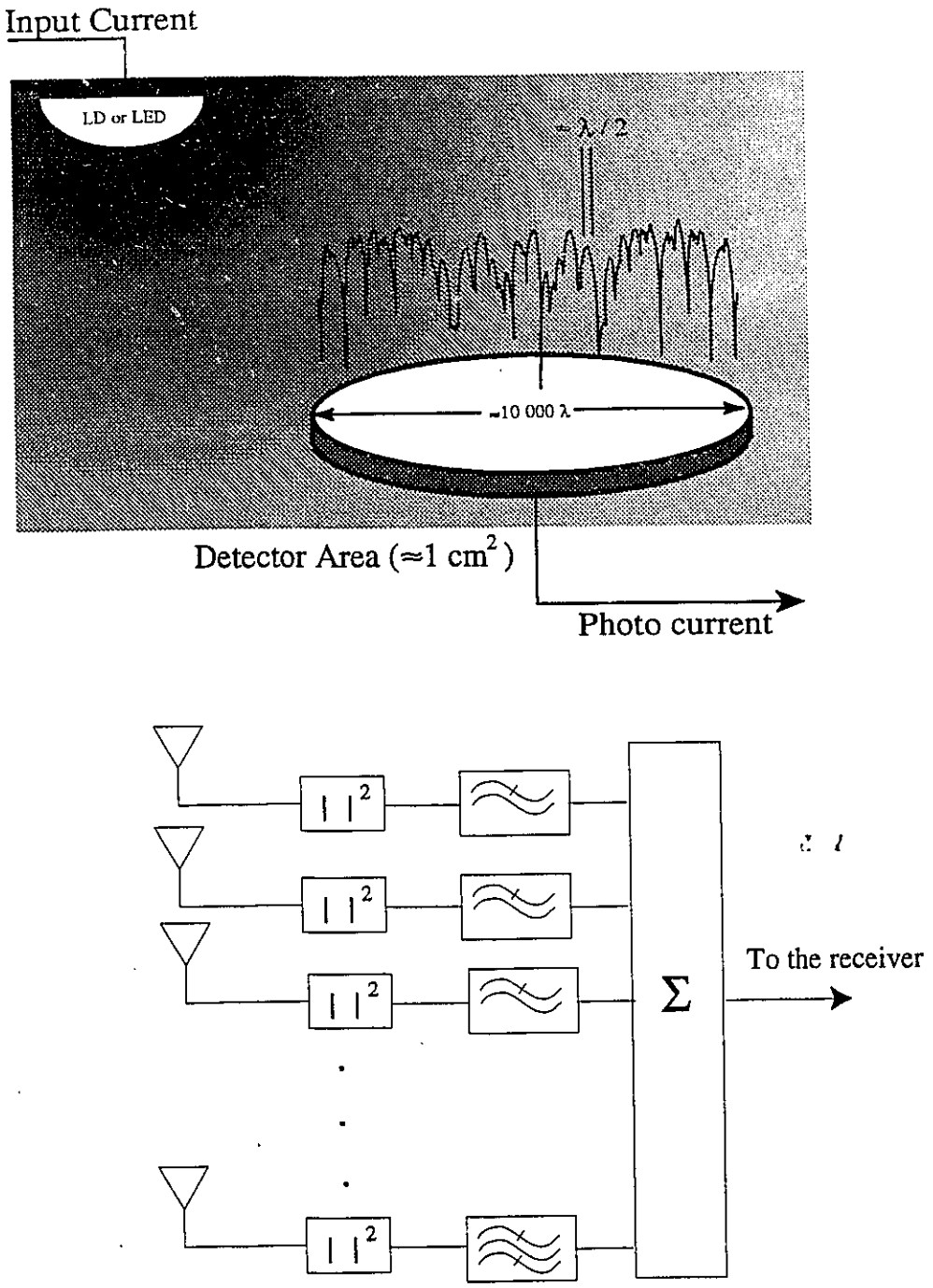

Figure 2.2 Size of a photodetector is several thousands times larger than the IR wavelength. Therefore, the photodiode averages out peaks and nulls resulting from cancellation of the carriers in the optical frequency range. The counterpart to this process in conventional RF channels is like when we use several thousands of antennas and feed the receiver with the sum of the squared filtered output of each antenna.(first figure modified from [51])

The process of averaging in a photodiode, is like if we place thousands of antennas, each with a size smaller than wavelength of operation, in the receiver. Then we use non-coherent square law detectors for each antenna branch and sum the results to produce the output. It is evident that we will not see any nulls due to carrier level signal cancellation in this configuration. Another view of a photodiode in DD systems is to consider it as a photon counting device that generates electrical current from detected photons. It is obvious that fading and cancellation will not cause nulls (zero photon reception) at the receiver.

As a conclusion, we see that processes like flat or Rayleigh fading in radio channels which distort the incoming signal regardless of bit-rate, are not present at the IM/DD optical channels. Distortion of the signal in an IR channel is a result of inter symbol interference which is caused by the spread in the impulse response of the channel. This kind of distortion is related to the signaling rate over the channel. Also, this averaging process, makes IR detectors less sensitive to location than a radio detector. Unlike RF channels in which huge differences can happen with small movements of the receiver, an IR receiver senses considerable changes when it is moved a few centimeters[3]. RF antennas are sometimes omni-directional, making them almost direction insensitive, but an IR photodiode can have a maximum FOV of 90°. In general, IR systems are much more sensitive to rotation than RF systems. Although, channel characteristics do not change in an IR system with small spatial movements, they change considerably with rotation.

As we discussed before, the channel input, *d(t)* should be positive everywhere. This results in another difference between IR channel and conventional RF channels . In IR channel, safety considerations limit the average intensity of the optical transmitted power,

$$\lim_{T\to\infty} \frac{1}{2T} \int_{-T}^{T} X(t)dt < P_{avg} \qquad (2\text{-}1)$$

while in the conventional RF channels, the power of the transmitted signal is limited,

[3]Noticable change in impulse response happens when displacement is in the order of ligh speed times resolution of measurment system. For a system with 500MHz bandwidth, time resolution is in the order of 2 ns. Such a system shouldn't sense noticable changes in channel charactristics with displacements of less than 0.6m [36].

$$\lim_{T\to\infty}\frac{1}{2T}\int_{-T}^{T}X(t)^2\,dt < P_{\max} \qquad (2\text{-}2)$$

To calculate Bit Error Rate (BER) for IR channels for a given modulation, we can't blindly apply the BER formulas of conventional channels. We should analyze these channels under the correct constraints.

2.4. Noise

In Fig. 2.3, we see the power spectral density of three common illumination sources: fluorescent light, sunlight, and incandescent light [56]. We see that the sunlight and the incandescent light both have strong components in the operating wavelength of an IR system. The power of the background light can be hundreds of times more than the received signal. When detected by the photodetector, this ambient light generates a dc current plus shot noise. This shot noise is proportional to the detected ambient light power and is the major source of noise in IR systems. This clearly shows the need for optical bandpass filters to reduce the amount of background radiation detected by a photodiode. Reduction of ambient light by a filter is very important in achieving the desired SNR in practical systems. Optical filters are usually sensitive to the direction of the incoming light beam. The need for a wide FOV at the receiver, that collects light from all directions, makes the design of optical filters a challenging problem [42][59][60][61][62].
The background induced shot noise is modeled as an additive white Guassian noise (AWGN) with a power spectral density (PSD) given by [42]:

$$S_n(f)=P_{bg}A_R\gamma q\equiv N_0 \ (A^2/Hz) \qquad (2\text{-}3)$$

where P_{bg} is the level of background radiation per unit area detected by photodiode and q is the charge of an electron (1.6×10^{-19} Coulombs).

In a typical lightning condition, P_{bg} is much more than power of the received signal. For example, in a typical lightning condition in the presence of sunlight, the level of received background power is 130 μW/cm² using a 23 nm optical filter [36]. As we will see in chapter three, the typical value of received signal power is 0.1 to 5 μW/cm². In the presence of background radiation, this noise is the dominant source of noise in the receiver. This is a major difference between IR receivers and optical fiber receivers. In the latter, the dominant source of noise is the noise generated by electronic components.

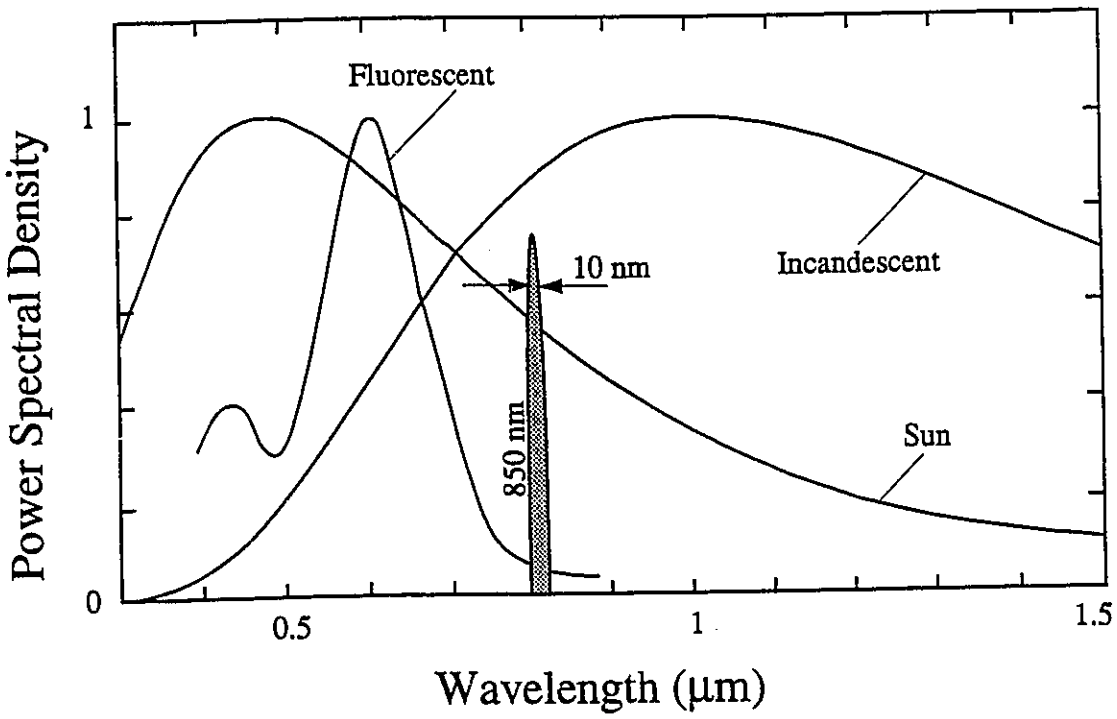

Figure 2.3 Power Spectral density of three major noise sources for infrared receivers. The IR system is assumed to work at 850 nm wavelength. (from [42])

In this model, we expressed the received signal $r(t)$ as the convolution of $d(t)$ and $\gamma A_R h(t)$. Therefore, signal power is proportional to $Y^2(t)$. Increasing the amount of received light in the receiver, increases both the signal and the noise power due to ambient light. Noise power is proportional to the detected background light power, P_{bg}, while signal power is proportional to the square of the detected optical signal power. Therefore, increasing the size of the detector or using concentrators or lenses to collect more light at the receiver improves the signal-to-noise ratio (SNR).

2.5. Multipath dispersion

Reflection of light by objects, causes a distortion called the *multipath-induced temporal dispersion* or simply *multipath dispersion* in an IR channel. For each transmitted impulse, a widened pulse is detected at the receiver[4]. Optical impulse undergoes several reflections and attenuated replicas arrive at different times causing the transmitted impulse to be received as an attenuated, widened pulse. Examples of impulse response of an IR channel are presented in chapter three. In a typical indoor environment, the spread of impulse response does not exceed 100 ns. The exact value of spread depends on the physical configuration. This spread causes a distortion that is baud rate dependent. Higher baud rate signaling over this channel results in more distortion. This distortion causes ISI in the received signal. If the period of the transmitted pulses is less than the spread of the impulse response of the channel, tails of previous symbol(s) will overlay the current symbol. This added component, reduces the noise margin, i.e. increases the possibility of wrong decisions by closing the eye of the received signal. To compensate for the reduced margin, the transmitted power should be increased somewhat in order to keep the system performance similar to an ISI-free system. This added power, opens the received signal eye pattern. If sum of the tails of the previous pulses is more than the value of the current pulse, then there is an irreducible error rate. In this case, increasing the transmitted power doesn't solve the problem because the amplitude of tails also increases. In this case, equalizers are used to compensate for ISI [48].

To quantify the spread of the channel impulse response, we can define *maximum excess delay* of $h(t)$ as

[4] More details on the mechanism of this distortion is given in chapter three.

$$D_{\max} = t_{\max} - t_{\min} \qquad (2\text{-}4)$$

where t_{max} is the last time that $h(t)$ drops below a threshold value, h_{th}, and t_{min} is the first time $h(t)$ goes above that threshold. The numerical value of D_{max} depends on h_{th} which is usually determined by system noise level. D_{max} gives us the maximum span of $h(t)$ in the time domain, which determines the ISI-free limits of the baud rate. For ISI-free communications, the baud rate of the signal, R_b, should be less than D_{max}^{-1}. Although D_{max} is a measure for width of $h(t)$, it does not contain any information about distribution of $h(t)$ values in time. It can tell us when communication is ISI-free but it can't tell us how much ISI would be there for a specific baud rate. Fig. 2.4 shows an example of two impulse responses both with the same D_{max} resulting in different amounts of distortion due to ISI. $h_1(t)$ is more concentrated at the origin than $h_2(t)$. Stronger tail of $h_2(t)$ generates more ISI compared to $h_1(t)$.

Another measure for the spread of $h(t)$ is the *root mean square delay spread* or simply *r.m.s. delay spread* defined by [36]:

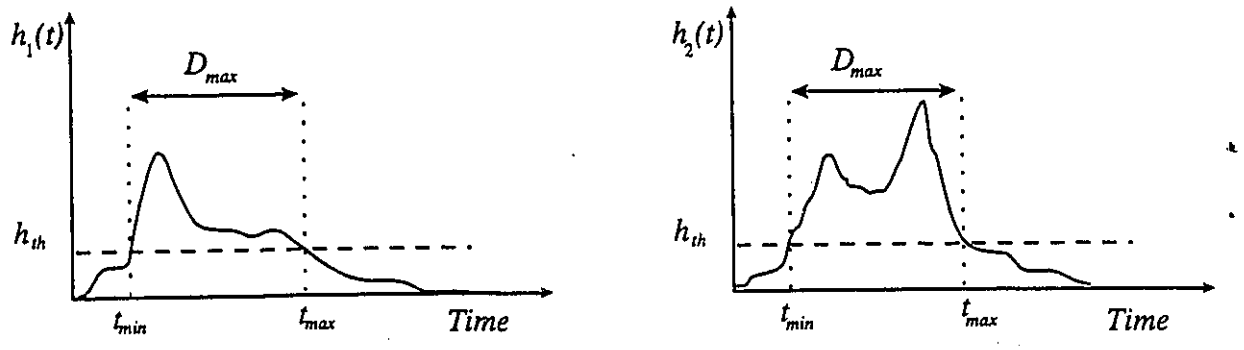

Figure 2.4 Illustration of maximum excess delay of two functions.

$$\sigma = \sqrt{\frac{\int_{-\infty}^{\infty}(t-\mu)^2 . h^2(t)dt}{\int_{-\infty}^{\infty}h^2(t)dt}} \qquad (2\text{-}5)$$

where μ is defined by:

$$\mu = \frac{\int_{-\infty}^{\infty}t . h^2(t)dt}{\int_{-\infty}^{\infty}h^2(t)dt} \qquad (2\text{-}6)$$

This definition accounts for the distribution of *h(t)* in time and therefore is a more suitable definition for the spread of impulse response. The r.m.s delay spread is defined in radio channels as the square root of the second central moment of the ensemble average of the magnitude squared channel impulse response. In deriving this definition, the channel is assumed to be a slowly varying, zero-mean, wide sense stationary, random function of spatial location or time. It has also been assumed that the values of *h(t)* are uncorrelated in time, namely $E[h(t).h(t')]=0$ for $t \neq t'$. These assumptions are not valid for an IR channel and so the relations between the r.m.s. delay spread and the channel performance which are derived for conventional RF channels are not applicable here. We define σ only as a means to compare width of *h(t)* for different configurations. It has been shown that there is a strong relationship between σ and the power penalty due to ISI [37].

2.6. Eye safety considerations

Infrared radiation may cause harmful damage to human eye or skin tissue. There are various standards specifying safe levels of optical radiation [63][64]. In this section we will briefly review the terms and conditions specified in these standards for safe use of lasers and apply standards for a diffusely radiating laser source.

2.6.1. Definition of terms

In order to clarify our discussion, we define the terms that will be used throughout this section[63][64].

Maximum Permissible Exposure (MPE):

This term refers to the level of laser radiation to which, under normal circumstances, persons may be exposed without suffering adverse effects. The MPE level represents the maximum level to which the eye or skin can be exposed without consequential injury immediately or after a long time and are related to the wavelength of the radiation, the pulse duration or exposure time, the tissue at risk and, for visible and near infra-red radiation in the range of 400 nm to 1400 nm, the size of retinal image.

In our application, the restriction due to retinal image of radiation source is the most restricting value for the radiation power of the source.

Angular Subtense (α):

This term refers to the visual angle subtended by the apparent source (including diffuse reflection) at the eye of an observer or at the point of measurement.(see Fig. 2.5.)

Depending on the value of angular subtense, viewing conditions are devided into intrabeam viewing condition and extended source viewing condition. In intrabeam viewing condition, the retinal image of the radiating device is smaller than 2μm and therefore there are more possibilities of damage to the retina. As illustrated if Fig. 2.5, decreasing the distance between the eye and the radiation source increases the angular subtense and therefore changes the viewing condition.

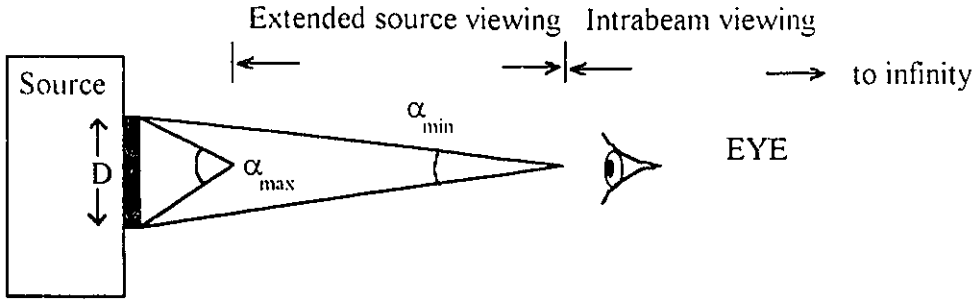

Figure 2.5. Minimum and Maximum angular subtense of an optical source.

Minimum Angular Subtense (Limiting Angular Subtense) (α_{min}):

This is defined as the value of angular subtense of the apparent source above which a source is considered an extended source. MPEs are independent of the source size for angular subtense less than α_{min}. For wavelengths between 0.4 and 1.050 μm and exposure time of more than 10 sec, α_{min} is 0.011 radian.

Maximum Angular Subtense (α_{max}):

This is defined as the value of angular subtense above which MPEs are independent of the source size. For wavelengths between 0.4 and 1.050 μm and exposure time of more than 10 sec, α_{max} is 0.1 radian.

Extended Source Viewing:

This is defined as the viewing condition whereby the apparent source at a distance of 100 mm or more subtends an angle at the eye greater than the limiting angular subtense α_{min}.

Intrabeam viewing:

This is defined as the viewing condition where the source subtends an angle at the eye which is equal to or less than α_{min}, the minimum angular subtense. This category includes most collimated beams and so-called point sources.

Irradiance (L):

This is defined as the quotient of the radiant flux incident on an element of the surface containing the point at which irradiance is measured, by the area of that element.

$$L = \frac{d\Phi}{dA \cdot \cos\theta \cdot d\Omega} \qquad (2\text{-}7)$$

where $d\Phi$ is the radiant flux transmitted by an elementary beam passing through the given point and propagating in the solid angle $d\Omega$ containing the given direction. dA is the area of a section of that beam containing the given point and θ is the angle between the normal to that section and the direction of the beam.

SI unit: Watt per square meter ($W.m^{-2}$)

Radiant Power; Radiant Flux (Φ,*P*):

This refers to the power emitted, transferred, or received in the form of radiation.

SI unit: Watt (W)

Radiant Intensity (of a source in a given direction)

This refers to the quotient of the radiant flux leaving the source, propagating in an element of solid angle containing the given direction by the element of solid angle.

SI unit: ($W.sr^{-1}$)

2.6.2. Case study

In this section, we want to calculate the maximum IR radiation power allowed by safety limits for a transmitter in a typical indoor condition. The radiation sources are assumed to be continuous wave optical devices[5] operating in the wavelength region near 800 nm and the exposure time of more than 8 hour is assumed through this section.

First we assume a diffusing point source with a total radiation power Φ at the ceiling of a typical office at the height of 3 m. Also, we assume a source that transmits IR signals at λ=850 nm.

The assumption of diffused radiation from a point source leads us to use MPE's for intrabeam viewing conditions where the angular subtence of source is smaller than α_{min}. In this case assuming a Lambertian pattern generated by the diffuser, exposure at the cornea may be estimated using the inverse square law relationship,

$$E = \frac{\rho \cdot \Phi \cdot \cos\theta}{\pi \cdot R^2} \qquad (2\text{-}8)$$

where E is the irradiance produced at a distance R from a diffusing surface with a reflection coefficient ρ, when the surface is irradiated by a laser with an output power Φ (Watts). The angle θ is the viewing angle relative to the normal to the surface. If the diffused pattern is generated by a diffuser in front of a laser, $\rho.\Phi$ is the total output power from the diffuser after illumination by the laser. So the laser power should be less than Φ_{max} to make sure that the received radiation level does not exceed MPE value.

$$\Phi_{max} = \frac{\pi \cdot (MPE) \cdot R^2}{\rho \cdot \cos\theta} \qquad (2\text{-}9)$$

[5]There are pulsed optical devices such as gas lasers.

For the wavelengths in the range of 400 nm to 1050 nm and for the exposure time of 10^3 to 3×10^4 seconds (30 minutes to about 8 hours) the MPE value for Ocular exposure to a laser beam (Intrabeam viewing) is given by[64][6]:

$MPE = 3.2\times10^{2(\lambda-0.7)} = 3.2\times10^{2(0.85-0.7)} = 3.2\times2 = 6.4\ (W.m^{-2})$

Under a normal condition, assuming a person sitting behind his desk, at a horizontal distance of 2 m from the laser source and at a height of 1.5 m (See Fig. 2.6), we will have:

$\theta = \arctan(2/1.5) = 53.13°$

$\cos(\theta) = 0.6$

$R^2 = (2^2+1.5^2) = 6.25$ m

assuming [7] $\rho = 0.95$,

$$\Phi_{max} = \frac{\pi\cdot(MPE)\cdot R^2}{\rho\cdot\cos\theta} = \frac{\pi\times6.4\times6.25}{0.95\times0.6} = 220.46 \quad W$$

This is a very high value which is far from the power levels required for optical indoor wireless communications. Even considering someone directly below the transmitter with his eyes at the height of 1.8 m looking directly into the transmitter for up to 8 hours, the result for maximum safe level of optical power would be:

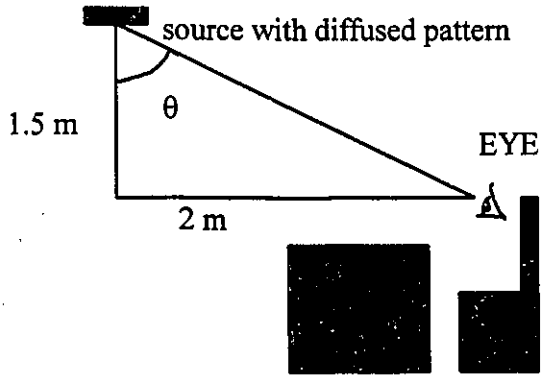

Figure 2.6. An example for MPE calculation for a LOS configuration.

[6]See Table 5 and Table 6 in [64].

[7] Typical values for reflection coefficients are 0.4 to 0.9 for objects inside a room. For transparent diffusers, the ratio of power passed through the diffuser to the radiated power are usually smaller than 0.95. So assuming a high ρ will result in a smaller Φ, increasing the margins from the actual received radiation.

$$\Phi_{max} = \frac{\pi \cdot (MPE) \cdot R^2}{\rho \cdot \cos\theta} = \frac{\pi \times 6.4 \times (3-1.8)^2}{0.95 \times 1} = 30.47 \quad W$$

which is again not a limiting factor in our application. Note that, the limitations due to skin exposure under the same conditions are 625 times larger [64][8]. So the main limitation is imposed by the so called "Ocular exposure" and we don't need to consider MPE for skin exposure in this application.

We would expect the main limitation on the radiation power imposed by the safety requirements of sources on the portables because they are closer to human eye. To discuss the portable IR transmission limits, we assume the portable be on a desk, in front of the user with a distance of 30 cm from the user's eye. We also assume a diffusing point source on the portable as a radiation source. Usually, sources from portables are looking toward the ceiling. Assuming a Lambertian pattern, radiation is maximum at $\theta=0$. Under the worst case conditions in which angle between looking direction and surface normal is zero and assuming a $\rho=0.95$, we have:

$$\Phi_{max} = \frac{\pi \cdot (MPE) \cdot R^2}{\rho \cdot \cos\theta} = \frac{\pi \times 6.4 \times (0.3)^2}{0.95 \times \cos(0)} = 1.9 \quad W \qquad (2\text{-}10)$$

We see this value is much less than the previous values. Note that we assumed intrabeam viewing conditions in these calculations because we assumed there exists a point source diffuser. This value can be increased if we transmit the same power from a larger area. This will result in the image of the transmitter in the retina to be larger and therefore resulting in less harm to retina. Holographic techniques has been used to create sources with controlled radiation pattern which makes them eye-safe[65][66][67][68]. Note that, increasing radiation area changes the viewing condition from "Intrabeam viewing" to "Extended source viewing " condition. The rules for calculation of MPE's are different under this condition. Assuming perpendicular viewing at a distance R, a radiation source of the size D, extended source viewing conditions hold if:

$$\frac{D}{\alpha_{min}} > R > \frac{D}{\alpha_{max}} \qquad (2\text{-}11)$$

where we used the following relation between R and D (See Fig. 2.5) :

$$R = \frac{D}{2\arctan(\alpha/2)} \cong \frac{D}{\alpha} \qquad (2\text{-}12)$$

[8]See Table 7 , page 43 in [64].

For example, assuming a diameter of D = 2 cm for the radiation circle, extended source viewing conditions apply for distances between 20 cm and 180 cm from the source.

Under extended source viewing conditions, the value of MPE should be multiplied by a correction coefficient $C_E=\alpha/\alpha_{min}$. This value is greater than 1 as long as the user stays within the specified limits. Therefore, the resulting value for MPEs are higher in this region. So the extended source viewing conditions impose less limitations on the maximum permissible radiation power of an optical source.

For an absolutely safe system, we may consider a case in which the distance between the source and the eye is very small (limited by packaging of source). Assume a source of diameter 4 mm, and a distance of 5 cm between eye and transmitter. In this case we have:

$$R_{\max} = \frac{D}{\alpha_{\min}} = \frac{0.4}{0.011} = 36.4 \ \ cm$$

$$R_{\min} = \frac{D}{\alpha_{\max}} = \frac{0.4}{0.1} = 4 \ \ cm$$

Since $R_{max} > R > R_{min}$, extended viewing conditions hold in this case and the safe level of radiation may be calculated as follows:

$$C_E = \frac{\alpha}{\alpha_{\min}} = \frac{D/R}{\alpha_{\min}} = \frac{0.4/5}{0.011} = 7.27$$

$$\Phi_{\max} = \frac{\pi \cdot (MPE) \cdot R^2}{\rho \cdot \cos\theta} \cdot C_E = \frac{\pi \times 6.4 \times (0.05)^2}{0.95 \times \cos(0)} \times 7.27 = 0.385 \ \ W$$

Note that the MPE level used for these calculation is for viewing duration of more than 10^3 seconds (about 16 minutes). Decreasing the duration of observation, results in an increase in the safe radiation level. For example if the duration of looking into the source is assumed to be 5 minutes, MPE level increases from 6.4 $W.m^{-2}$ to 8.65 $W.m^{-2}$ and the maximum safe level of radiation will increase accordingly to 0.520 W. Since it is very unlikely that a person looks at such a close distance for a long time to a receiver we may use the safety level mentioned in (2-10) for practical purposes.

Chapter 3

Simulation Of Indoor Infrared Channel

3.1. Introduction

A non-directed Infrared optical channel can be categorized as either a Line-Of-Sight (LOS) one or a diffuse one. In the LOS configuration, receiver relies on a direct unobstructed path between a transmitter and itself. In other words, the transmitter should always be within the Field-Of-View (FOV) of the receiver. In the diffused configuration, the transmitter illuminates ceiling and walls and the receiver collects the reflected rays. In this configuration no LOS between the transmitter and the receiver is necessary. Fig. 3.1 shows these two configurations.
In both cases, multiple reflections of light from walls, ceiling and objects inside the room cause temporal dispersion in the received signal. Inter-Symbol-Interference (ISI) produced by multipath scattering, is one of the major impairments to high-data rate communications over an indoor infrared channel. As mentioned in chapter two, a direct detection indoor infrared optical system can be completely characterized by its real-valued impulse response $h(t)$. Having $h(t)$, a deterministic function for a fixed physical configuration, path loss and multipath-induced delay spread can be calculated. Path loss is very important in power budget analysis of an indoor infrared system and the delay spread is used in selection of communications subsystem, including modulation scheme, coding, type of detection and anti-multipath countermeasures.

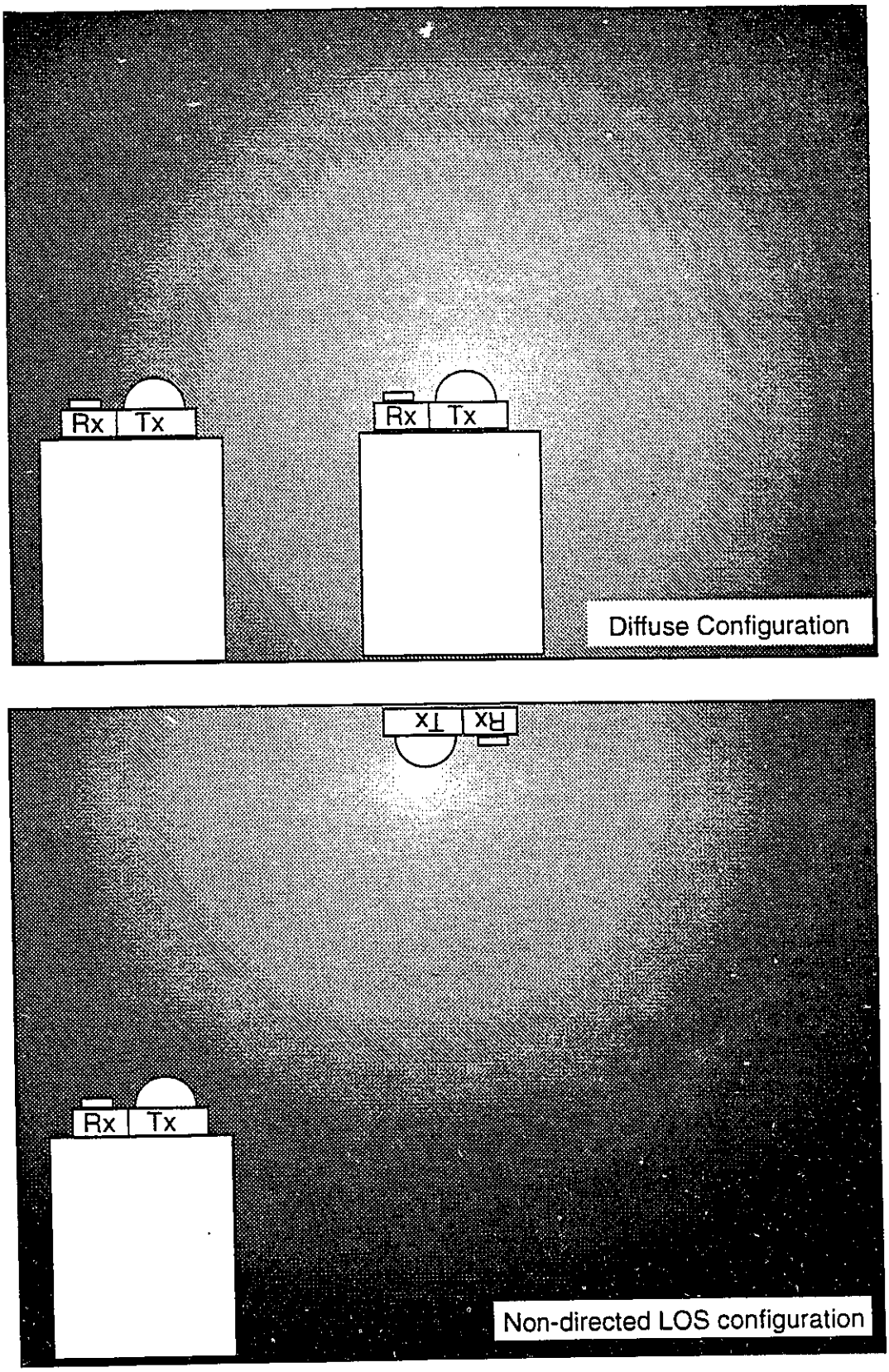

Figure 3.1 Illustration of non-directed LOS and diffuse configuration.

Modeling and simulation of indoor infrared channel has been addressed in literature with the first steps taken by Gfeller *et al.* [56] who pioneered the idea of using infrared for indoor wireless communications. They modeled the radiation pattern of a Light Emitting Diode (LED) by a Lambertian pattern and showed that the reflections of Infrared light from the surface of most indoor materials can be approximately modeled by a diffused Lambertian pattern. The reflection coefficient, ρ, of a unit area of the surface can be defined as the ratio of the light power reflected from the surface to the light power received by that area. Parameter ρ was measured in [56] for many materials used in building construction and it was noted that most of these materials are good reflecting objects with a reflection coefficient in the range 0.5 and 0.8. The relatively high value of ρ is a major motivation behind using the diffused configuration that relies on reflections from reflectors inside a room.

The analyses by Gfeller *et al.* [56] was meant for power-budget calculations, so they were interested in calculating the total received power at the detector. They accounted only for single reflections of light. Hash *et al.* [32] extended their work to account for double reflections, as well. These analyses did not take temporal dispersion of the channel into account. In other words, the only interest was in the total received optical power which can be expressed as the dc component of the frequency response of the channel, $H(0) = \int_{-\infty}^{\infty} h(t)dt$. For power-budget analysis, two reflections is usually enough because of the safety margins usually included in the calculations. However for a complete system design, more comprehensive information about channel characteristics is required. Hortensius, *et al.* [33] simulated impulse response of the channel for the first time, accounting for a single reflection. A set of measurements at the University of Ottawa was performed [35] to characterize indoor IR channel over a 40 MHz band. The limited bandwidth of the equipment's in that measurement setup was not sufficient for an accurate estimation of the channel impulse response. A major step in the estimation of impulse response of indoor infrared channels was taken by J.R.Barry, *et al.* [34][42]. They presented an algorithm to calculate the impulse response of this channel, taking into account an arbitrary number of reflections. This algorithm was verified by a set of channel measurements by Krause *et al.* [36] showing a good agreement between the estimated and the measured channel impulse responses.

Although their simulation algorithm was implemented for a rectangular empty room, the algorithm is general and can be applied to more complicated environments. The simulation procedure described in this chapter is an extension of the latter work by including additional features and capabilities into the program which is proving to be useful for many applications. Controlling the transmitter FOV may be beneficial in reducing the multipath components of the received signal. Also, in some designs we may use more than one transmitter in each room. Several sources may be used to shape the pattern of the received power profile across the room or to provide smaller cells to make a LOS system more feasible. Both of these capabilities were added to the simulation package. The package is also capable of generating power and delay spread profiles over the area of a room, examples of which will be seen in the next few sections.

In the following sections we will define the transmitter and the reflector model. An algorithm for calculation of impulse response and its implementation aspects [34] will be discussed next. Some examples of the results will be presented at the end of this chapter.

3.2. Models

In this section, models for source, receiver and reflector will be presented and line-of-sight impulse response is defined [34]. On the basis of the LOS impulse response, multiple reflections impulse response will be derived and the implementation issues will be discussed.

3.2.1. Source and receiver model

Following Gfeller [56], we can describe the radiation pattern of a wide beam optical source by a generalized Lambertian law:

$$R(\phi) = \frac{n+1}{2\pi} P_s \cos^n(\phi) \qquad \text{for} \quad \phi \in [-\pi/2, \pi/2] \tag{3-13}$$

Here, n is the mode number of the radiation lobe defined by:

$$n = \frac{\ln(0.5)}{\ln[\cos(HPBW)]}$$

where $HPBW$ is the half power emission angle of the LED. The higher value of n corresponds to more directive radiation pattern of the LED. Effect of n on the radiation pattern of an LED can be seen in Fig. 3.2 Note that, $(n+1)/2\pi$ is a

normalizing factor used to ensure the total radiated power of LED over the hemisphere equals P_s.

A point source S can be described by a set of scalars and vectors:

$$S \begin{cases} r_S: & \text{A three element vector describing the location of transmitter.} \\ \hat{n}_S: & \text{A three element normalized vector describing orientation of transmitter.} \\ P_S: & \text{Total optical power radiated from the source.} \\ R(\phi,\theta): & \text{Radiation pattern of the source.} \\ FOV_S: & \text{Source Field - Of - View.} \end{cases}$$

A receiver of the light can also be described by a set of scalars and vectors:

$$\Re \begin{cases} r_R: & \text{A three element vector describing the location of receiver .} \\ \hat{n}_R: & \text{A three element normalized vector describing orientation of receiver .} \\ A_R: & \text{Receiver area .} \\ FOV_R: & \text{Receiver Field - Of - View.} \end{cases}$$

3.2.2. Line-of-sight impulse response

Assume an environment without any reflectors. The impulse response between a source S and a receiver $\Re$, is given by [34]

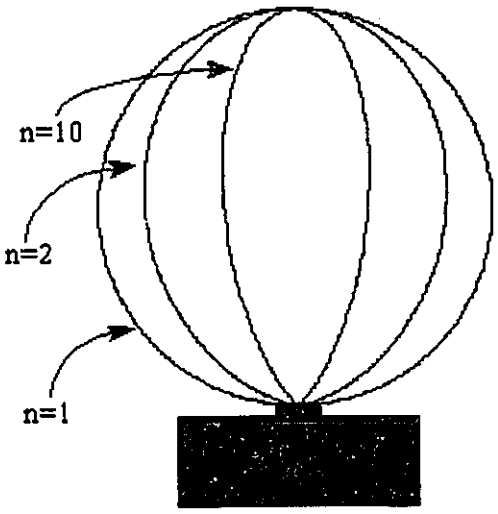

Figure 3.2. Normalized Radiation pattern of a generalized Lambertian source for several values of n.

$$h^{(0)}(t;S,\Re) \approx \frac{n+1}{2\pi}\cos^n(\phi)d\Omega\, rect(\theta / FOV_R)rect(\phi / FOV_S)\ \delta(t - R/c) \qquad (3\text{-}14)$$

where $d\Omega$ is the solid angle subtended by the receiver's differential area

$$d\Omega = \cos(\theta)A_R / R^2 \qquad (3\text{-}15)$$

R is the distance between the source and the receiver:

$$R = \|r_s - r_R\| \qquad (3\text{-}16)$$

θ is the angle between $\hat{n}_R$ and $(r_s - r_R)$:

$$\cos(\theta) = \hat{n}_R \cdot (r_s - r_R) / R \qquad (3\text{-}17)$$

ϕ is the angle between $\hat{n}_s$ and $(r_R - r_S)$:

$$\cos(\phi) = \hat{n}_s \cdot (r_R - r_s) / R \qquad (3\text{-}18)$$

The rectangular function is defined by:

$$rect(x) = \begin{cases} 1 & for\ \ |x| \le 1 \\ 0 & for\ \ |x| > \end{cases} \qquad (3\text{-}19)$$

and c is the speed of light.

In deriving (3-2), it is assumed that the receiver area is much smaller than the distance between transmitter and receiver, so the received optical power is constant over photodetector area and all optical energy reaches the receiver at the same time.

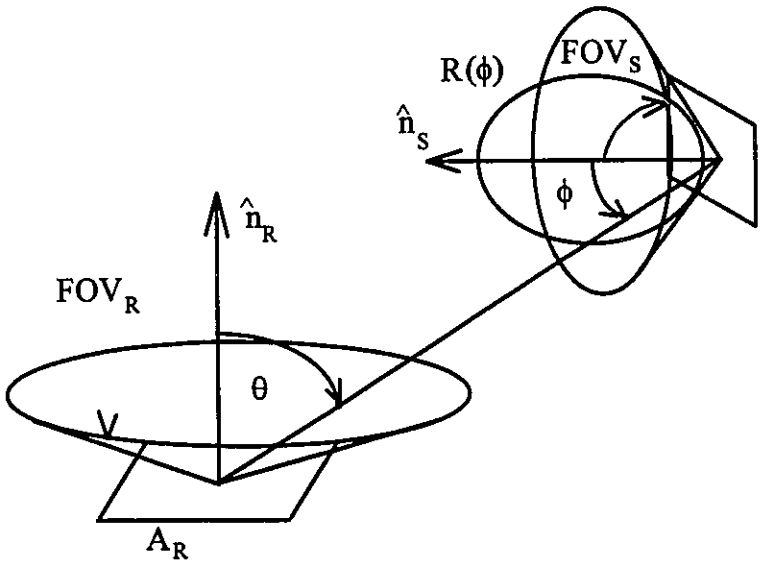

Figure 3.3. Transmitter and receiver geometry

3.3. Multiple Bounce Impulse Response

In a room with a receiver $\Re$ and a transmitter S, one can write the impulse response of the channel as the sum of the impulse responses from the lights reflected just once, plus those who are reflected twice and so on. In other words, impulse response of the channel can be written as:

$$h(t;S,\Re)=\sum_{k=0}^{\infty}h^{(k)}(t;S,\Re) \qquad (3\text{-}20)$$

where $h^{(k)}(t;S,\Re)$ represents the light undergoing exactly k reflections to reach the receiver $\Re$ from the source S. The Line of sight path, the path without any reflection, is given by (3-14). Higher order reflections can be calculated recursively using:

$$h^{(k)}(t;S,\Re)=\int h^{(0)}(t;S,\{r,\hat{n},\pi/2,dA\})\otimes h^{(k-1)}(t;\{r,\hat{n},1\},\Re) \qquad (3\text{-}21)$$

where symbol $\otimes$ denotes convolution. Here, the LOS impulse response from source S to the an element of size dA (as the intermediate receiver/transmitter) is convloved with the (k-1)-th bounce impulse response from that element to the receiver $\Re$ and integrated over all the reflector areas. Substituting (3-14) in (3-9) will result in:

$$h^{(k)}(t;S,\Re)=$$
$$\frac{n+1}{2\pi}\int_{S}\frac{\rho_r\cos^n(\phi)\cos(\theta)}{R^2}\,rect(2\theta/\pi)\;h^{(k-1)}(t-R/c;\{r,\hat{n},1\},\Re)\;dA \qquad (3\text{-}22)$$

These integrations are performed with respect to the position r on the surface S of all reflectors and the notations used in the integration are as follows:

$\hat{n}$: Normal to the reflector surface S at position r.

dA: Differential area of the reflector surface at position r.

ρ_r : Reflectivity at position r.

R : Distance between differential area and receiver, ($R=\|r-r_R\|$)

ϕ : Angle between source normal and the line connecting source and differential area, so $\cos(\phi)=\hat{n}_s\cdot(r-r_s)/R$.

θ : Angle between differential area normal and the line connecting source and that area., so $\cos(\theta)=\hat{n}\cdot(r_s-r)/R$.

From this integration, we see that the k-bounce impulse response, depends on the (k-1)-bounce impulse response. In other words, to find the k-bounce impulse

response from source *S*, we shall find the distribution of power and its timing over all reflectors and then assume each differential area as another source, and compute the (k-1) bounce impulse response.

3.3.1. Implementation

To calculate the integral in (3-21), we shall divide the reflecting surfaces into smaller elements, each with area ΔA. Each of these elements, receive an amount of power with a certain delay and then act as a transmitter with a Lambertian pattern by reflecting a portion of their received optical energy back into the media. Assuming total number of elements to be N and noting the i-th element with E_i we may approximately write $h^{(k)}(t)$ as:

$$\begin{aligned} h^{(k)}(t;S,\Re) &\approx \sum_{i=1}^{N} h^{(0)}(t;S,E_i) \otimes h^{(k-1)}(t;E_i,\Re) \\ &= \frac{n+1}{2\pi} \sum_{i=1}^{N} \frac{\rho_i \cos^n(\phi)\cos(\theta)}{R^2} rect(2\theta/\pi) h^{(k-1)}(t-R/c;\{r,\hat{n},1\},\Re)\Delta A \end{aligned} \tag{3-23}$$

It is obvious that E_i plays the role of a source in calculating the (k-1) bounce impulse response while acting as a receiver in the first bounce (power directly from source). Approximating the integral by a discrete sum, results in a piece-wise continuous function $h^{(k)}(t)$. In fact, the resulting $h^{(k)}(t)$ would be a finite sum of scaled and delayed delta functions. We may divide time axis into bins of width Δt and sum the total power received in each bin. The result would be a histogram that closely represent *h(t)*. For more accurate representation of *h(t)* we have to increase time and spatial resolution.

For reflection orders greater than one, it is not efficient to implement (3-23) directly. It can be seen that a direct implementation would require identical operations to be performed several times. It is obvious that for a specific room with N differential reflector elements, all that is needed to calculate impulse response is the delay between i-th element and the j-th element, $\tau(i,j)$, and the power received from i-th element to the j-th element, $\Delta p(i,j)$. A direct implementation, calculates each of these, k times, and therefore is very time consuming. Instead, we may store these elements in two table look-ups and retrieve them as they are needed in the calculations. The procedure for calculation of impulse response using table lookup method is given by [34]:

```
function h(t;i,j,k)
begin
        if(k=0)
                return ΔP(i,j) * delta(t-τ(i,j))
        else
                return sum from e=1 to N
                        rho(e) * ΔP(i,e) * h(t-τ(i,e);e,j,k-1)
        end if
end
```

Although table lookup method results in much less computation time, it requires much more memory. Assuming 4-byte space is required for the storage of a floating point number, table look-up method would require $8N^2$ bytes of memory. For example, considering a 5m × 5m × 3m room with ΔA=10 cm × 10 cm, there will be N=11000 small elements. To create a look up table for these elements, 968 Mbyte of memory is required which is well beyond the limits of today's computers. For this example, assuming 32 Mbyte of available memory, the size of elements should be greater than 25 cm × 25 cm.

Clearly there is a trade-off between the speed and the available memory in practical implementation of this algorithm. When more accuracy is required, a smaller size for the elements should be chosen, which in turn will result higher N and therefore the direct calculation should be used. With small values of N, table lookup is practical and faster. Running the program on a SUN SPARC STATION 10™, the time required for estimation of impulse response using the direct algorithm was approximately $16N^k$ μsec. This means that for the same size room ,with element size of 10 cm × 10 cm, and k=2 approximately 35 minutes were required. Increasing to k=3, the required time would be approximately 254 days. This shows the effect of k on the computing time.

The calculations made in this program, can be done in parallel and the algorithm is well suited in nature for parallel implementation. Optimization of this algorithm is an open area for the interested researchers.

3.4. Simulation Results

The simulation procedure discussed in the previous sections is used to analyze various aspects of indoor infrared channel to give us the required knowledge about system design. In the next sections, we will briefly overview some of the simulation results and discuss them briefly.

3.4.1. Impulse response and related parameters

After calculating *h(t)*, we can easily find frequency response of the system, *H(f)*, total received electrical power, P_E and the root mean square delay spread of impulse response, σ, using these formulas:

$$H(f) = \int_{-\infty}^{\infty} h(t) e^{-j\omega t f} dt \qquad (3\text{-}24)$$

$$P_E = \int_{-\infty}^{\infty} h^2(t) dt \qquad (3\text{-}25)$$

$$\sigma = \sqrt{\frac{1}{P_E} \int_{-\infty}^{\infty} (t-\mu)^2 . h^2(t) dt} \qquad (3\text{-}26)$$

where μ is defined as:

$$\mu = \frac{1}{P_E} \int_{-\infty}^{\infty} t . h^2(t) dt \qquad (3\text{-}27)$$

Because of the discretization used in the simulation, we have a discrete version of *h(t)* that can be referred to as *h[n]*. if *h[n]* is non-zero in [*0,M*] we can rewrite (3-24) to (3-27) as follows:

$$\boldsymbol{H(k) = \frac{1}{M} \sum_{n=0}^{M} h[n] . e^{-jkn(2\pi/M)}} \qquad (3\text{-}28)$$

$$P_E = \sum_{n=0}^{M} h^2[n] \qquad (3\text{-}29)$$

$$\sigma = \sqrt{\frac{1}{P_E} \sum_{n=0}^{M} (n-\mu)^2 . h^2[n]} \qquad (3\text{-}30)$$

$$\mu = \frac{1}{P_E}\sum_{n=0}^{M} n.h^2[n] \qquad (3\text{-}31)$$

In the LOS configurations, there is a strong impulse at the beginning of the impulse response that usually carries most of the received energy. The fact that a large amount of energy is received at a very short time, makes this impulse a very important component of *h(t)*. As a result of this impulse, which concentrates energy at the beginning of impulse response, delay spread of LOS channels are much less than diffuse channels. We define a variable LP as:

$$LP = \frac{\text{Power in the LOS Impulse}}{\text{Total received Optical Power}}$$

Parameter LP varies between 0 (No LOS component in the impulse response) and 1 (No multipath[9]). Clearly, a higher value of LP corresponds to a lower value for delay spread and less ISI due to multipath.

Sometimes it is important to have information about spatial variations of the channel. Distribution of received power and delay spread over the area of a room and sensitivity of these distributions to environment conditions are among important information required for a complete design. We can also define PDF and CDF for the results that are important for designing a channel with a minimized outage. For example, if we calculate channel parameters for 1200 locations in a 3m × 4m × 3m room, (one simulation per 10 cm × 10 cm cell all over the room at the height of 1m) generating a vector p for the received power across the room, we can define these two functions:

$$PDF_p(x) = \frac{1}{M}\sum_{i=1}^{M} Count[x < p(i) < x + \Delta x] \qquad (3\text{-}32)$$

$$CDF_p(x) = \frac{1}{M}\sum_{i=1}^{M} Count[x < p(i)] \qquad (3\text{-}33)$$

where M is the size of vector p and $Count[x]$ is defined by:

$$Count[x] = \begin{cases} 1 & \text{if x is FALSE} \\ 0 & \text{if x is TRUE} \end{cases} \qquad (3\text{-}34)$$

[9]LP=0 happens in diffused IR channels and LP=1 happens when both transmitter and receiver have very narrow FOV and are aligned.

These two functions provide us with some more information about the distribution of the values of a specific channel parameter that is useful for system design and comparison.

The simulation software is capable of generating results for these purposes by dividing the area of a room (or a specified part of it) into smaller cells of specified size. In each cell, impulse response and the corresponding parameters are calculated. These results are then fed into a set of visualization programs written in MATLAB™ to generate proper graphs and charts containing spatial and numerical distribution of channel parameters. We will compare and analyze our simulation results using these parameters and graphs in the following sections.

3.4.2. LOS and Diffuse: A comparison

Consider a 3m × 4m × 3m room with an IR base station inside. Depending on the configuration, the base station can be on the ceiling, (LOS configuration) or at the center of the room shining the ceiling (Diffuse configuration). Fig. 3.1 shows these two configurations. For comparison, we assume the same transceiver and reflection parameters for both cases. The only difference would be in the direction and location of the transmitter in both cases. Parameters used for this simulation are specified in Table 3-1. Three locations, R1, R2 and R3 were chosen and impulse response was calculated for each. Fig. 3.4 shows the impulse and frequency responses for each location in diffuse and LOS configurations. The LOS impulse response consists of a strong delta function at the origin[10] plus some residual power coming later, as a result of multipath effect. The first delta function carries most of the received energy (LP=0.76, 0.84 and 0.88 for R1, R2 and R3). This strong LOS delta has an advantage for LOS configuration. It causes the delay spread of this type of channel be negligible. Therefore, we expect minor degradation due to ISI in this type of channel compared to the diffuse channel. If the direct path between transmitter and receiver is blocked, the receiver loses most of its received power. The rest of impulse response has much less energy compared to a shadowed diffuse channel, because the diffuse configuration receives its energy from all reflectors, and consequently is very hard to block. This clearly shows the sensitivity of LOS to shadowing.

[10]Origin was chosen to be at t=R/c where R is the distance between the transmitter and the receiver and c is the speed of light. The peak of this delta is much higher compared to the multipath components, so in the LOS impulse response plots, a clipped version of it is shown.

Room	Room A		
Length (L_x)	4 m		
Width (L_y)	3 m		
Height (L_z)	3 m		
Reflectivity (ρ)			
North wall	0.6		
South wall	0.6		
East wall	0.6		
West wall	0.6		
Ceiling	0.7		
Floor	0.1		
Bounces (k)	k=1	k=2	k=3
N_x	400	100	40
N_y	300	75	30
N_z	300	75	30
Run time	6 sec	112 min.	160 hour

Source in A	Diffuse	LOS
Power (Ps)	1 W	1 W
X (m)	2	2
Y (m)	1.5	1.5
Z (m)	1	3
Elevation	90°	-90°
Azimuth	0°	0°
FOV_s	85°	85°

Rx in room A	R1	R2	R3
Area (A_r) (cm^2)	1	1	1
X (m)	0.5	1.5	2.5
Y (m)	0.5	2.5	0.8
Z (m)	1	1	1
Elevation	+90°	+90°	+90°
Azimuth	0°	0°	0°
FOV_r	85°	85°	85°

Table 3.1. Room A, Source and receiver parameters

Considering the impulse response of the diffuse system, we can clearly see the spread of the received energy over a wider time span. This makes such diffuse systems more vulnerable to ISI and shows that antimultipath techniques should be used for high data rate transmission. Table 3.2 shows a summary of the results obtained by simulation for room (A), at locations R1, R2 and R3. The other important difference observed is the received power which is 2 to 3 times more for LOS compared to diffuse configuration. This advantage of LOS should be considered in system design because IR systems are power-limited for eye safety reasons and power budgeting is very important in the design.

Spatial variations of the received power, delay spread, and the corresponding numerical distributions are illustrated in Fig. 3.5 to Fig. 3.9. The spatial variations of power in Fig. 3.5 and Fig. 3.7 look almost the same with a higher received power in the center of the room. The ratio of the maximum received power to the minimum received power is near 3 for both cases of LOS and diffuse configuration corresponding to about 5 dBo variation [11] in the received optical power across different locations of the room. Numerical distribution of the received power show that in LOS configuration, 80% of the cells receive more than 3.5$\mu W/cm^2$ while in diffuse this value is 2 $\mu W/cm^2$.

Another interesting point is that in a diffuse configuration, less than 10% of cells receive $P<P_{max}/2$ where P_{max} is the maximum received power in the room center, while this ratio for LOS is about 50%. This means that a receiver that can handle 3 dBo variation in received power and is designed under a maximum power constraint, receives signals properly in more locations in a diffuse configuration compared to a LOS configuration. In another words, the PDF of the received power for a diffuse configuration has more concentration in higher values of P compared to the PDF of P in a LOS configuration.

[11] dBo is optical dB and is defined by $y=10\log_{10}(x)$.

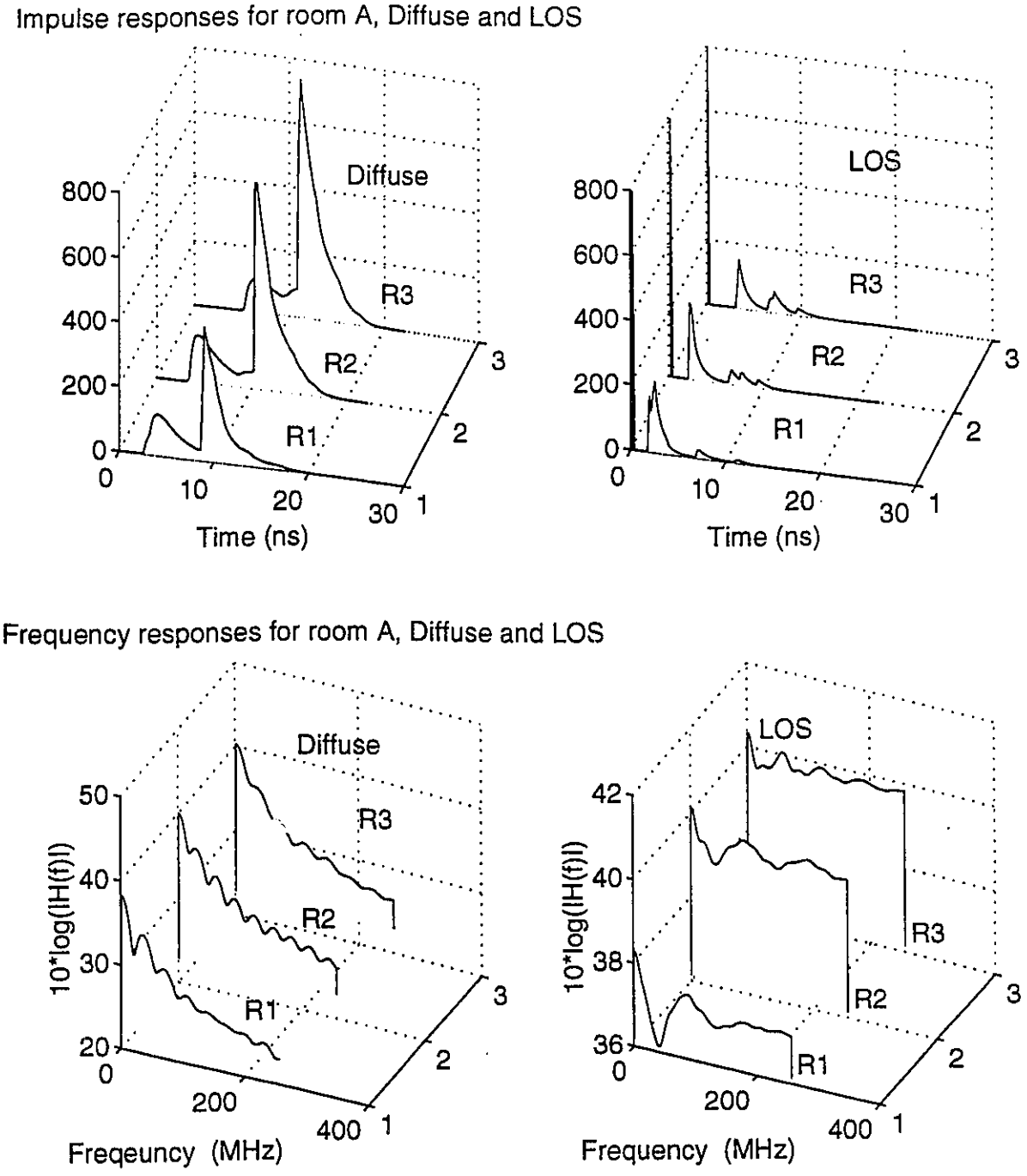

Figure 3.4 Impulse responses and frequency responses for three locations (R1, R2 and R3) in room A.

Fig. 3.6 and Fig. 3.8 show spatial variations of delay spread in room (A) for diffuse and LOS configurations, respectively. Both figures show a higher delay spread near reflecting objects. In diffuse configuration, walls in x-direction cause higher values of delay spread in nearby locations, because they receive more power from a Lambertian source compared to the walls in y-direction. The delayed reflected power makes stronger multipath components for cells near these walls. From numerical distribution of delay spread for diffuse configuration we see that 80% of cells have delays less than 2.4 nsec which is $0.7\sigma_{max}$, where σ_{max} is the maximum delay spread. In other words, considering $0.7\sigma_{max}$ for the design yields sufficient coverage. Although this is true for this example, we shall always use σ_{max} as the design criteria because we may not get this 80% coverage using $\sigma_{design}=0.6\sigma_{max}$.There are examples showing that this coverage might even go to zero by designing for $\sigma_{design}=0.7\sigma_{max}$.(Refer to section 3.4.7) Comparing the delay spread values for LOS and diffuse, we see that the delay spread of the LOS configuration is almost ten times less than the diffuse configuration. This can be described by the fact that there is a very strong impulse in the impulse response of a LOS system which makes its delay spread very small.

Fig. 3.9 shows spatial and numerical distribution of LP for LOS configuration. In this configuration, LOS impulse carries 60% to 88% of the received power(LP), with an almost flat spatial and numerical distribution for LP. The large value of LP shows the sensitivity of this configuration to the presence of a LOS between transmitter and receiver.

Location in room A	R1		R2		R3	
Configuration	Diffuse	LOS	Diffuse	LOS	Diffuse	LOS
Power ($\mu W/cm^2$)	1.35	3.162	2.06	5.48	2.16	6.44
Delay Spread (ns)	6.4	0.02	7.47	0.006	6.67	0.004
LP	--	0.76	--	0.84	--	0.88

Table 3.2 Summary of simulation results for room (A)

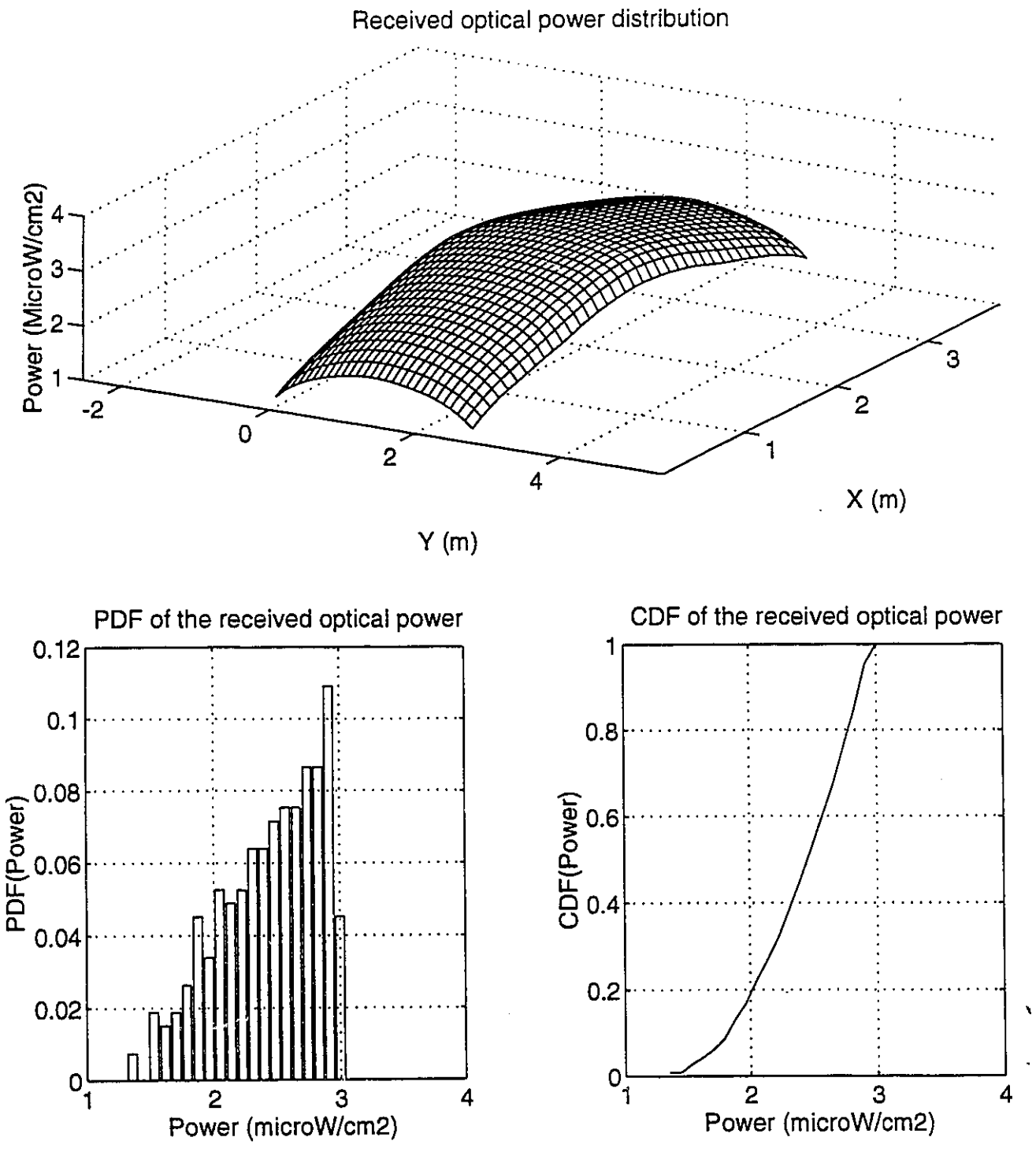

Figure 3.5 Spatial and numerical distribution for the received power in room A, diffuse configuration.

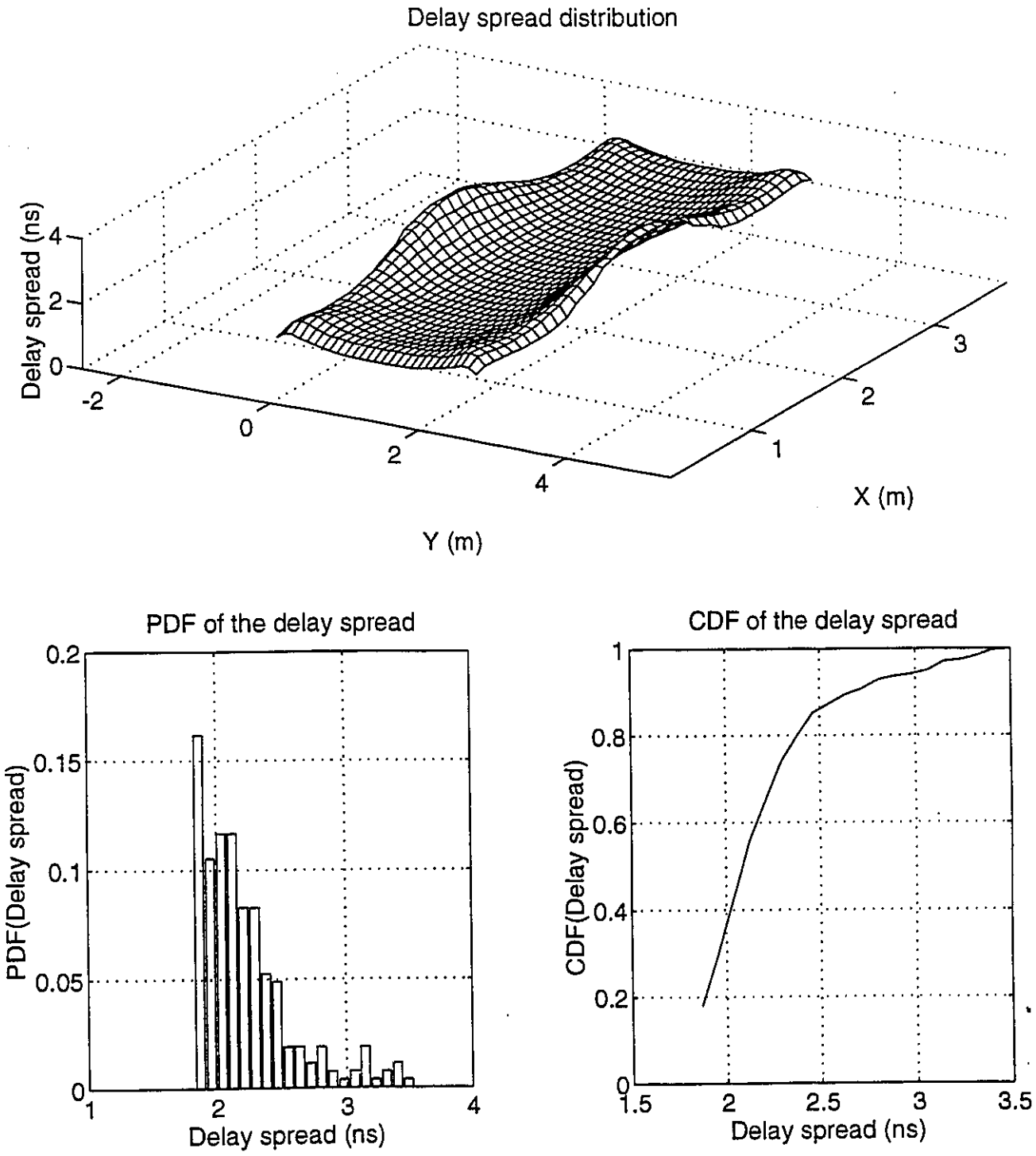

Figure 3.6 Spatial and numerical distribution for the delay spread in room A, diffuse configuration.

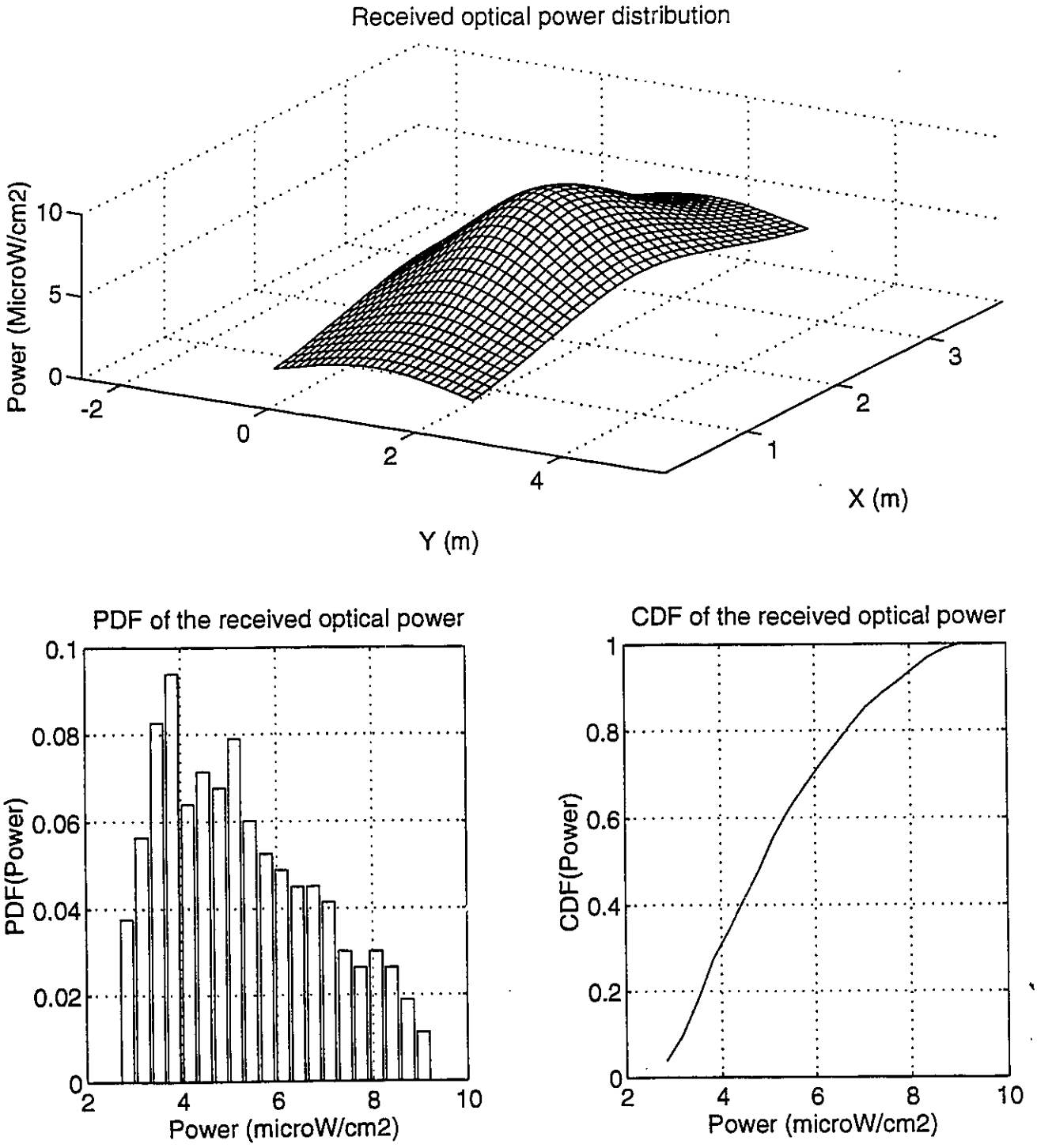

Figure 3.7 Spatial and numerical distribution for the received power in room A, LOS configuration.

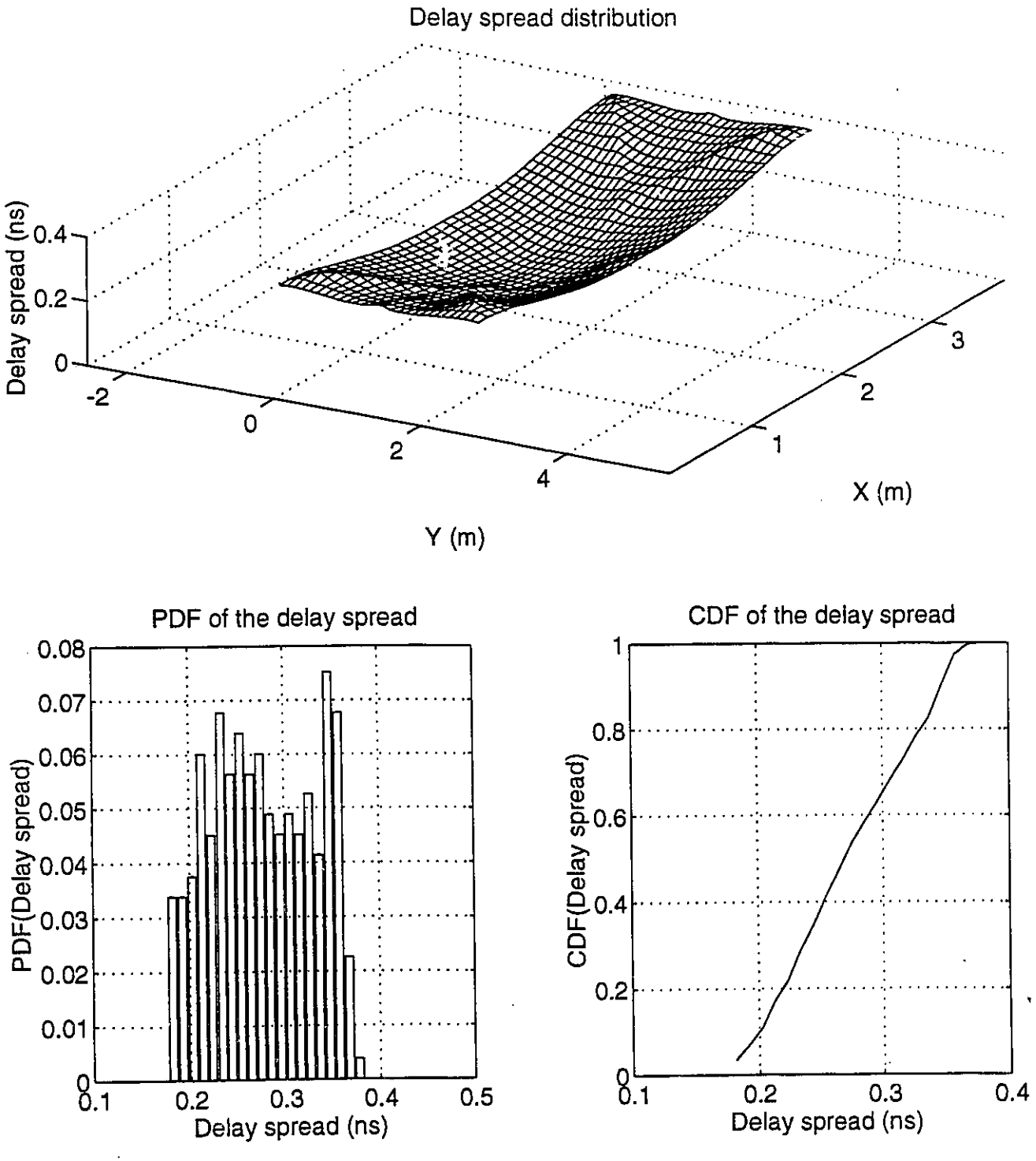

Figure 3.8 Spatial and numerical distribution for the delay spread in room A, LOS configuration.

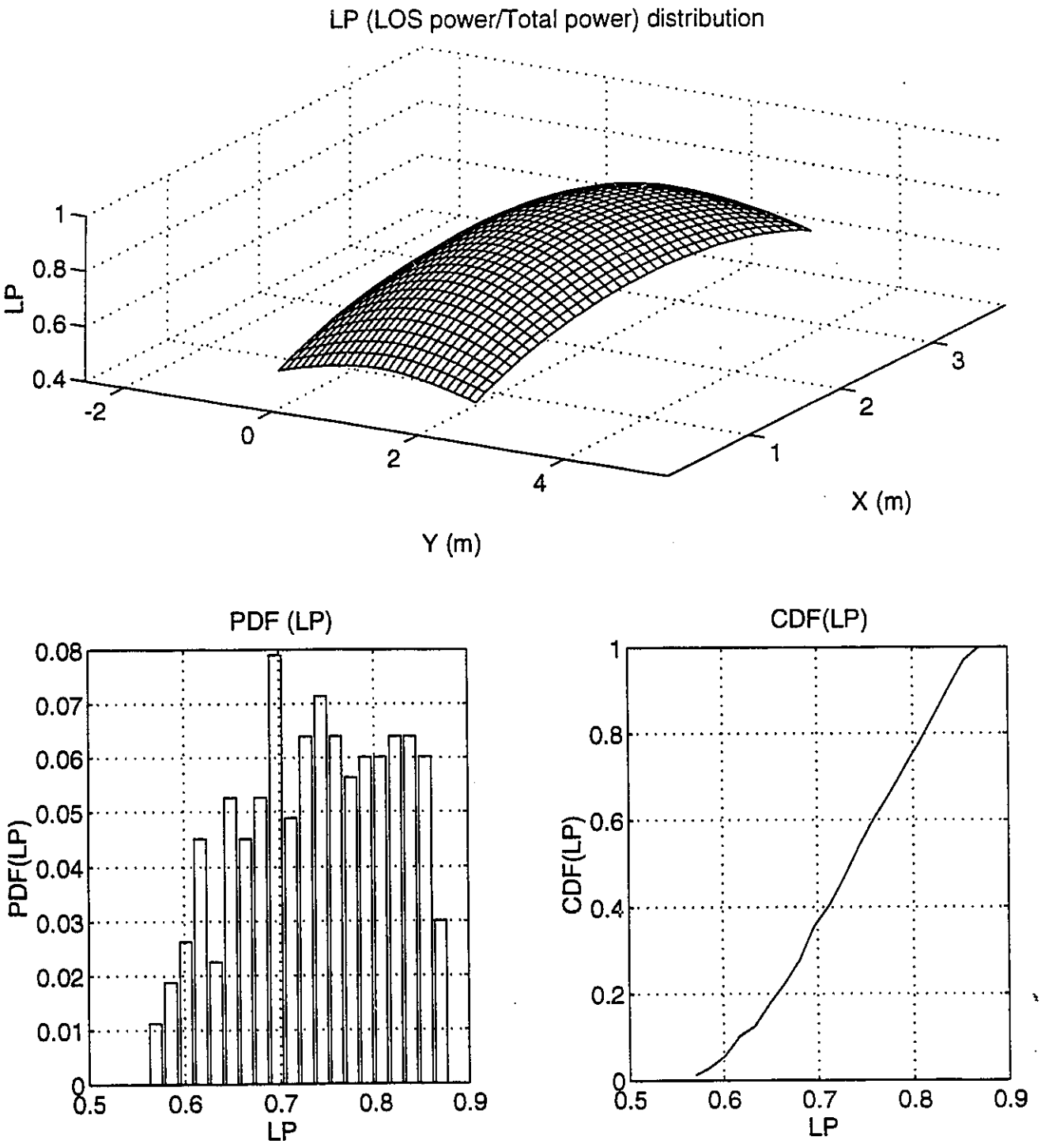

Figure 3.9 Spatial and numerical distribution for the ratio of LOS power to the total received power (LP) in room A, LOS configuration.

3.4.3. Relation between delay spread and received power

A very interesting point is the relation between the received optical power and the delay spread of impulse response. This is important in designing receivers with angular diversity reception. Fig. 3.10 shows two figures plotting received power versus delay spread for different locations. The interesting point is that there is a clear relationship between power and delay spread for LOS systems, while there is no such a relation for diffuse configuration. This is a clear example that using power as an indication of a low-multipath impulse response is valid for LOS configurations, but not otherwise. In other words, diversity techniques that try to maximize the received signal-to-noise power ratio do not necessarily reach an optimized value for delay spread depending on the channel configuration. This is one of the important results of this chapter.

3.4.4. Receiver and transmitter FOV

Another important parameter of an optical transmitter or receiver is its FOV. Intuitively, a wider FOV yields more received power and less sensitivity to rotation of the receiver, but at the same time, allows more multipath components in the impulse response. This effect is illustrated in Fig. 3.11 and Fig. 3.12. We simulated channel impulse response at location R1, room (A) in a LOS configuration for several values of transmitter FOV. Fig 3.11 shows the results of this simulation. These plots show that there are no clear change in the shape of impulse response or frequency response of the system. As we increase the transmitter FOV, delay spread of impulse response is increased and the LP is decreased. A wide FOV transmitter shines broader areas on the walls and other reflecting surfaces, producing more powerful multipath components. These components are detected by the receiver and increase the delay spread and the total detected power, decreasing the LP with a fixed LOS power .

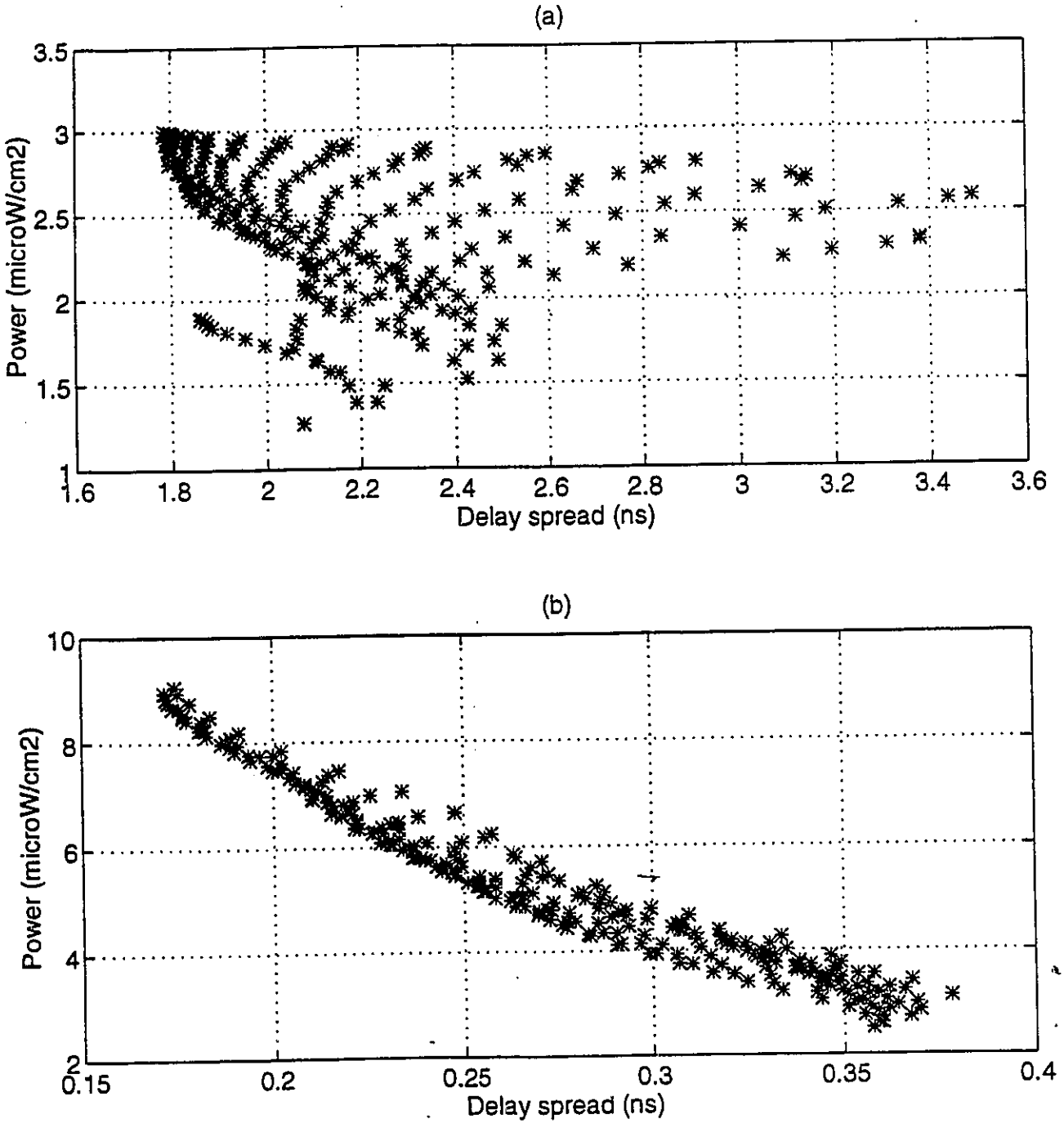

Figure 3.10 Scatter diagram of the optical power vs. delay spread for the diffuse (a) and the LOS (b) configurations . (room A).

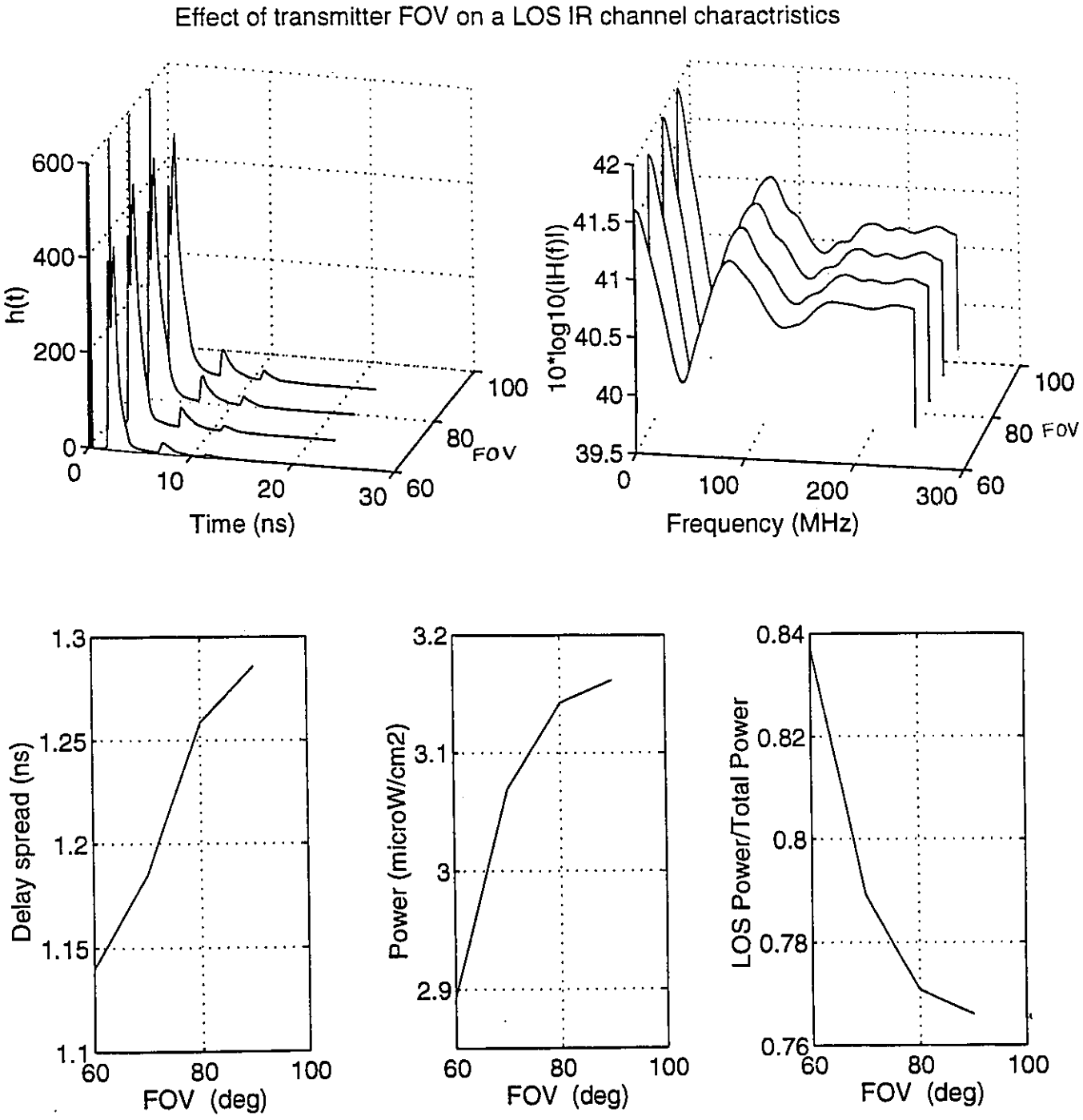

Figure 3.11 Effect of transmitter field-of-view on the impulse response, the frequency response, the delay spread, the received power and the LOS power ratio for a LOS configuration. (room A, location R1)

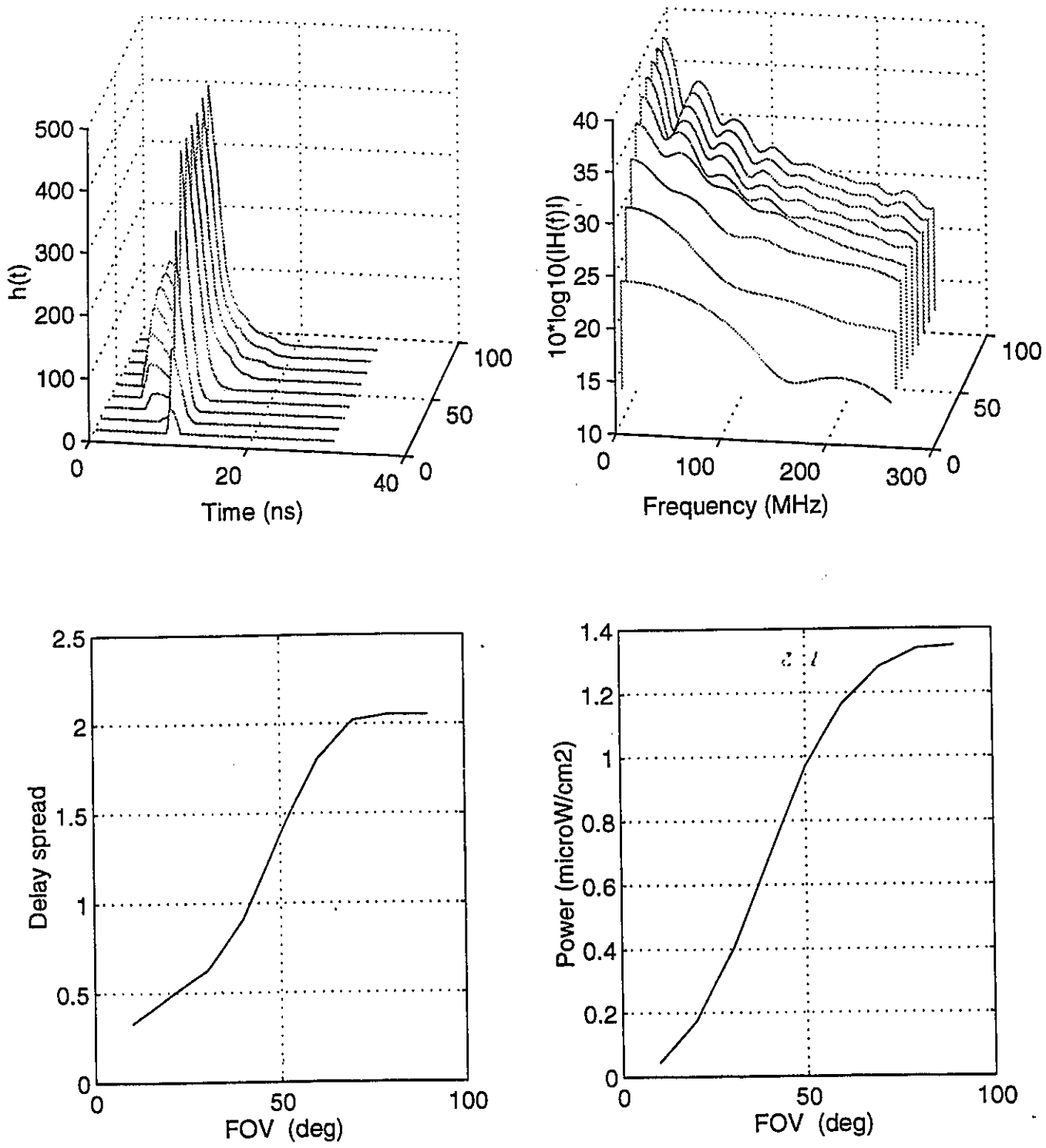

Figure 3.12 Effect of receiver field-of-view on the impulse response, the frequency response, the delay spread and the received power for a diffuse configuration.

Fig. 3.12 illustrates the effect of receiver FOV on the impulse response. By changing the receiver FOV from 90° to 10°, there is a clear change in the shape of impulse response and frequency response. Delay spread is 4 times less when decreasing the receiver FOV and the received power is down from 1.3 $\mu W/cm^2$ to 0.2 $\mu W/cm^2$. This shows that, although reducing multipath is possible for diffuse systems by limiting the receiver FOV, a high price should be paid namely loss in the received power. There is a trade-off between the received power and the delay spread. Perhaps a 40° FOV is a proper choice. At this value, delay spread is reduced by 50% while a decrease in the received power is only 20%.

3.4.5. Effect of resolution and the number of bounces

In calculating the impulse response of the system, the reflection surfaces are divided into several smaller elements, each acting as a receiver and then as a transmitter with a fraction of the received power. As mentioned in section 3.3.1, there is an exponential relationship between the required simulation run-time of the simulation program and the number of bounces used for calculation of the impulse response, namely $T \propto N^k$ where T is the required run-time of the computer program using a direct method, k is the number of bounces used in such a simulation and N is the number of elements used for this simulation. Assuming an empty room with a rectangular shape, dividing each of dimensions along X, Y and Z axis into N_x, N_y and N_z pieces will result in $N=2(N_xN_y+N_xN_z+N_yN_z)$ small reflecting cells. To illustrate the effect of N and k on the run-time and the accuracy of the results, we calculated impulse response of configuration A, position R1 with k=1,2 and 3. Fig. 3.13 shows the effect of k on the normalized impulse response and the frequency response of the system. Increasing k results in a more accurate estimation of channel. The price is a much higher simulation run-time as shown in Table 3.1. From Fig. 3.13 we see that increasing k, reveals more multipath components of *h(t)*. Delay spread increases from 6.4 ns for k=1 to 7.2 ns for k=2 and 7.7 ns for k=3. The 3-dB band of the system which is 95 MHz for k=1 changes to 75 MHz for k=2 and 60 MHz for k=3. Table 3.3 summarizes these results.

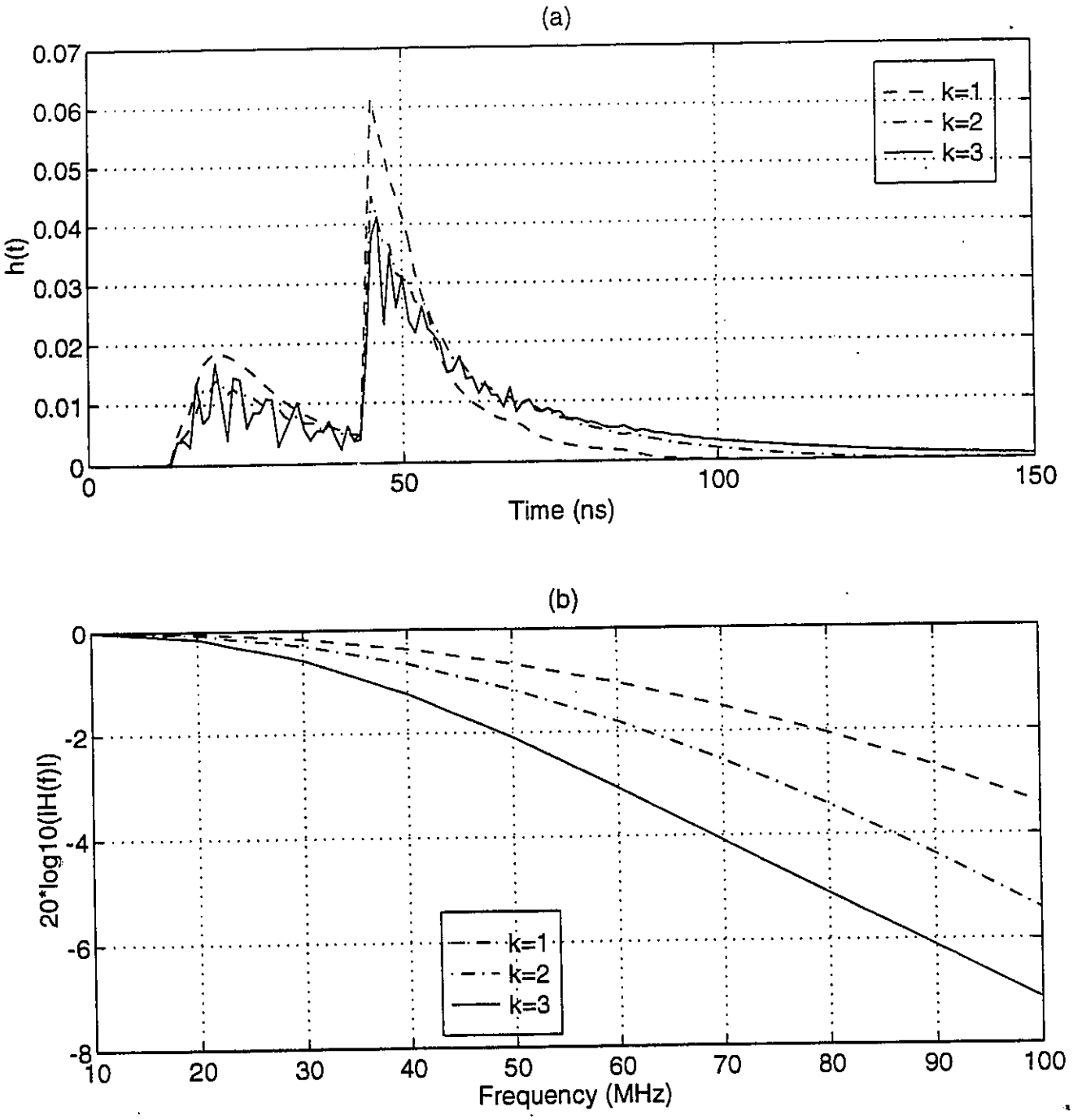

Figure 3.13 Effect of k on the simulation results. Figure (a) shows the change in the shape of the impulse response when higher order reflections are considered in the simulation. Note the increase in the spread of the impulse response. Figure (b) shows the change in the estimated 3-dB bandwidth of the system. Increasing k results in lower estimated bandwidth for the channel.

There is always a trade-off between the program run-time and accuracy. Beyond a certain point, the resulting accuracy is not worth the extra run-time that it takes. For this example we noted that decreasing ΔA from 4 cm × 4 cm to 2 cm × 2 cm increases the simulation run-time by a factor of 8 while there is less than 10% difference in the results. As a consequence, we simulated most of these configurations for generating spatial variation results with k=2 and elements of size 4 cm × 4 cm in order to have enough accuracy with a reasonable run-time.

3.4.6. Effect of Reflection coefficients

To have a feeling about the effect of reflection coefficients on the channel characteristics, we simulated the spatial variation of power and delay spread for room (C) which is the same size as room (A) but with different reflection coefficients for walls. Table 3.4 contains specification of room (C). Fig. 3.14 illustrates the effect of reflection coefficients on the spatial variation of the received power and the delay spread. There is a slight shift of the received optical power shape toward the higher reflection area, corresponding to a higher received power due to higher reflection of walls. The change is more clear in delay spread profile. In Fig. 3.14, near higher reflection walls, there are more strong multipath components resulting in higher values for delay spread. As a result, we would expect stronger multipath components near highly reflecting materials like glasses or shiny metals.

Bounces	k=1	k=2	k=3
Received power ($\mu W/cm^2$)	1.35	1.42	1.48
Delay spread (ns)	6.4	7.2	7.7
3-dBo bandwidth (MHz)	95	75	60
cell size ΔA	1 cm × 1 cm	4 cm × 4 cm	10 cm × 10 cm
Simulation time	6 sec	112 min.	160 hour

Table 3.3. Effect of k on the results obtained by simulation

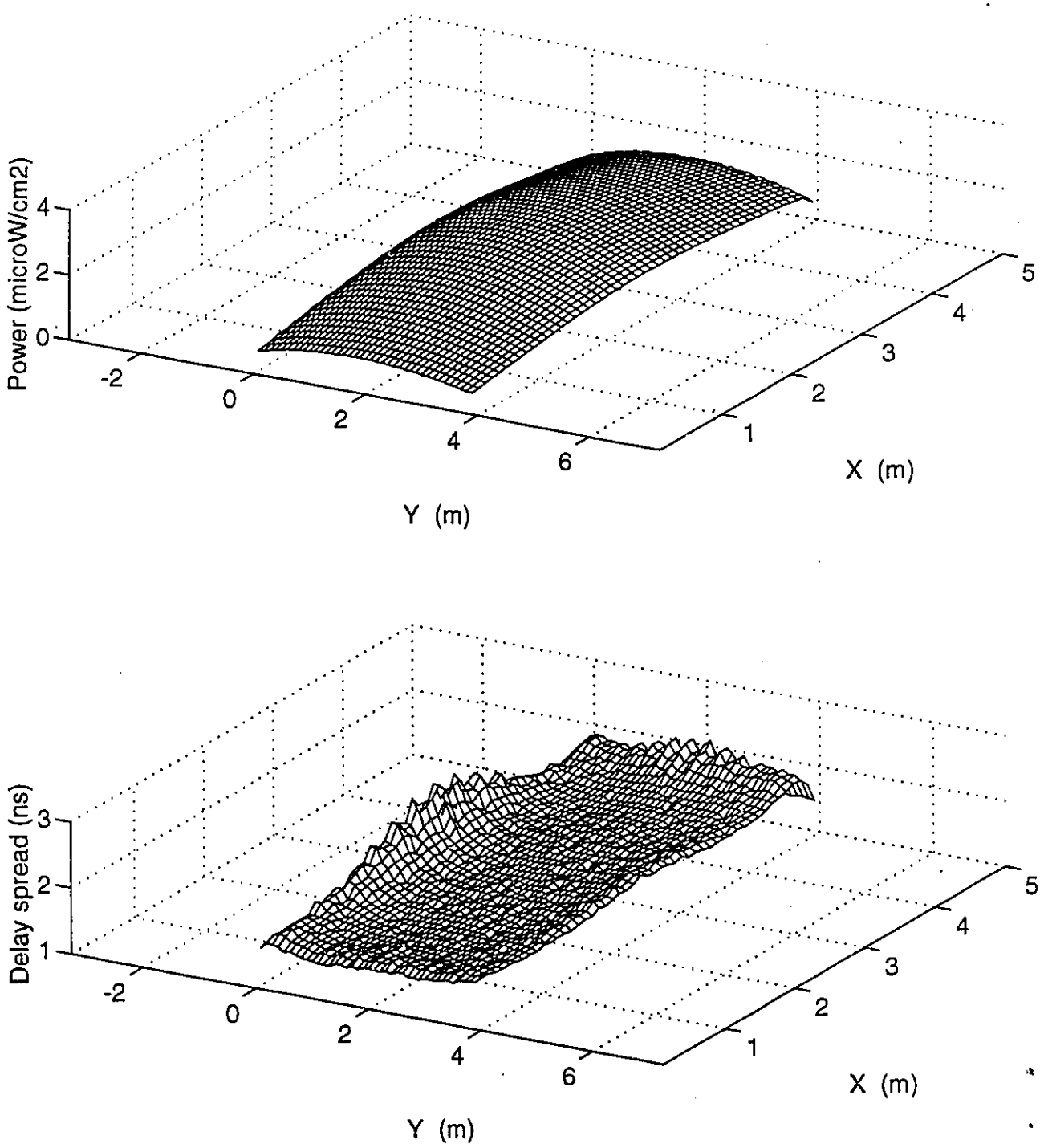

Figure 3.14 Effect of the reflection coefficients of walls on the distribution of received optical power and delay spread. Note higher delay spread values near higher reflecting walls.

3.4.7. Room Size

As a complement, we simulated the channel for a larger room (B), which is the size of a conference room. Table 3.4 contains the relevant parameters for this room.

As illustrated in Fig 3.15, the spatial variation of the received power is almost the same for room (A) and room (B). Comparing Fig. 3.15 with Fig. 3.5 (room (A) and room (B) in diffuse configuration) we see that although the maximum and the minimum values of the received power are almost the same, (P_{max}=2.2 $\mu W/cm^2$ and P_{min}=0.7 $\mu W/cm^2$) their numerical distribution are not exactly the same. In room (A), 80% of the cells receive more than 1.9 $\mu W/cm^2$ while in room (B), this value is 1.5 $\mu W/cm^2$. Overall, we don't see major difference between the received powers by increasing the room area by almost 3 times. This is a very good point for the diffuse configuration. It means that a diffuse system with proper power margins, wouldn't be much sensitive to room dimensions.

Room	Room B	Room C
Length (L_x)	8 m	4 m
Width (L_y)	5 m	3 m
Height (L_z)	3 m	3 m
bounces (k)	2	2
Cell size (ΔA)	4 cm × 4 cm	4 cm × 4 cm
Reflectivity (ρ)		
North wall	0.6	0.8
South wall	0.6	0.3
East wall	0.6	0.6
West wall	0.6	0.2
Ceiling	0.7	0.7
Floor	0.1	0.1

Table 3.4. Specifications of room (B) and room (C) used in simulations

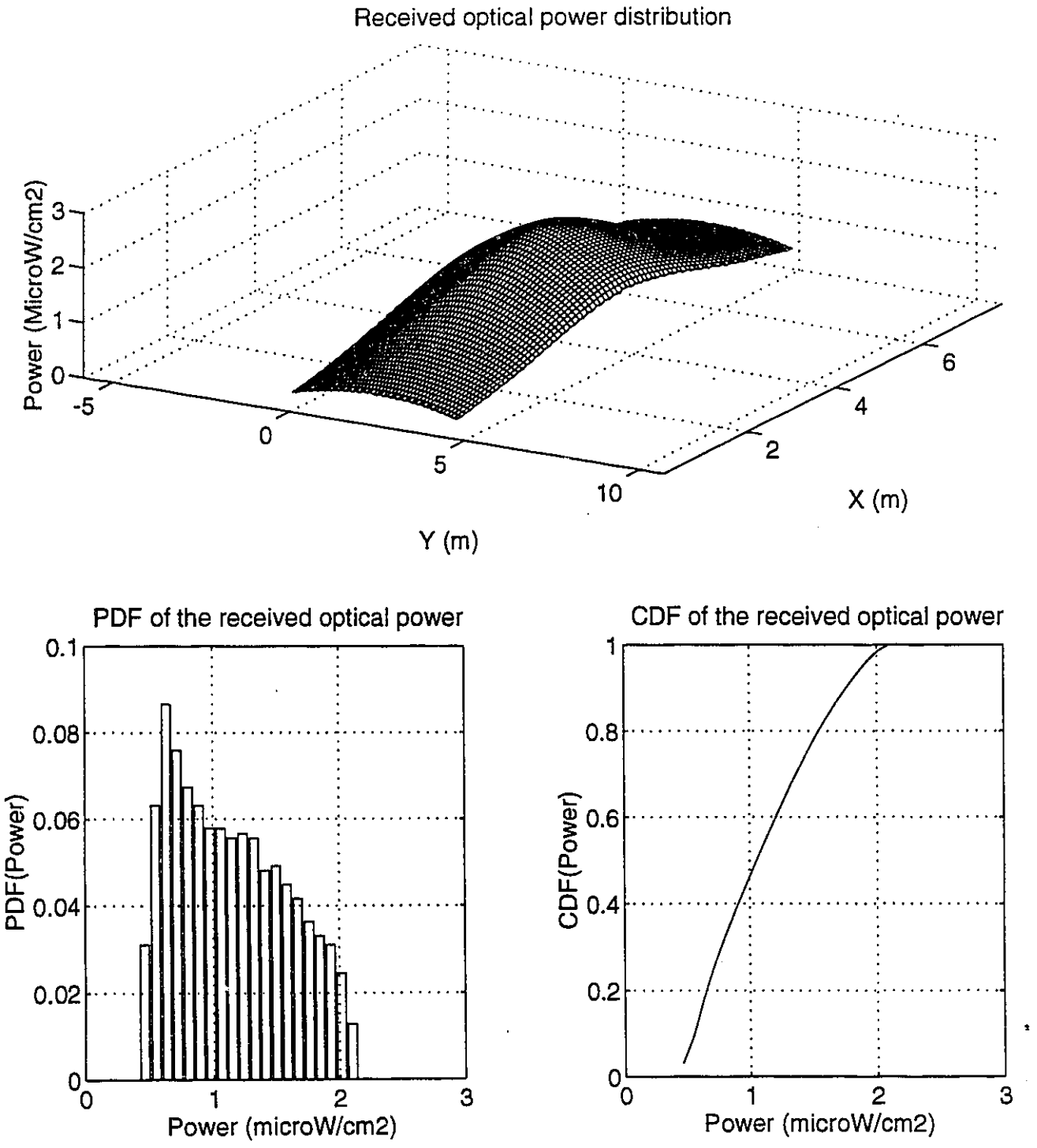

Figure 3.15 Spatial and numerical distribution of the received optical power in room B, diffuse configuration.

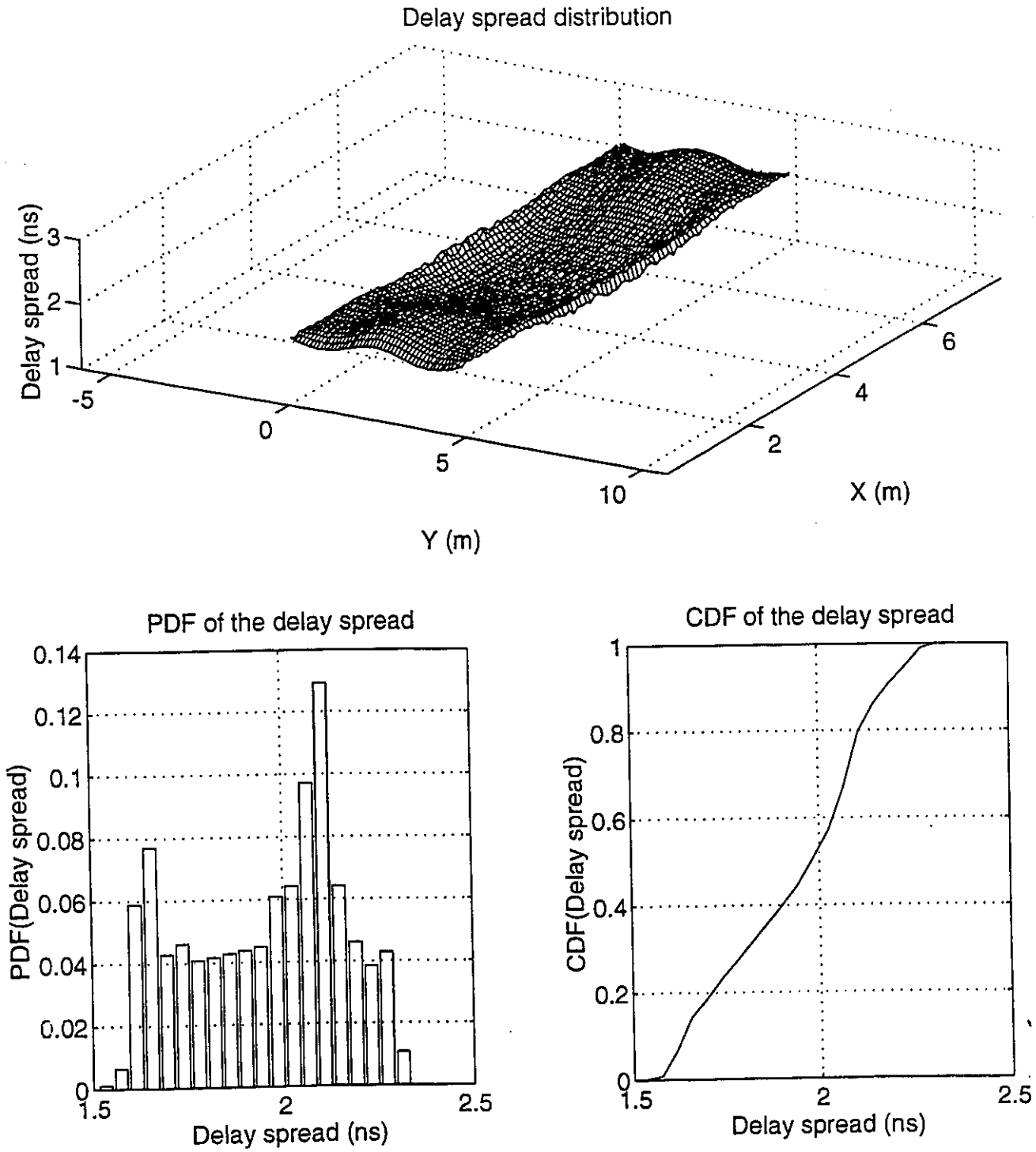

Figure 3.16 Spatial and numerical distribution of the delay spread in room B, diffuse configuration.

The more important difference between room (A) and room (B) is their delay spread distributions. Spatial and numerical distributions of delay in room (B) are illustrated in Fig. 3.16 and 3.18. Spatial distribution of delay spread shows an area of low delay near transmitter and two areas with almost flat distributions of delay at the first and the last quarter of the room. This shows an area with strong multipath components beyond a certain horizontal separation between the transmitter and the receiver. Looking at numerical distribution of the delay spread for diffuse configuration in Fig. 3.16 we see that almost all the cells have larger delays than $0.6\sigma_{max}$ (σ_{max} is the maximum delay spread in a certain configuration) while in room (A) only 20% of cells have delays more than $0.6\sigma_{max}$. This shows that for design of a robust system we should always use the maximum delay spread as the criteria. Considering room (B) with a LOS configuration, we see similar differences.

Fig. 3.17 to Fig. 3.19 illustrate results for LOS configuration in room (B). There is no important change in the shape of power profile. Numerical distribution of power shows that the minimum received power in room (B) is less than half of that in room (A) (1.1 $\mu W/cm^2$ for room (B) compared to 2.8 $\mu W/cm^2$ for room (A)).

Another interesting point is the distribution of LP in room (B) shown in Fig. 3.19. It shows that 80% of cells in room (B) receive 70% or more of their received power from LOS component of impulse response. The ratio of cells in room (A) that receive 70% or more of their power from LOS is 60%. This shows that in larger rooms, LOS component becomes more important to the receivers. In other words, the receiver becomes more sensitive to shadowing.

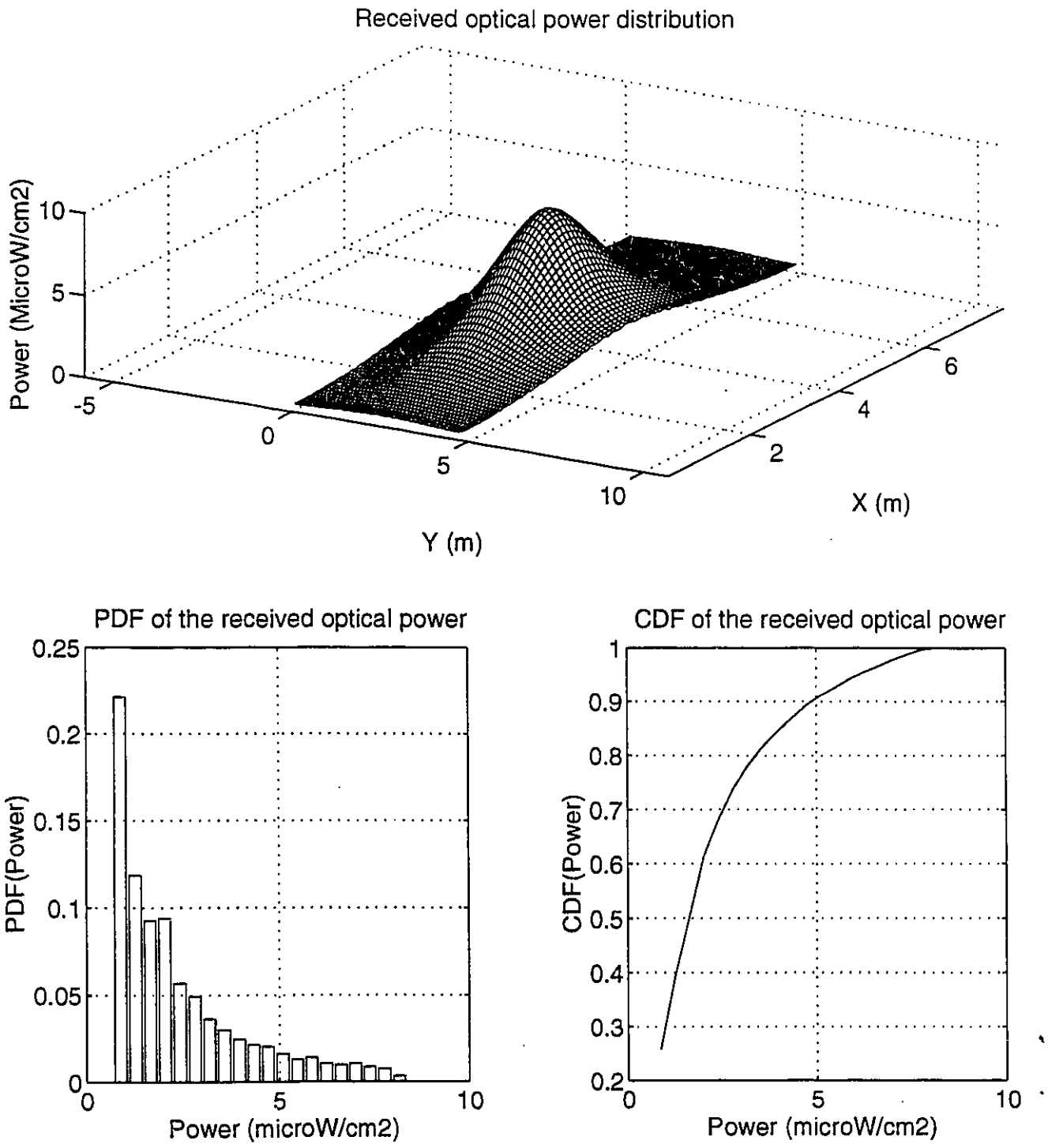

Figure 3.17 Spatial and numerical distribution of the received optical power in room B, LOS configuration.

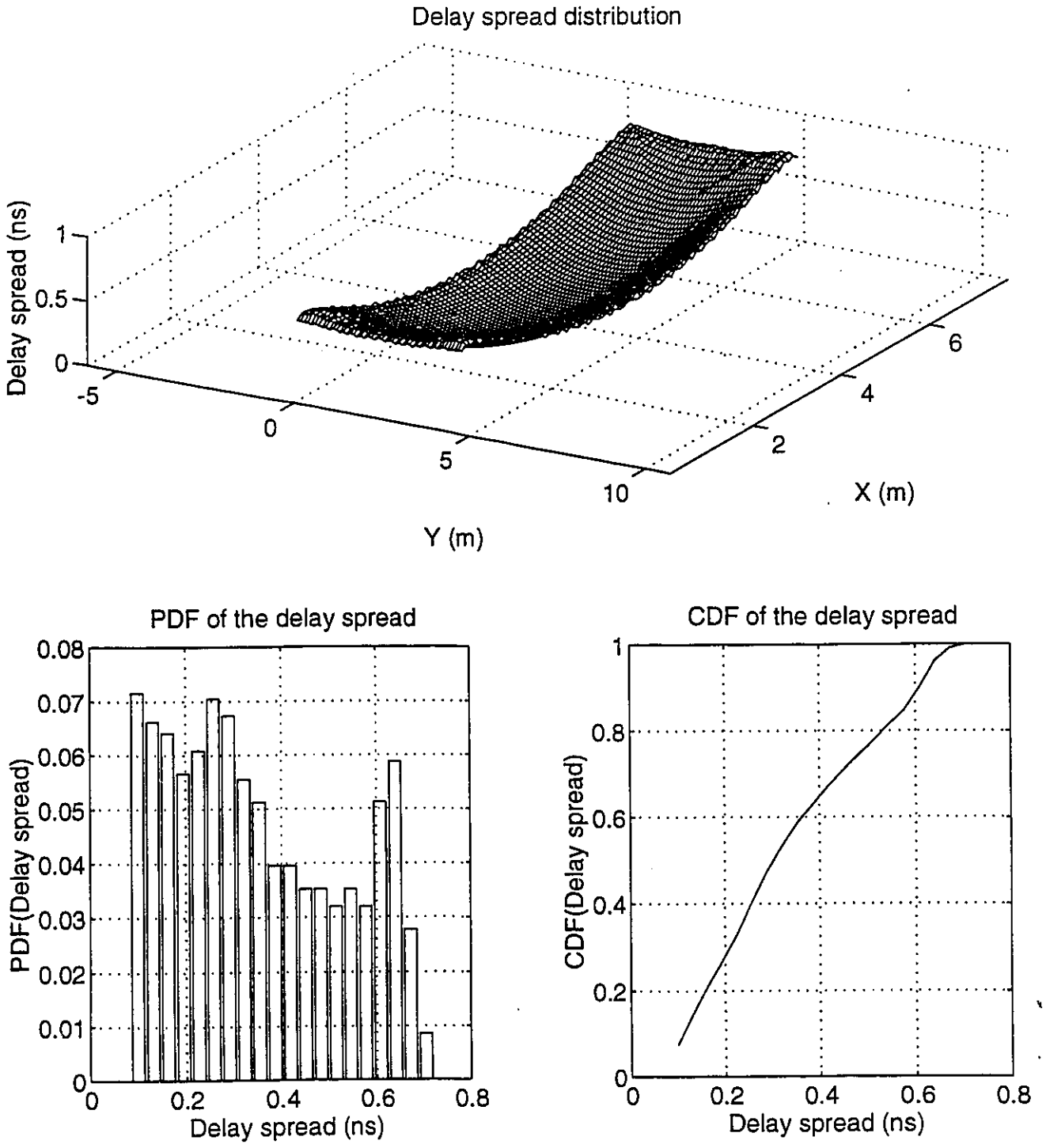

Figure 3.18 Spatial and numerical distribution of the delay spread in room B, LOS configuration.

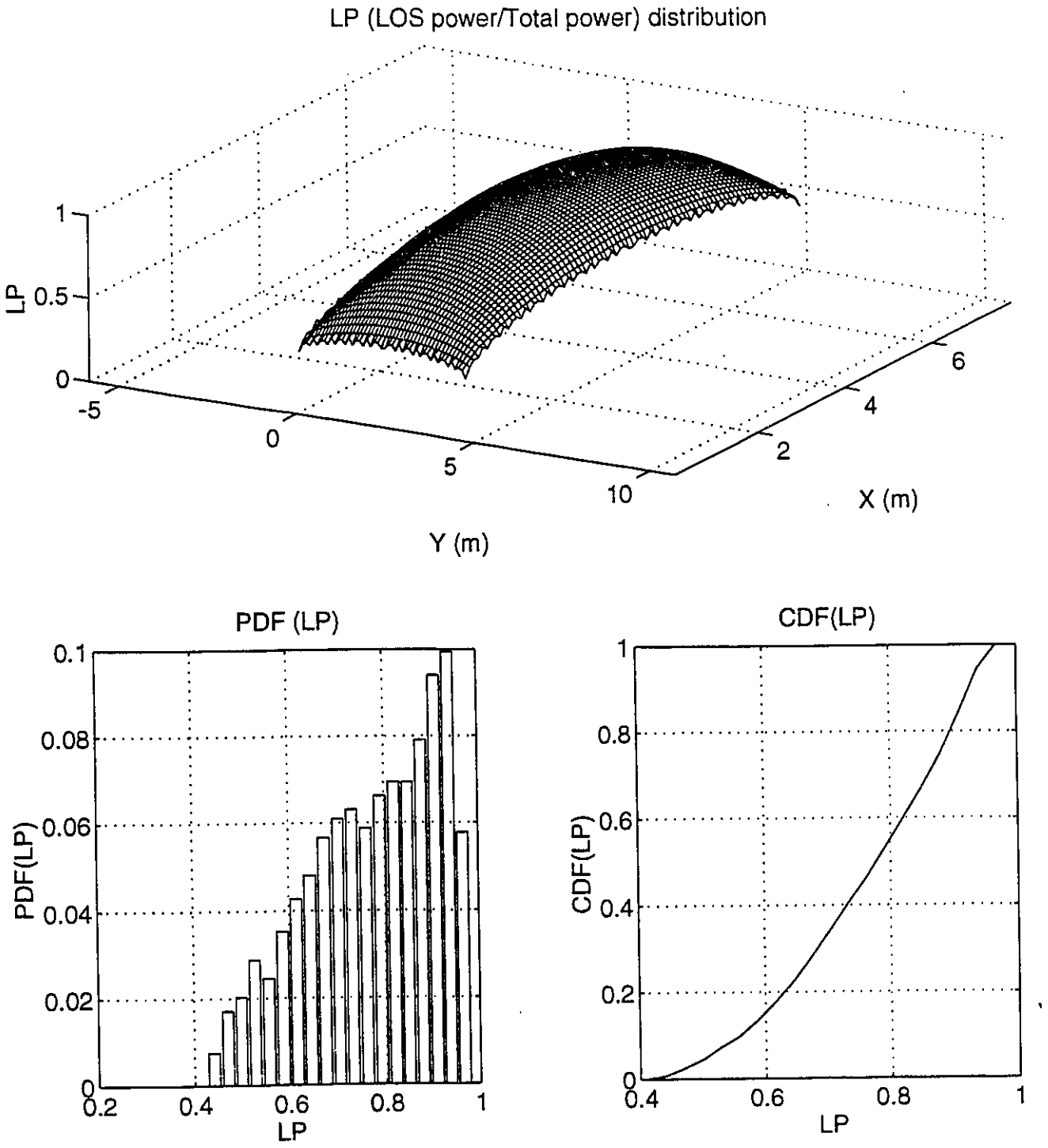

Figure 3.19 Spatial and numerical distribution for the ratio of LOS power to the total received power (LP) in room B, LOS configuration.

3.4.8. Passive optical components for optical power distribution

We propose a configuration that has the advantages of a single source LOS configuration while solving the shadowing problem. We can use optical passive components to make an optical IR transmission configuration less sensitive to shadowing. Fig. 3.20 shows the optical passive component and the proposed configuration. This passive component, reflects the incoming collimated beam and diffuses it in a desirable direction. Several of these components can be installed on the ceiling of a large room. The central base station sends a collimated optical beam to each of these devices making them a source, without the need for wiring and complex installations. There will be several of these elements in the ceiling so the system will be less sensitive to shadowing. A large FOV receiver can see at least one of them most of the time (unless total FOV of the receiver is blocked). The presence of a concentrated energy as an impulse, coming from direct LOS, is maintained making delay spread of this configuration less than that of diffuse configuration. Note that, because of the delays between several impulses in this configuration, delay spread would be more than that in a single source LOS configuration. Fig. 3.21 shows the spatial power distribution of this configuration, which shows a different shape compared to previous profiles. This is due to the spatial distribution of the energy source which now consists of 4 points in the ceiling.

The delay spread profile, shown in Fig. 3.22 is similar to a LOS system with higher values. Considering numerical distribution of the delay spread, there are 80% of cells with the delay spread of less than 1.2 nsec. This value is 2.2 nsec for diffuse configuration in the same room, (70% more delay spread). So we see that we have the advantage of less delay spread while avoiding shadowing problem to some extent. We can consider the diffuse configuration as an extension of this configuration with K points on the ceiling each transmitting a portion of the transmitter energy where K is very large (K goes to infinity in a mathematical description).

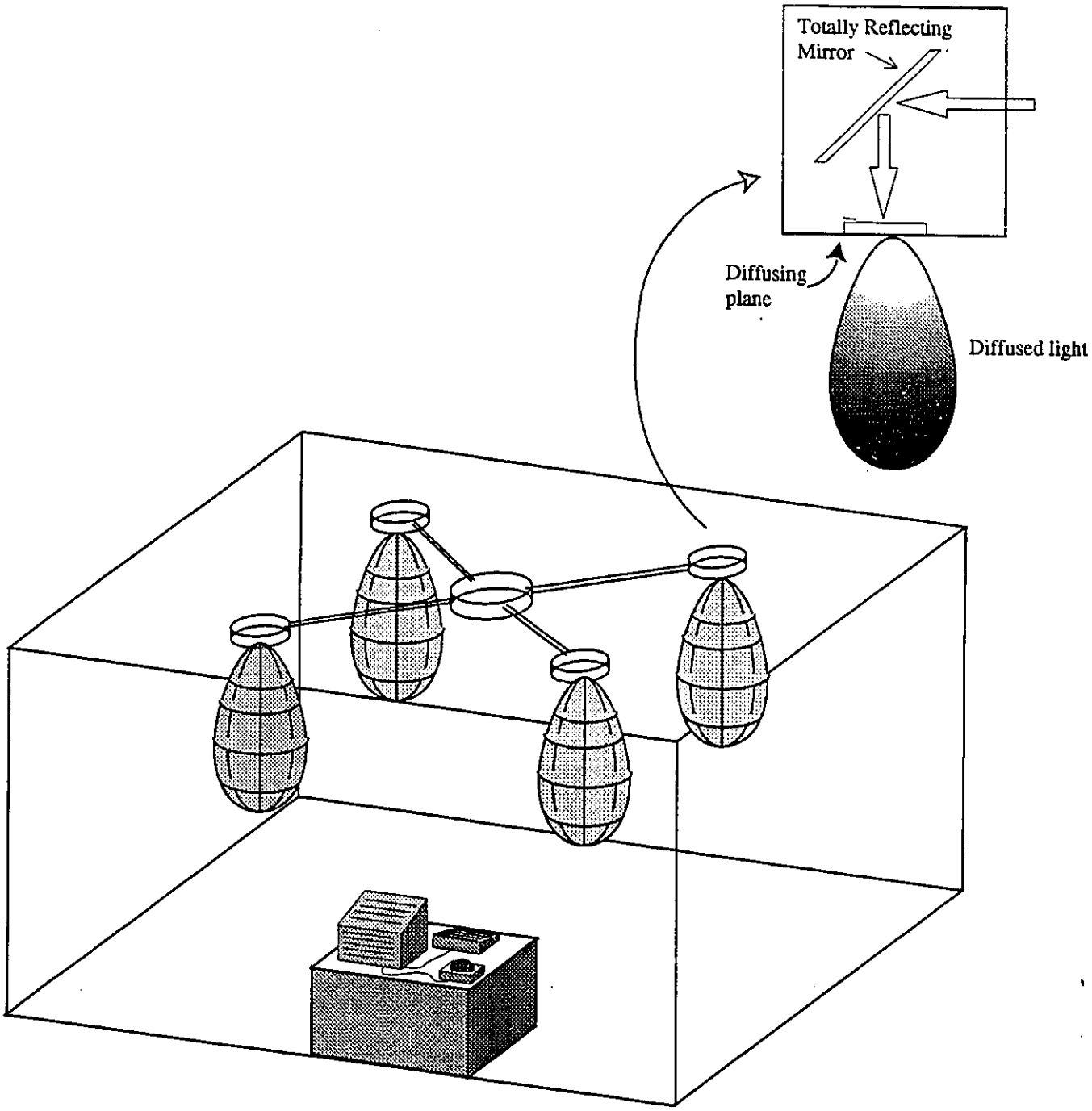

Figure 3.20 Use of passive optical reflectors to make a LOS system more tolerant to shadowing.

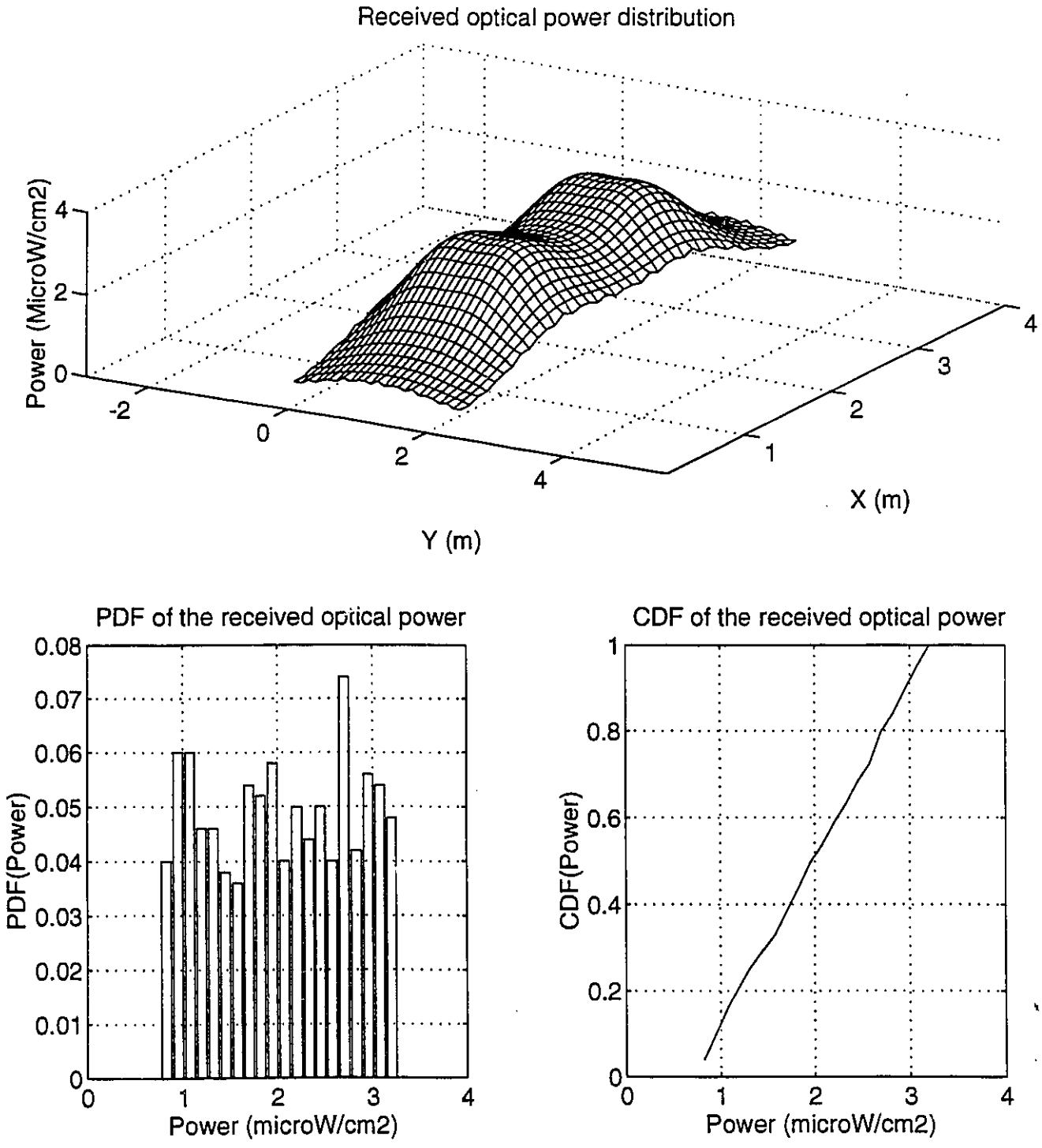

Figure 3.21 Spatial and numerical distribution of the received optical power in room B using 4 passive optical diffusers.

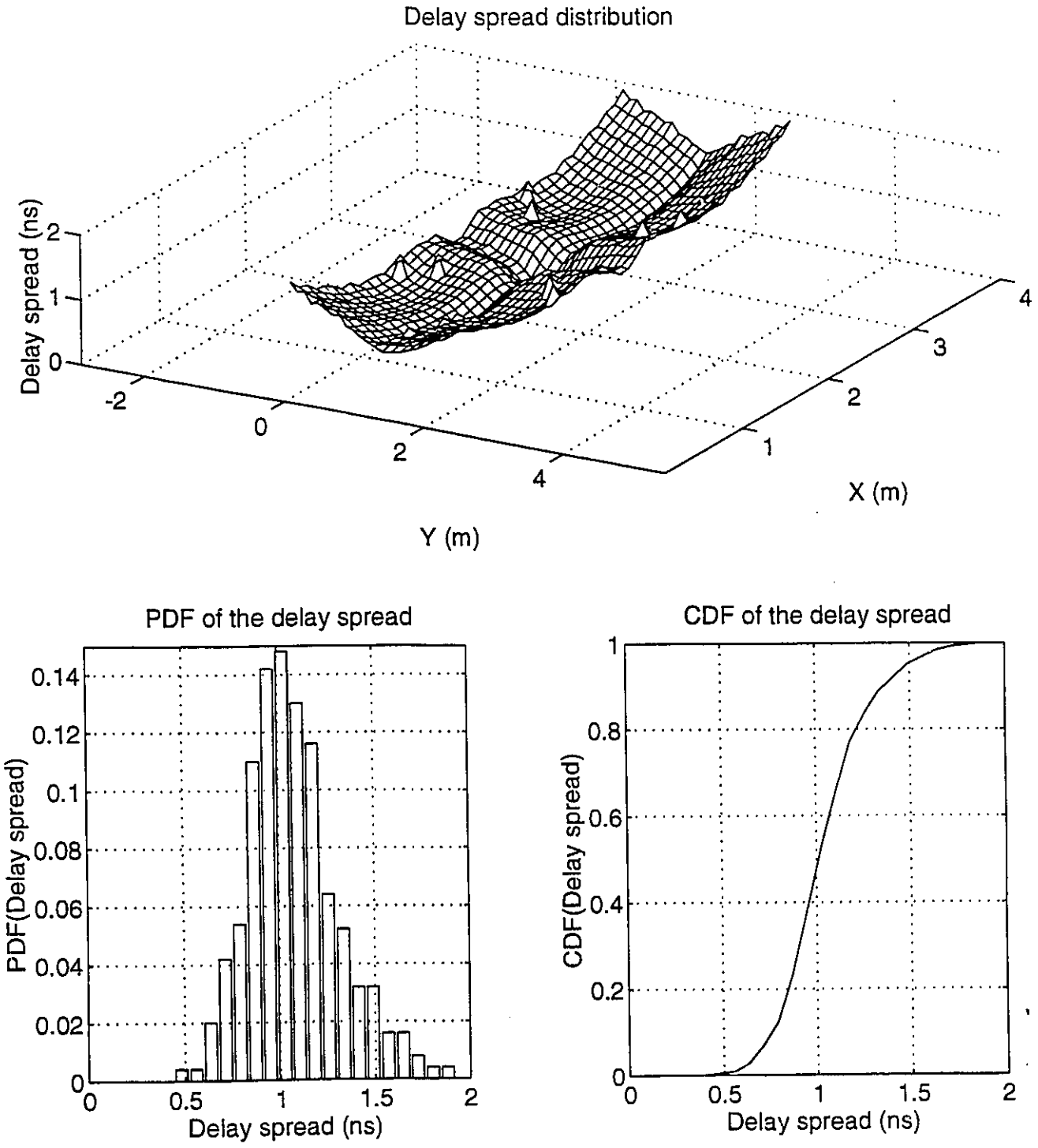

Figure 3.22 Spatial and numerical distribution of the delay spread in room B using 4 passive optical diffusers.

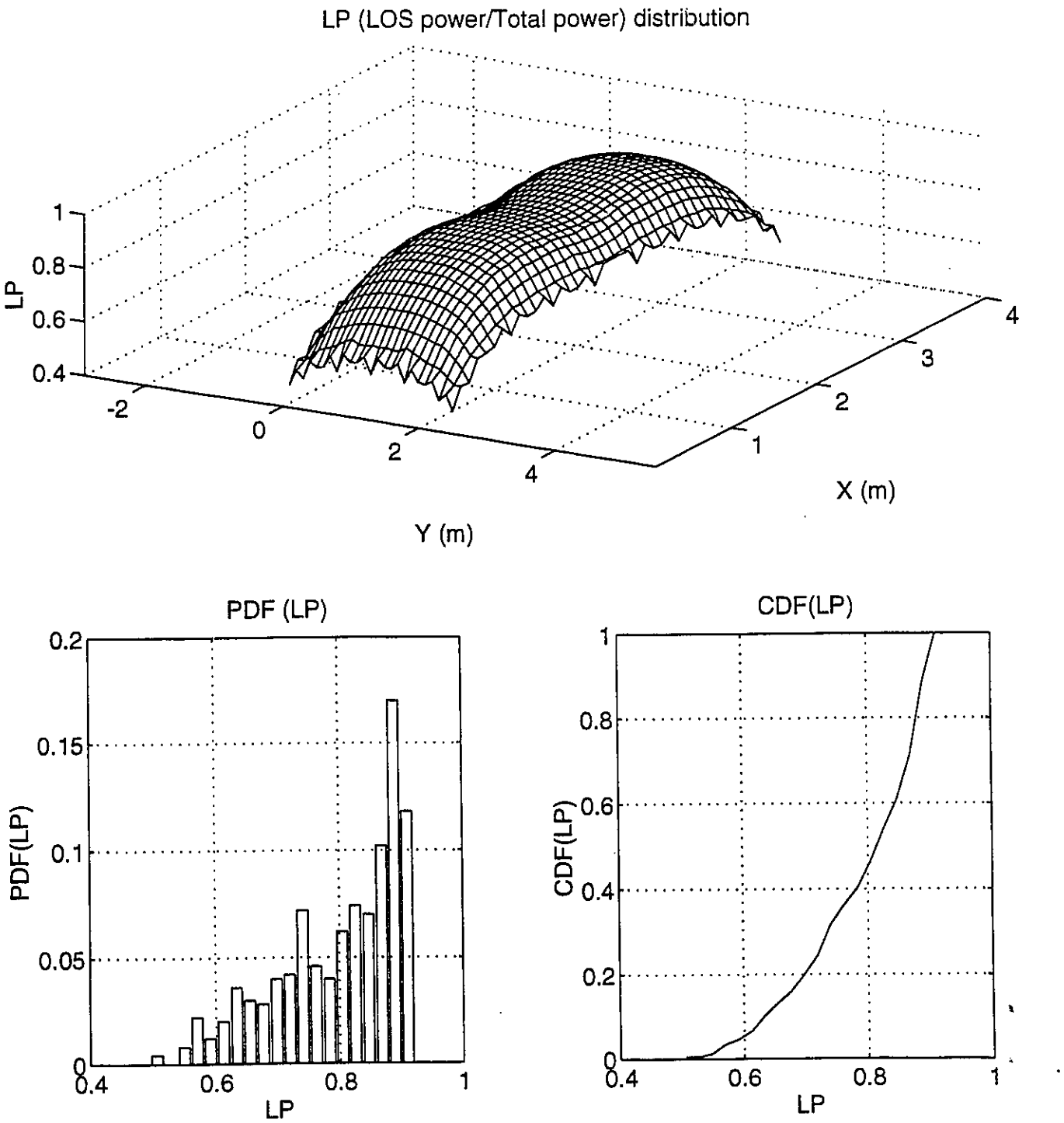

Figure 3.23 Spatial and numerical distribution for the ratio of LOS power to the total received power (LP) in room B using 4 passive optical diffusers.

Chapter 4

Angular diversity

4.1. Introduction

Errors occur in the reception when the channel attenuation is large. Diversity techniques are based on the notion that if the receiver is supplied with several replicas of the same information, the probability that all the received signals are attenuated together is reduced considerably and a lower BER would be achievable. There are several ways by which we can provide a receiver with replicas of the same signal. One method is to employ frequency diversity by sending information on different carriers. Another method is to transmit the same signal, several times that is called time diversity. Since time and frequency are important scarce resources in a communication system, in many applications, we may not want to choose methods that provide diversity at the cost of spending these resources for performance improvement. Another commonly employed technique is use of several receivers (antennas or photodiodes) to collect signals from different locations or directions. The receiving devices should see different channel characteristics to benefit from diversity advantages. For example in a RF system, antennas should be separated by a multiple wavelengths to allow independent fading. In other words, each antenna should see an independent snap-shot of the channel.

As we noted in previous chapters, non-directed optical channel, is not very sensitive to the position of the receiver. We do not expect major fluctuations in channel impulse response by moving the receiver a few centimeters back and forth. Instead, this channel is very sensitive to direction of reception, i.e., rotation of the receiver changes the channel characteristics considerably. For these channels, angular diversity seems a promising technique to overcome channel impairments due to multipath and the ambient light. A receiver employing angular

diversity uses several photodiodes, each looking in a different direction with a limited FOV. Considering the eye as an optical receiver of light signals, we recognize how the direction of looking is important to receive proper information from the environment. As an example, consider an optical receiver which is placed near a window under the direct sun-light. The level of noise generated by this strong ambient light, reduces the SNR and prevents the receiver from proper operation. If the receiver can somehow look in other directions where a smaller amount of ambient light is detected, it can achieve a much higher SNR regardless of the strong ambient light in the environment. In other words, directivity of the noise sources in unguided optical communications channels makes angular diversity an important part of an optical receiver.

4.2. Combining criteria

No matter how we receive replicas of the same signal, we have to combine them to produce the best possible signal for detection. To decide the type of combining suitable for an application, we should first decide on combining criteria. There are two possible criteria for combining. The first one is combining in order to maximize the SNR and the second is combining to minimize the delay spread. Minimizing the delay spread results in a lower ISI and improves the system performance. We will briefly review these two criteria below.

4.2.1. SNR

Consider an L-branch diversity receiver as shown in Fig. 4.1. Assume the signal power in each branch is S_i and the noise power is N_i . So we have, $SNR_i=S_i/N_i$. A combiner that maximizes the SNR uses the received signals from each branch to produce an output signal with a maximized SNR.

Combining techniques assume a known SNR on each branch. For an optical receiver, this can be determined easily. Electrical current generated by ambient light is the major noise source on each branch. This current is the sum of a dc component and shot noise. Amplitude of the shot noise and the dc component are both proportional to the level of the detected ambient light. Since the dc component of the incoming signal is much less than the dc component generated by the ambient light, we can assume that the dc component of the photodiode current is proportional to the level of ambient light. Therefore, by monitoring this

level, we can have an estimate of the noise on each branch. This dc component is removed from the signal as we noted in chapter 2. The result is signal plus shot noise. Having an estimate of the noise, it is easy to estimate the signal power. The SNR estimation is performed in each branch and is used for Maximal Ratio combining (MRC).

4.2.2. Delay spread

Combining techniques can also be used to minimize Co-Channel-Interference (CCI)[12] and ISI[71][72]. ISI is the major impairment of indoor IR channel when using high data rates. There is a direct relationship between the channel delay spread and multipath induced ISI [37]. Therefore, minimizing the delay spread of the channel, reduces the ISI. Such a combiner generates a signal, S_o from L input branches, $S_1, S_2, ..S_L$ such that the delay spread of S_o is minimized.

[12]Optical signals do not penetrate through walls and this makes CCI less important in IR communications. CCI might be considered a problem when several users are operating inside a single room, but proper use of time and frequency resources may solve this problem.

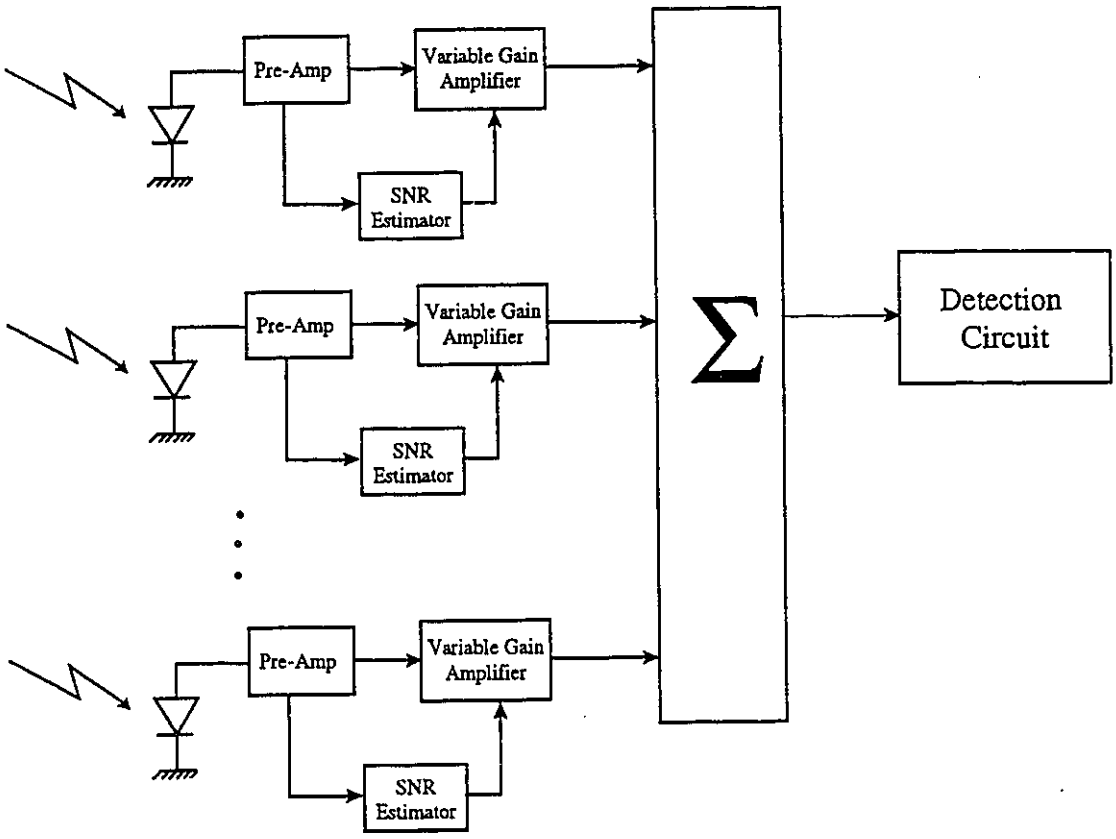

Figure 4.1. Maximal ratio combining for an optical receiver employing angular diversity technique.

4.3. Combining Techniques

4.3.1. Maximal ratio combining

Fig. 4.1 shows the block diagram of a maximal ratio combiner. In this combining technique, output of each branch is weighted by its SNR and the squared sum of the results is introduced to the receiver,

$$\left(\frac{S_o}{N_o}\right)_{MR} = \sqrt{\sum_{i=1}^{L}\left(\frac{S_i}{N_i}\right)^2} \qquad (4\text{-}1)$$

High-SNR branches are amplified more and therefore, the weighting used in this combiner, increases the contribution of high-SNR branches to the output SNR. In this combining technique, L variable gain amplifiers are needed.

4.3.2. Selection combining based on SNR

In selection combining, the best branch with maximum SNR is chosen by the combiner, therefore,

$$\left(\frac{S_o}{N_o}\right)_s = Max_i\left(\frac{S_i}{N_i}\right) \qquad (4\text{-}2)$$

As we see, this is a simpler combining technique. It does not require L variable gain amplifiers and the output is determined by a simple switching device that chooses the highest SNR branch. This decision is based on the information provided by the SNR estimators used on each branch. Fig. 4.2 shows a block diagram of this combining method.

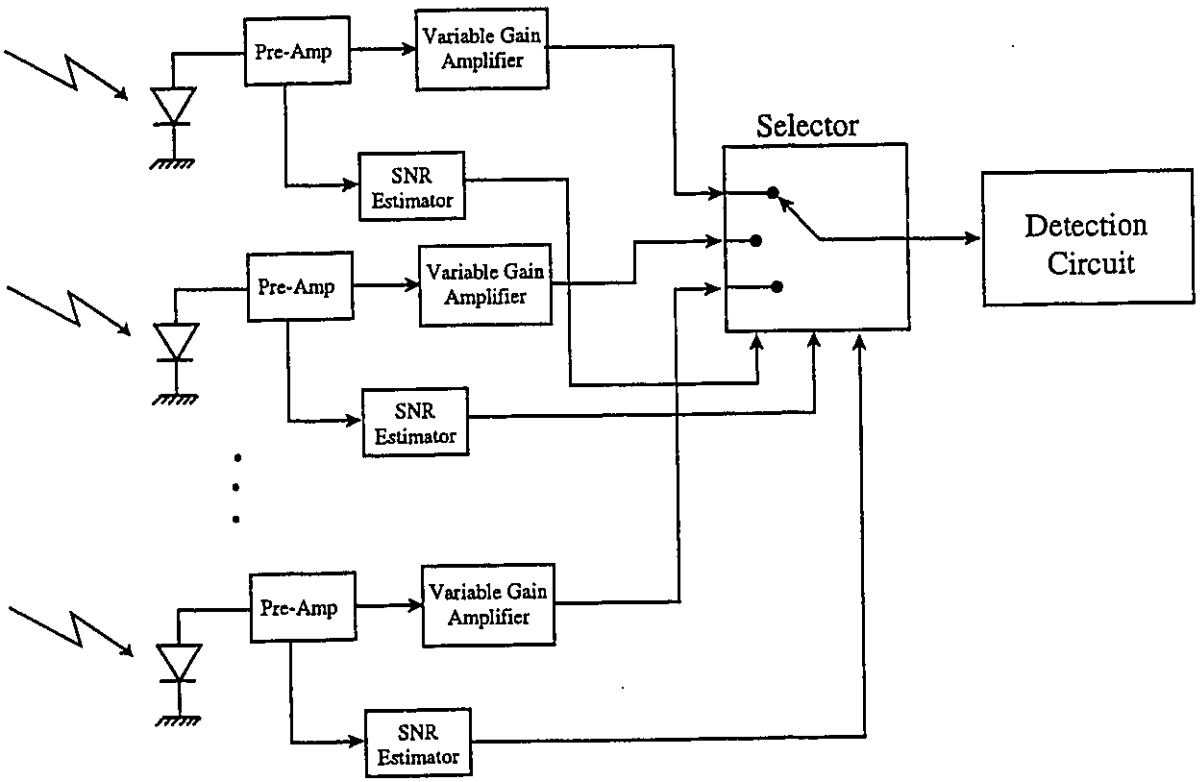

Figure 4.2 Selection diversity combining based on the SNR of each branch used in angular diversity optical receiver.

4.3.3. Minimizing delay spread

There are highly complex techniques for reduction of ISI by applying optimal filtering on the diversity branches. Since the complexity of digital signal processing techniques is a technological limit for the high data rates in our application (150 Mbps), we focus on simple combining techniques to minimize the delay spread. The simpiest combining technique, is selection combining based on delay spread. This combiner chooses the branch with minimum delay spread regardless of the induced noise in this specific branch. A block diagram of this combining technique is the same as that illustrated in Fig. 4.2, with SNR estimators replaced by delay spread estimators. We will compare this technique with other combining techniques in the following section.

4.4. A design example

As an example, we design an angular diversity receiver. Using the simulation software, we calculate the performance of several combining techniques applicable in designing angular diversity systems.

4.4.1. Receiver FOV and number of branches

Receiver FOV is an important factor in the design of angular diversity receivers. A wide FOV increases the received signal power, the delay spread and the detected ambient background light on a branch. On the other hand, a smaller FOV photodetector receives less signal power and ambient radiation from the environment. Delay spread is also less when FOV is small. Effect of FOV on the received power and the delay spread was discussed in chapter-3 without considering receiver rotation. In this section, we will see how rotation and receiver FOV change the delay spread and the received power.

An important aspect in the receiver design is the limitations imposed by light concentration techniques and optical bandpass filters on the receiver FOV. Optical concentrators can be an essential part of an IR receiver. They increase the detected signal power, without increasing the actual photodetector area[13][51][73]. One kind of concentrator, the dielectric compound parabolic concentrator (CPC), used for unguided optical communication reduces the receiver FOV, namely $\Omega_{in} / \Omega_{det} \approx n^2 A_{in} / A_{det}$, where n is the CPC refractive index. Narrow-band optical bandpass filters also limit the receiver FOV. Since we prefer optical filters to be narrow-band to reject as much ambient light as possible, we have to accept the imposed limitation on the FOV. Note that, these limitations show how wide we can choose the FOV of each branch. Depending on other design criteria, we may choose even an smaller FOV for each branch.

[13]Increasing the photodetector area, increases the input capacitance of the receiver preamplifier. This greatly reduces the amplifier bandwidth and increases the receiver thermal noise.

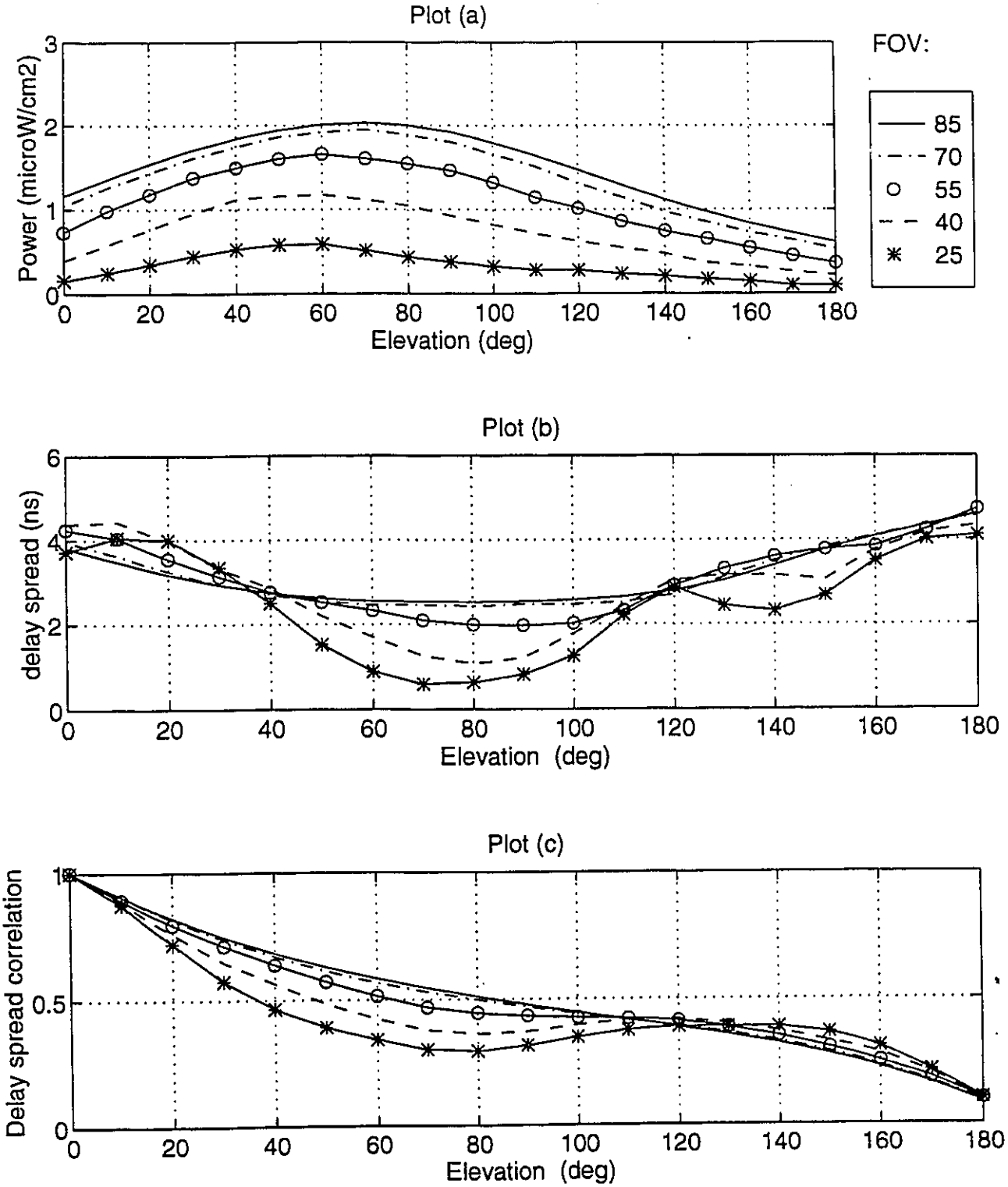

Figure 4.3 Effect of the receiver FOV and rotation on the channel characteristics.

To study the effect of receiver FOV on the channel characteristics, we place a receiver at location R1 in room B and change the elevation angle, θ, from 0° to 180° in steps of 10° (See Fig. 4.8 for definition of θ). Detected power and delay spread of impulse response in each step were recorded. This simulation was done for several values of receiver FOV to investigate the effect of FOV on the detected power and the delay spread. Fig. 4.3 illustrates the result of this simulation. Plot (a) shows the relation of the received power to the receiver direction for several values of FOV. As we expect, the highest power is received when the receiver looks toward the center of the ceiling (In this example receiver is in the corner of room and transmitter is at the center). Decreasing FOV from 85° decreases the level of the received signal power. Considering the power levels, we see that a decrease in the detected power from FOV=85° to FOV=70° is much less than a decrease from FOV=55° to FOV=40°. This confirms the results presented in chapter-3. Effect of rotation on the measured delay spread is shown in plot (b) of Fig. 4.3. As we expect, delay spread shows more fluctuation as FOV decreases. In other words, smaller FOV receivers are more sensitive to rotation. For example, compare delay spread for FOV=85° to FOV=25°. When FOV is large, the maximum and the minimum of delay spread are 3.8 ns and 2.6 ns and change of delay spread vs. elevation angle is very smooth. When FOV is set at 25°, the maximum delay spread is 4 ns and the minimum is 0.8 nsec, and there are fluctuations in the curve.

To describe the relation between the FOV and the channel characteristics seen by a tilted receiver, we calculate the normalized autocorrelation of each of the curves in plot(b). Normalized autocorrelation of a discrete time-limited function *d(n)* is defined by:

$$R_d(n) = \frac{1}{M} \sum_{j=0}^{N+n} d(j)d(j+n) \qquad (4\text{-}3)$$

where *d(n)* is non-zero in $n \in \{0,1,....,N\}$ and

$$M = \sum_{j=0}^{N} d^2(j) \qquad (4\text{-}4)$$

Plot (c) in Fig. 4.3 shows how $R_d(n)$ changes with FOV. The curves in this figure show how correlated are the channel delay spreads when rotating the receiver by n degrees. We see that increasing the FOV increases the correlation. This is

intuitively justified, since we expect a wide FOV receiver to be more tolerant to rotation. For example, assuming a threshold of 0.4 for the correlation, we see that for a FOV=25°, rotating the receiver by 45°, a new channel is seen by the receiver (Correlation drops below 0.4). For a FOV=85°, we have to rotate the receiver by about 110° before the correlation drops below 0.4. Therefore, in order to have independent channels on each branch of an angular diversity receiver, we should limit the FOV of each branch. Number of branches should be determined by using a curve as plot(c) in Fig. 4.3 to have independent channels seen by each receiver. In our example, we choose a FOV=40°. This reduces the peak received power by about 30% in that specific location for the receiver looking toward the ceiling. According to plot(c) and assuming a threshold of 0.4, we can have almost independent branches at angular separations of 60°. We choose a system with seven diversity branches as shown in Fig. 4.4. Six branches looking at an elevation of 40° and azimuth angles of {0°,60°,120°,180°,240°,300°} and one branch at an elevation angle of 90° and azimuth angle of 0° (looking directly toward the ceiling).

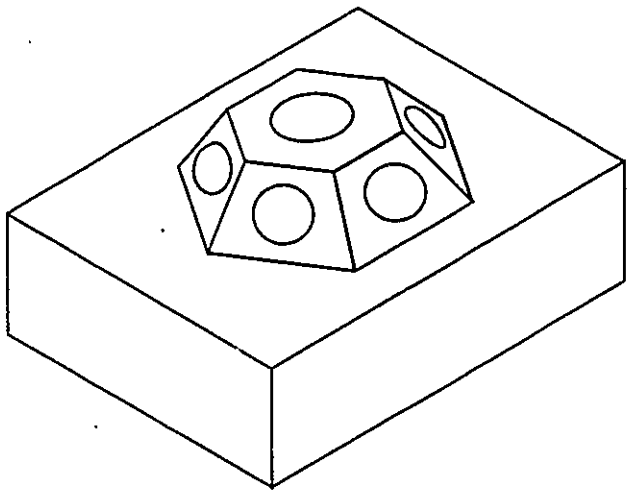

Figure 4.4 Angular diversity receiver used for the simulations.

4.4.2. Effect of diversity on the received power

It was mentioned in the previous discussions that limiting the receiver FOV reduces the detected optical power by the photodiode. However we should note that the reduction only affects the received power in one branch and not the received power of the receiver. To clarify this point, we simulated the received power on each branch of our angular diversity receiver in room B. At each location in this room, we measured the received power and the delay spread of the diversity branches assuming a diffused transmission configuration. Fig. 4.5 shows the detected power by each of the six photodiodes mounted on the sides of the receiver. It is seen that different photodiodes receive their peak power at different locations. For example, branch No. 1 (plot(a)), receives its maximum power when the receiver is at {x=2.6, y=2.5} while, branch No. 2 (plot(b)) receives its maximum power at {x=3.2, y=1.3}. This is due to different directions of the photodiodes mounted on the receiver. Each branch receives its maximum power when it looks toward the center of the ceiling that is highly illuminated by the diffused transmitter. We applied a selection diversity based on received power in each branch. At each location, the branch with the maximum received power was chosen. Fig 4.6 shows the distribution of power[14] across room B, applying selection diversity. Compare this result with Fig. 4.7 that shows the power distribution when a single wide FOV receiver is used in the receiver. Interestingly enough, we see that the maximum and the minimum received power are almost the same in both cases. We have limited the FOV of each receiver from 85° to 40° but we have not lost any power after selecting the best branch at each location. Considering an 80% coverage, the minimum received power for a wide FOV receiver is -61.9 dBo and for the best branch is -62.4 dBo, a difference of only 0.5 dBo. As a conclusion, we see that limiting receiver FOV for diversity combining is not reducing the received power when a proper combining method is used.

[14] Power is shown in dBo defined by: X(dBo)= 10*log10(x)

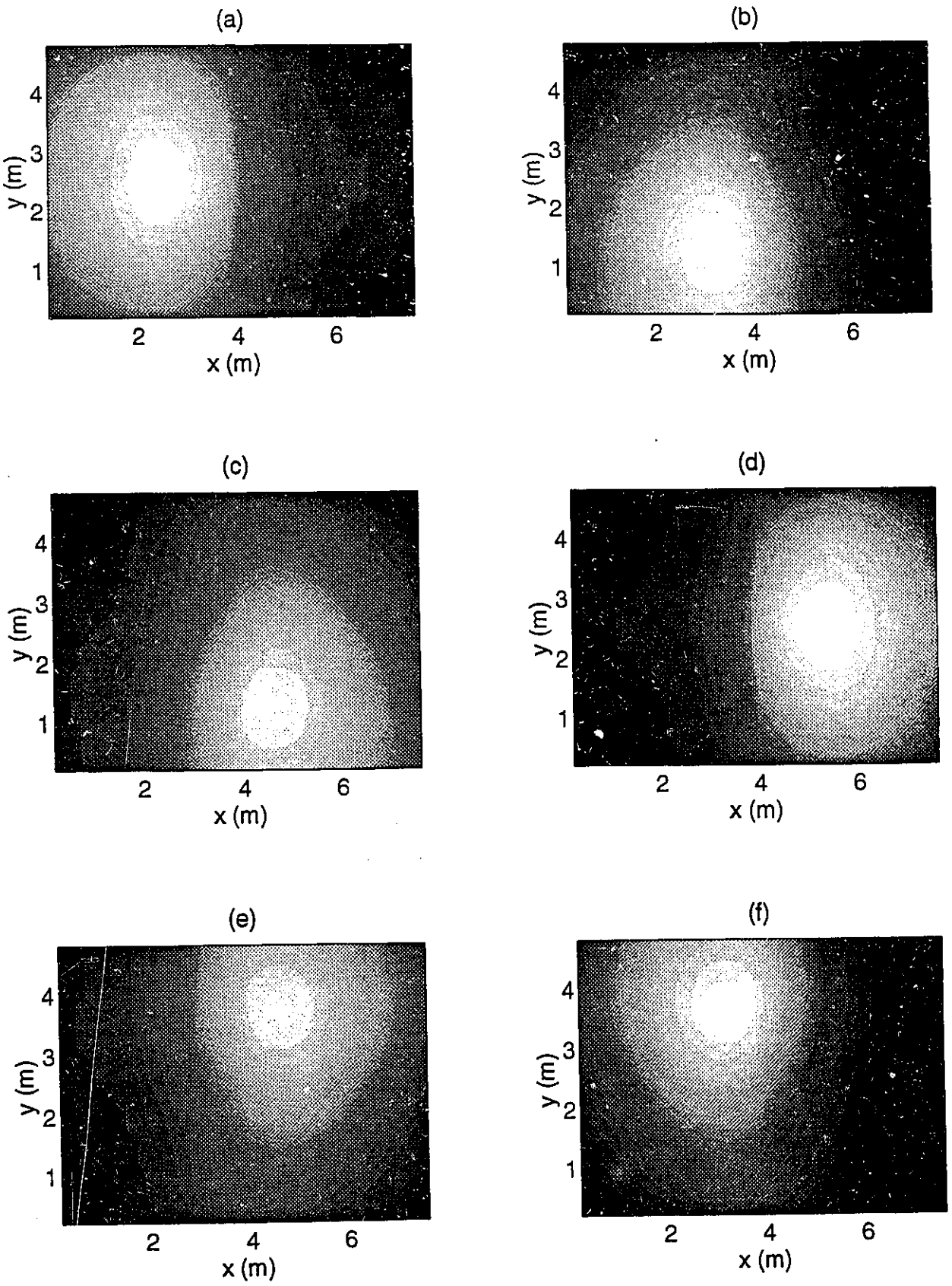

Figure 4.5 The received power on six branches of the angular diversity receiver.

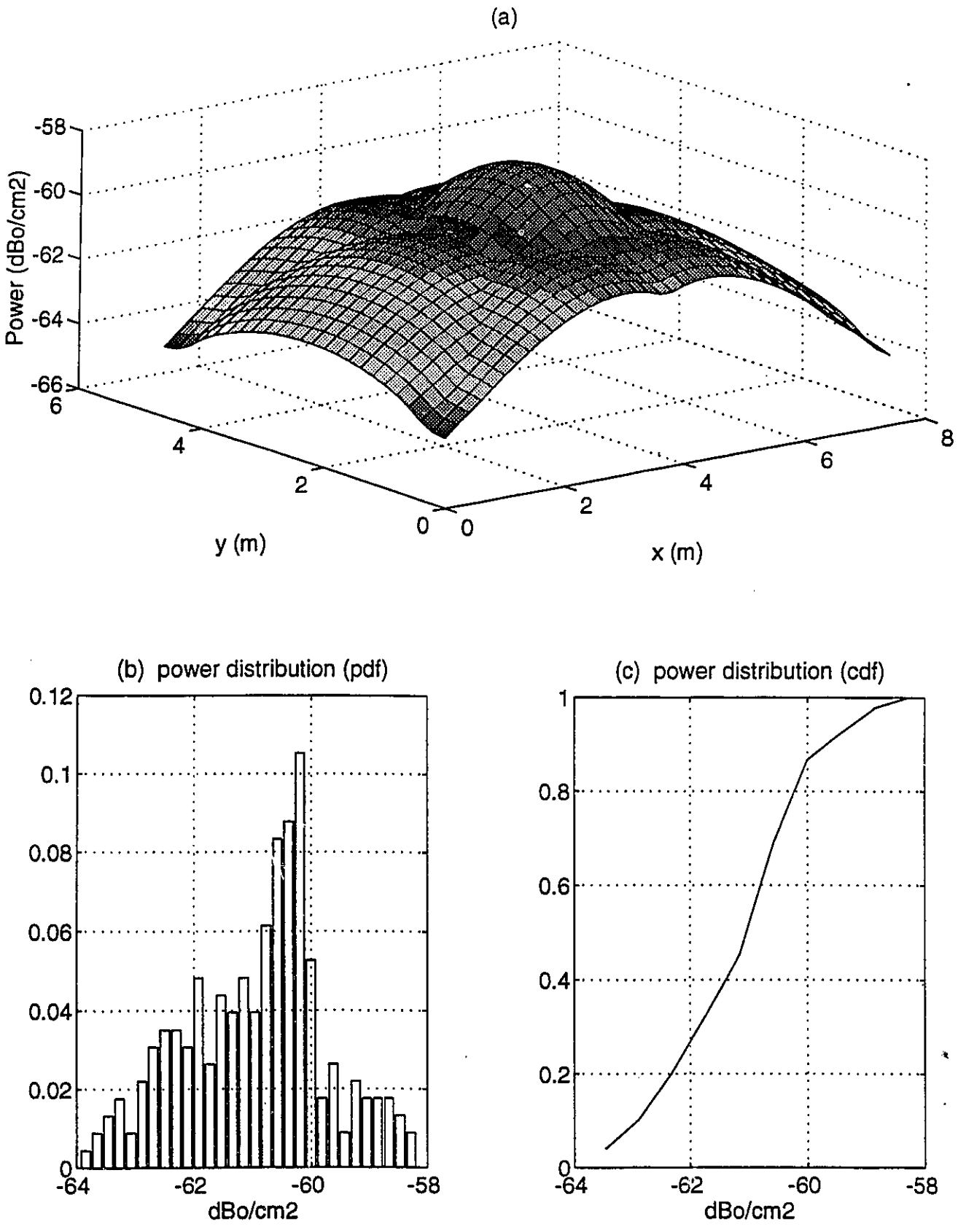

Figure 4.6 Spatial and numerical distribution of the received optical power when the highest power branch is chosen.

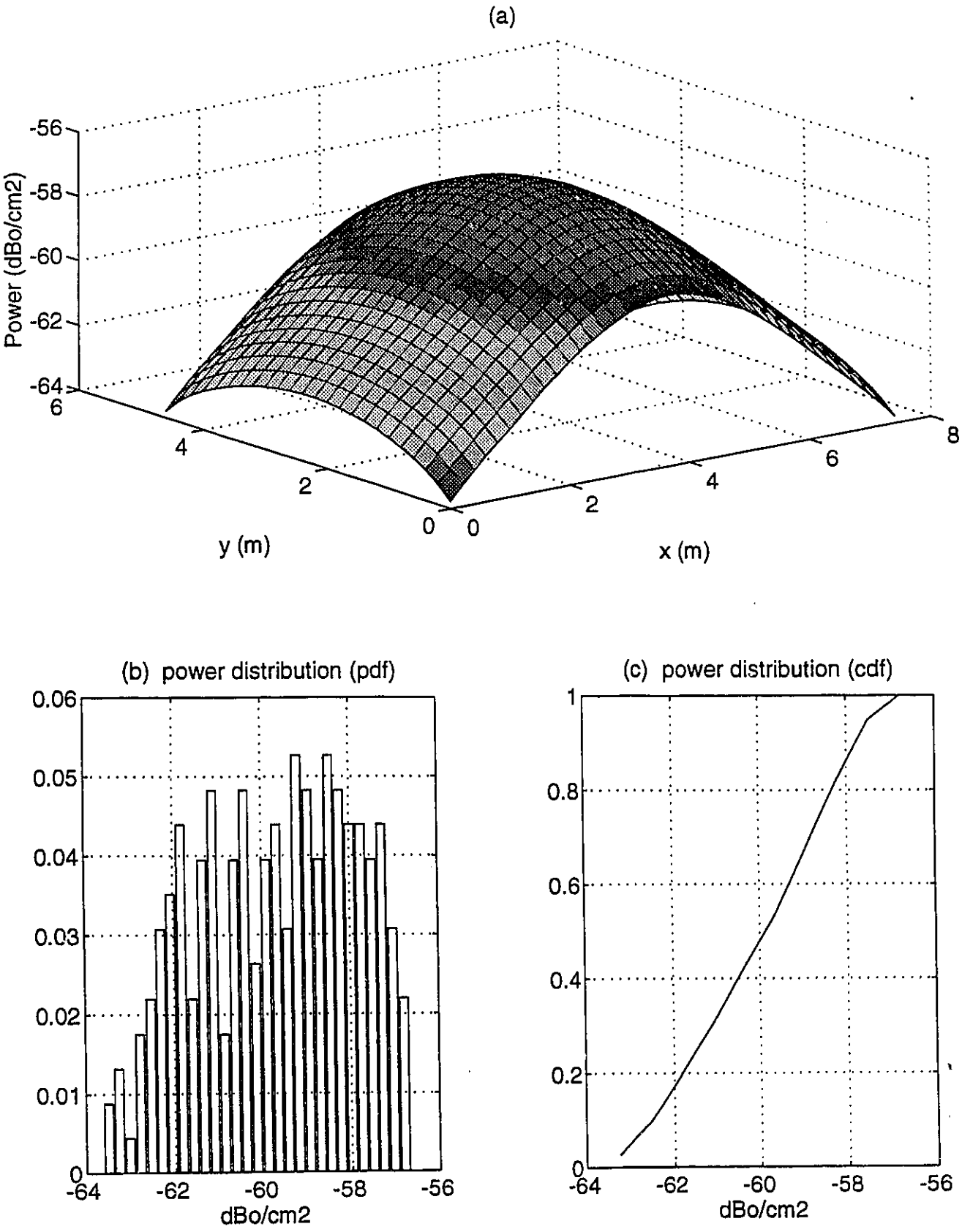

Figure 4.7 Spatial and numerical distribution of the received optical power using a single wide-FOV photodiode.

4.4.3. Power and delay spread

Considering samples of impulse response from the simulation software, there seems to be some correlation between power of an impulse response and its width. But this is not always true. To illustrate this, we simulated a receiver with a wide FOV (FOV=85°) at three sample locations in room B at a height of 1 m and (x,y)∈ {(0.5,0.5),(3,3},(5,1)}. A wide FOV of 85° was chosen for the receiver. Table 3.2 shows the specification of room B. As shown in Fig. 4.8, direction of reception is specified by the elevation angle, θ, and the azimuth angle, φ. In each location, we changed the elevation angle from 0° to 180° in steps of 10 and azimuth angle from 0° to 160° in steps of 20 to cover all possible directions in which a receiver may look. Fig 4.9 shows the directions in which each simulation is performed (receiver is placed in the direction of small planes shown in this figure). In each step, we simulated the impulse response and measured the corresponding power and delay spread.

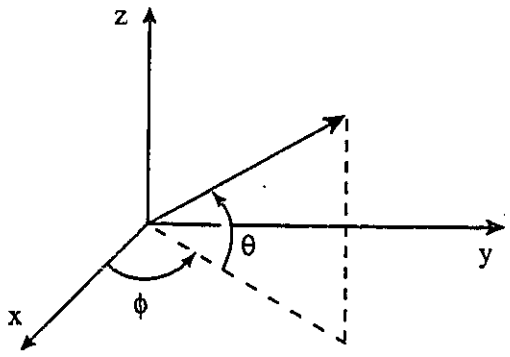

Figure 4.8 Illustration of the azimuth angle, θ, and the elevation angle, φ.

The received power and delay spread in each location is plotted as a function of φ and θ. Fig. 4.10, 4.11 and 4.12 show the results of these simulations. In each of these figures, plot (a) and (b) show the surface of power or delay spread as a function of φ and θ. plot (c) shows the contour of the received power superimposed on a plot representing the delay spread. This plot is a good way of showing the correlation between the delay spread and the received power in a specific location. We can see that at two locations, R2 and R3, in the direction corresponding to the highest level of received power, the delay spread of impulse response is minimum. However, this is not the case for the location R1. In other words, peak of the power plane in $\{z,\theta,\varphi\}$ space does not always coincide with the minimum of the delay spread plane. This is a good indication that the received power can not be used as a good indicator of the small delay spread for this type of channel.

Therefore a combining technique aimed at minimizing the delay spread, or ISI at the receiver should choose the branch with the lowest delay spread from the L available diversity branches.

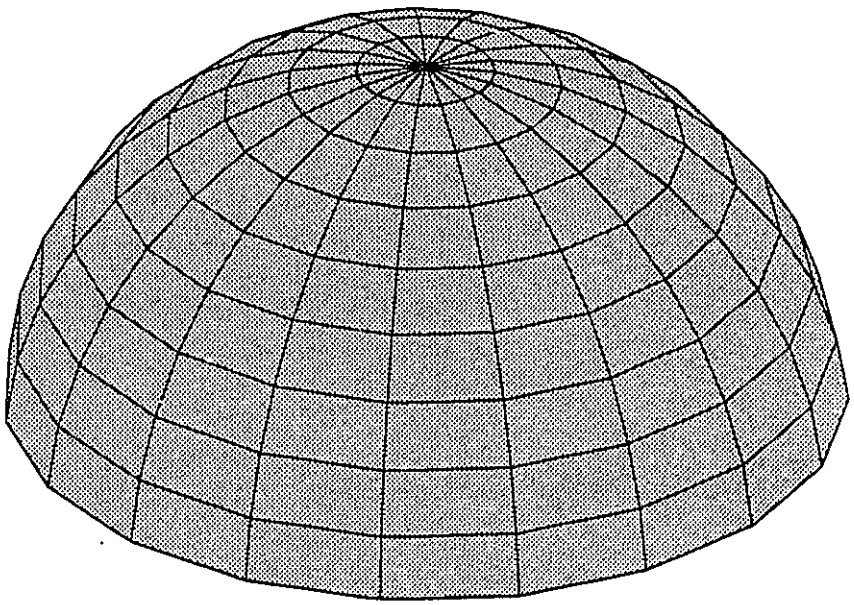

Figure 4.9 Directions used in the simulation to see the effect of rotation on the detected power and delay spread.

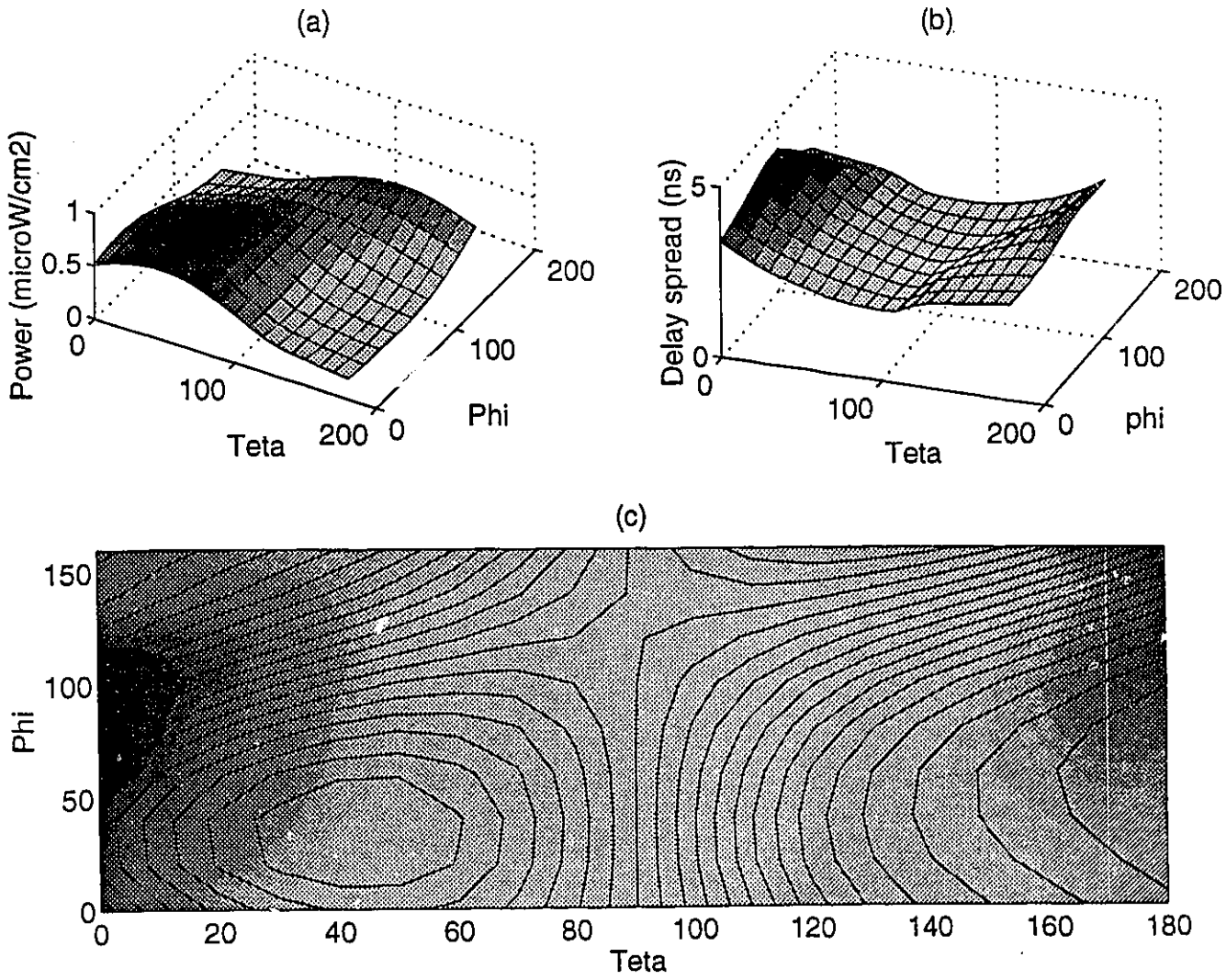

Figure 4.10 Relation between the delay spread and the detected power at location R1 in room B.

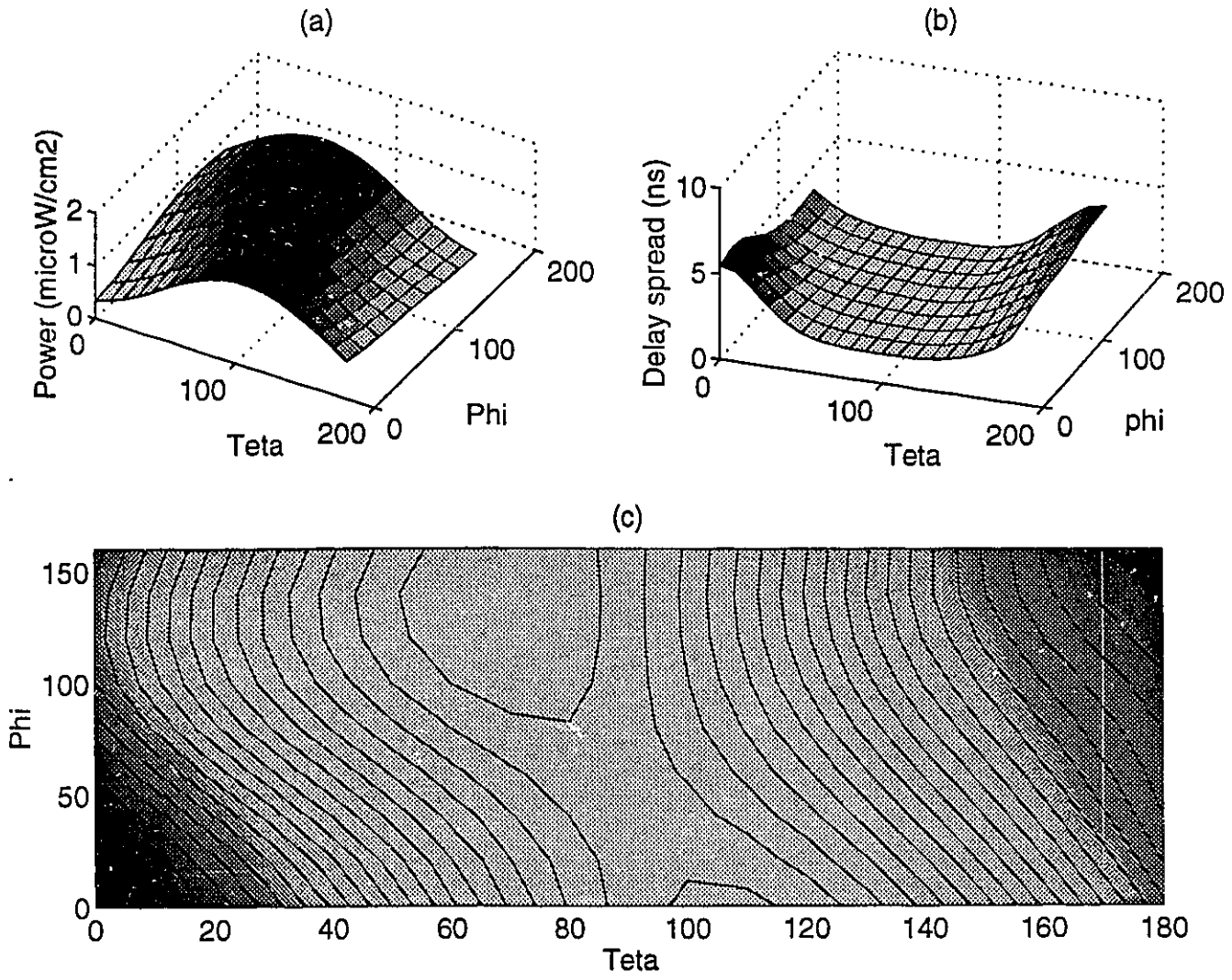

Figure 4.11 Relation between the delay spread and the detected power at location R2 in room B.

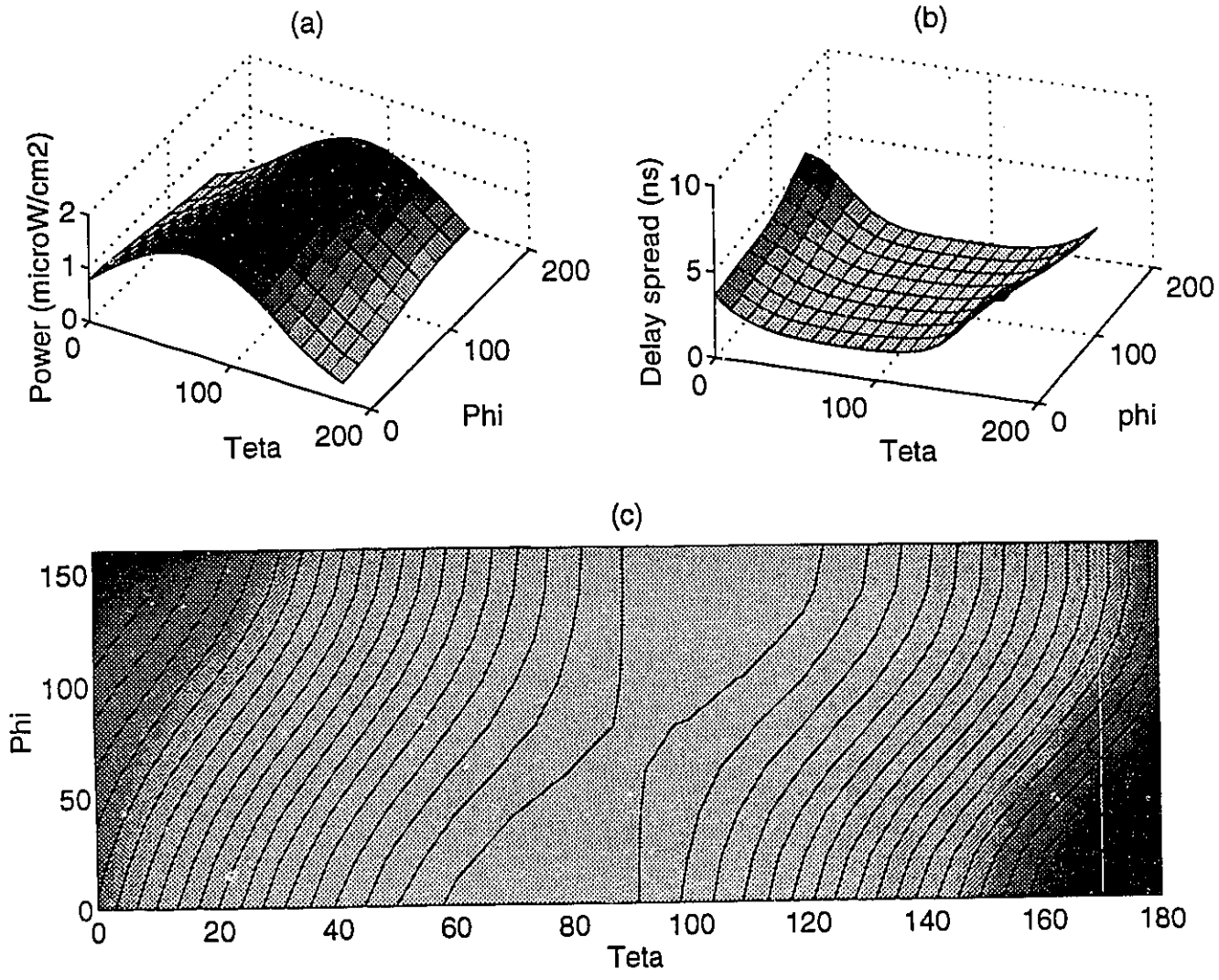

Figure 4.12 Relation between the delay spread and the detected power at location R3 in room B.

4.5. Comparison between combining techniques

To compare the combining techniques, the following setup is used for simulation. A transmitter located at the center of room B, looking toward the ceiling at a height of 1 m with a FOV=85°. Receivers are moved at 1 m height all over this room for impulse response measurements. Impulse response simulations were performed using k=2 bounces and a ΔA=10 cm × 10 cm. Receiver is a seven branch angular diversity receiver illustrated in Fig. 4.4.

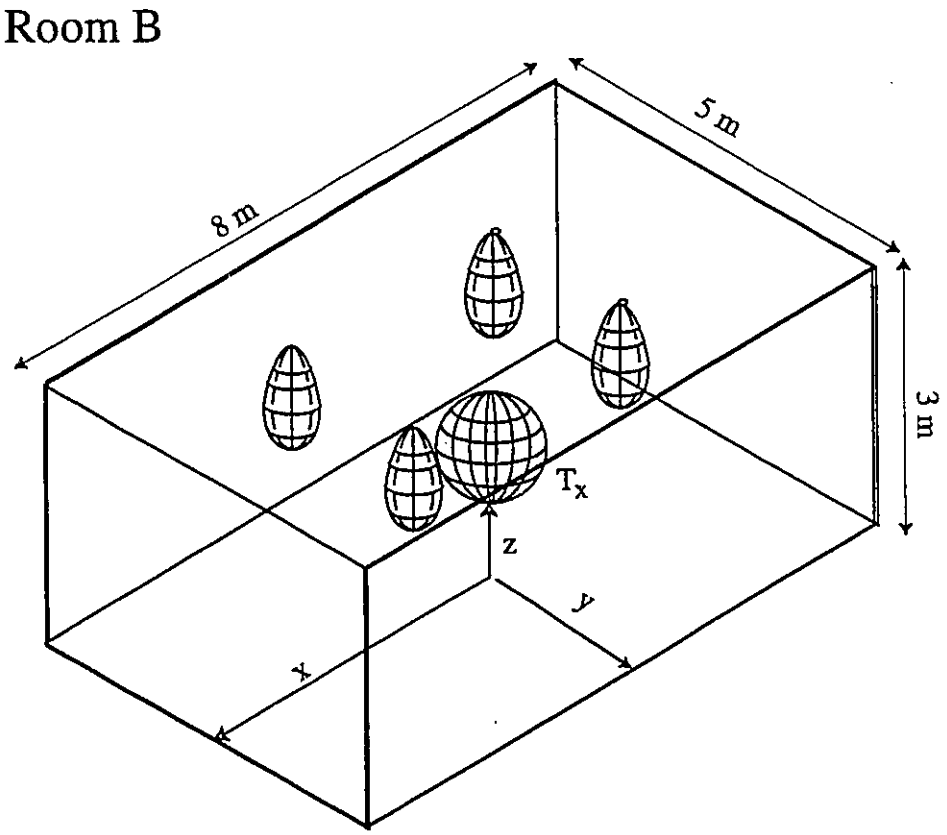

Figure 4.13 Physical configuration of the room B with the noise sources and transmitter location.

To simulate the noise sources, we put four optical sources at the ceiling looking down generating optical power with a first order Lambertian pattern. Location of these sources are (x,y)∈{(2.5,1.5),(5.5,1.5),(2.5,3.5),(5.5,3.5)}. The sources are lamps used for illumination of a typical office. We assume 100W optical power is generated from each lamp and no filtering to reduce the amount of detected background light. Effect of background light from windows has not been included in this simulation, but it should be easy to account for such an effect. As we saw in chapter 3, the most received power from an optical source is carried by its LOS component. Considering noise sources as optical transmitters, the same argument is true. A branch that looks toward one of these sources, receives a lot of noise induced by background radiation. Therefore, the received noise highly depends on the direction of reception. This clarifies the meaning of *directional noise* that we use throughout this chapter. A selection diversity technique that tries to maximize the SNR should try to choose a branch that doesn't have a noise source in its FOV or reduce the effect of such a branch. Fig 4.13 illustrates the transmitter, the noise sources and the receiver locations.

For comparison, we simulated the channel impulse response with the same transmission configuration, with a single branch wide-FOV receiver. This receiver was also moved across the room in steps of 20 cm, and at each location signal and noise power and channel delay spread were calculated and used for comparison.

To calculate the SNR on each branch, we calculated the total detected optical signal power P_{signal} and the optical noise power (optical background radiation) P_{bg} on each branch. As we noted in chapter 2, the noise power is proportional to P_{bg}, while the signal power is proportional to P_{signal}. Induced shot noise due to background radiation is given by [42]:

$$\sigma^2=2qrA_{det}BI_2P_{bg}$$

where q is the electron charge,r is the photodiode responsivity ,I_2 is a noise bandwidth factor, A_{det} is the photodetector area and B is the system bandwidth. Electrical signal power is given by:

$$S=A^2_{det}r^2P^2signal$$

Assuming B=150 MHz, I_2=0.562, A_{det}=1cm^2, r=0.53(A/W) [42] and expressing powers in W/cm^2, SNR on each branch is given by:

$$SNR = \frac{S}{\sigma^2} = \frac{(0.53) \times P^2_{signal}}{(1.6 \times 10^{19})(0.562)(150 \times 10^6) P_{bg}}$$

$$= 3.93 \times 10^{10} \times \frac{P^2_{signal}}{P_{bg}}$$

4.5.1. Maximum ratio combining

Fig 4.14 illustrates the received power on six branches from the noise sources. It is clearly seen that different branches receive different power patterns. The interesting point is the fact that each branch receives much more noise when a noise source comes within its FOV. In fact from this pattern of power, one can easily guess the location of noise sources. This confirms the fact that LOS is very important in carrying the optical power between a source and its destination and clarifies the meaning of the *directional noise*. For maximum ratio combining, received SNR on each branch is squared and the root square of the sum is calculated for each point. Fig 4.16 illustrates the results of maximum ratio combining. As we see in plot(a), the SNR is almost flat across the room. Plot(c), shows that almost 85% of locations, have SNR values of more than 35 dB. Compare this with Fig. 4.15 that shows the SNR distribution for a single branch wide FOV receiver. In a wide FOV receiver, noise sources are always within receiver's FOV resulting in a higher level of detected noise. This shows why SNR in this configuration is lower. As shown in plot(c), Fig. 4.16, only 55% of this room provides an SNR value of more than 35 dB. This shows an almost 40% reduction in the covered area with the same transmitted power (assuming a 35 dB as the threshold). Note that, when higher power noise sources such as direct sunlight from windows are present, a diversity system performs even much better because of the receiver capability in avoiding noise detection.

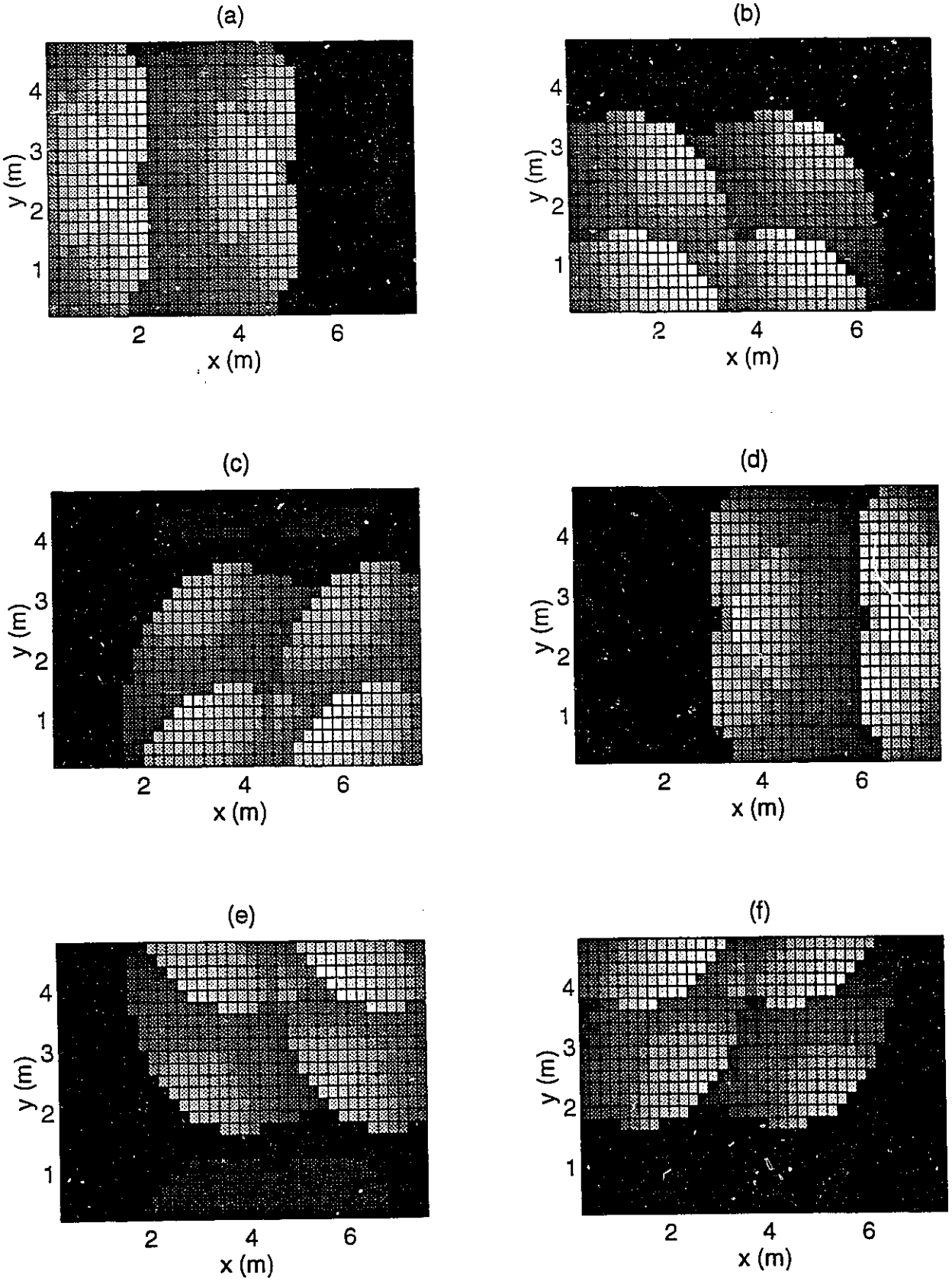

Figure 4.14 Received optical power on each branch of the receiver from the background radiation sources in the room B.

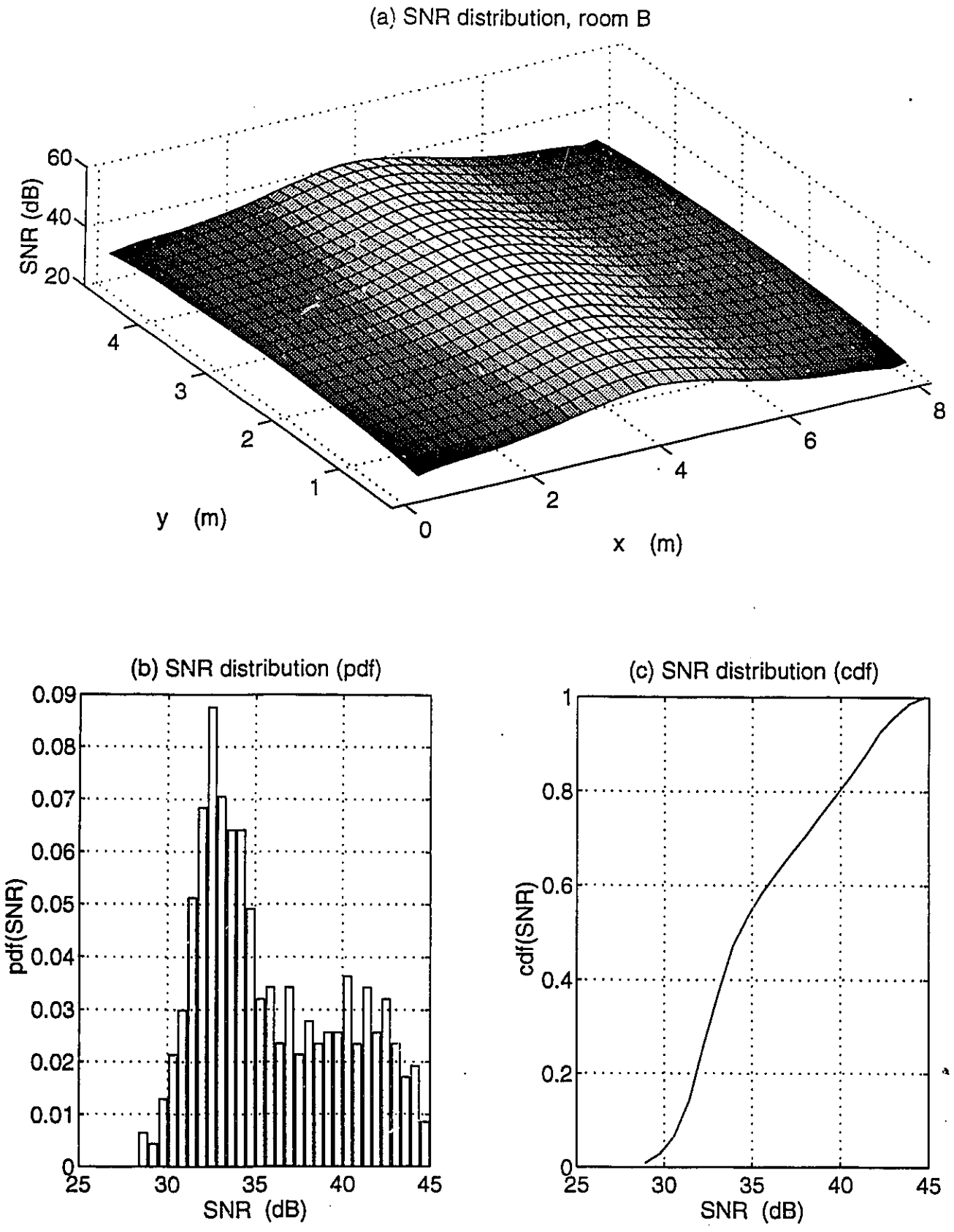

Figure 4.15 Spatial and numerical distribution of the SNR values for a wide-FOV single branch optical receiver.

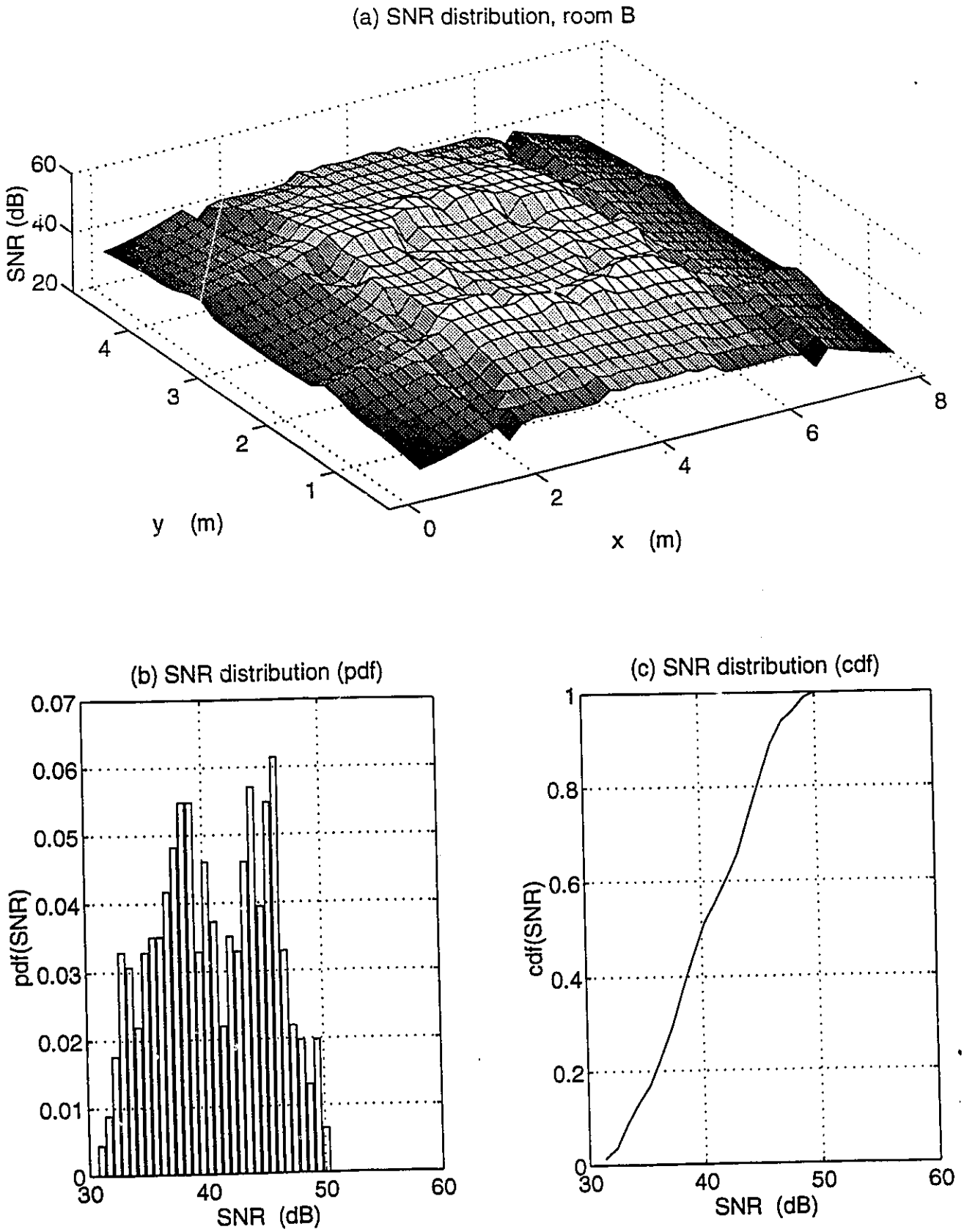

Figure 4.16 Spatial and numerical distribution of the SNR for the diversity receiver when maximum ratio combining is used.

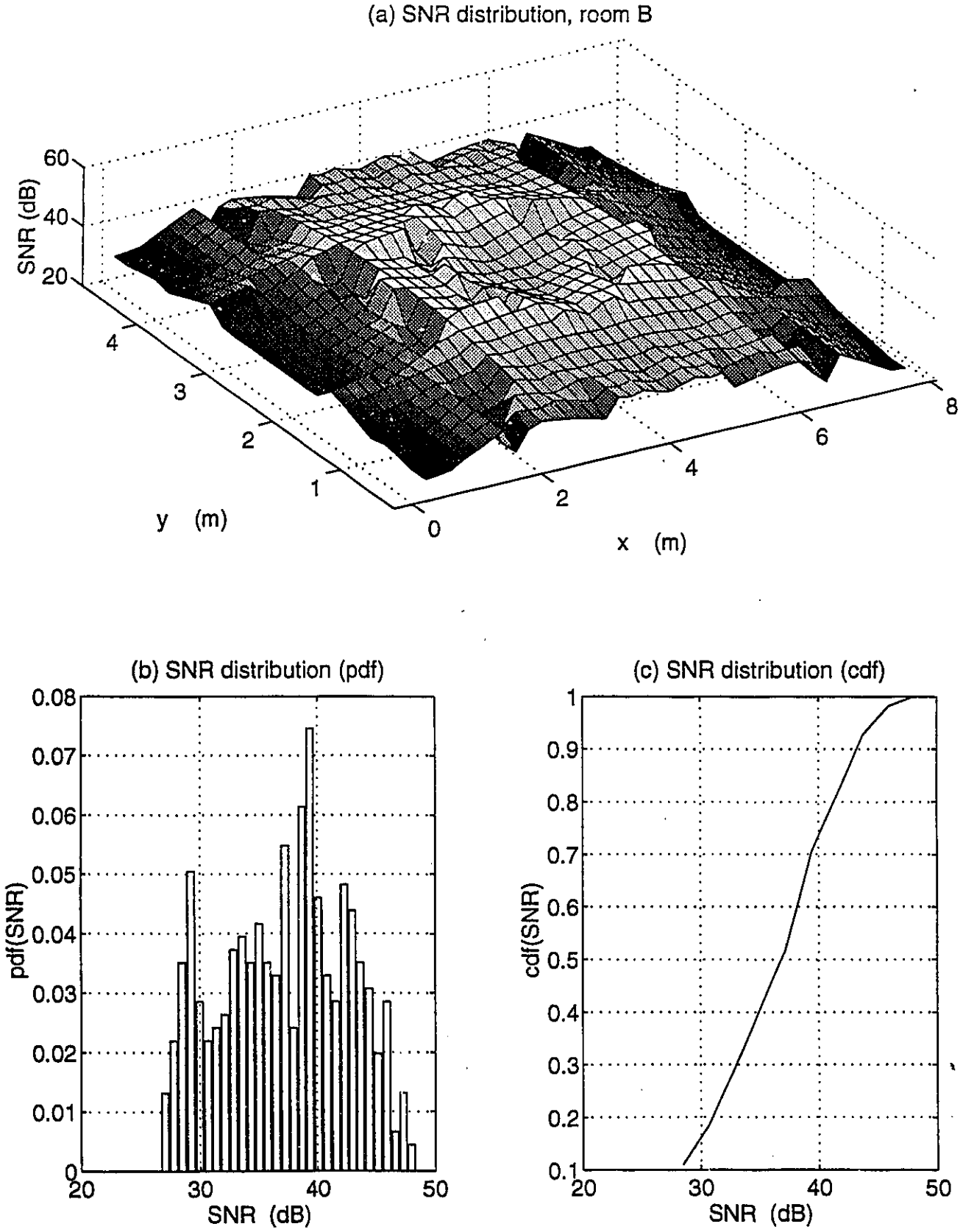

Figure 4.17 Spatial and numerical distribution of the SNR for the diversity receiver when selection combining based on the SNR is used.

4.5.2. Selection combining based on SNR

The same simulation is performed this time using selection combining. At each location, the maximum SNR branch is chosen as the input to the receiver. Results of this combining technique are illustrated in Fig. 4.17. The distribution of SNR is not as flat as that of maximum ratio combining. Abrupt changes in SNR are the results of switching from one branch to another. This combining technique is much simpler than MR combining, yet capable of achieving a high SNR and avoiding high powered directional noise sources such as office lamps and sunlight. Coverage area assuming 35 dB as the threshold, would be about 65% which is a 20% decrease from the MRC coverage area. Note that this is the price we pay for the simplicity of the system. Another interesting point is that although signal power reaches its maximum at the center of the room, SNR is not maximum at this point. This is because almost all the branches have at least one source of noise in their FOV and they can not effectively avoid the noise sources. For a better comparison between the coverage area and the distribution of SNR for the three combining techniques, we plotted the CDF for SNR together in Fig. 4.18.

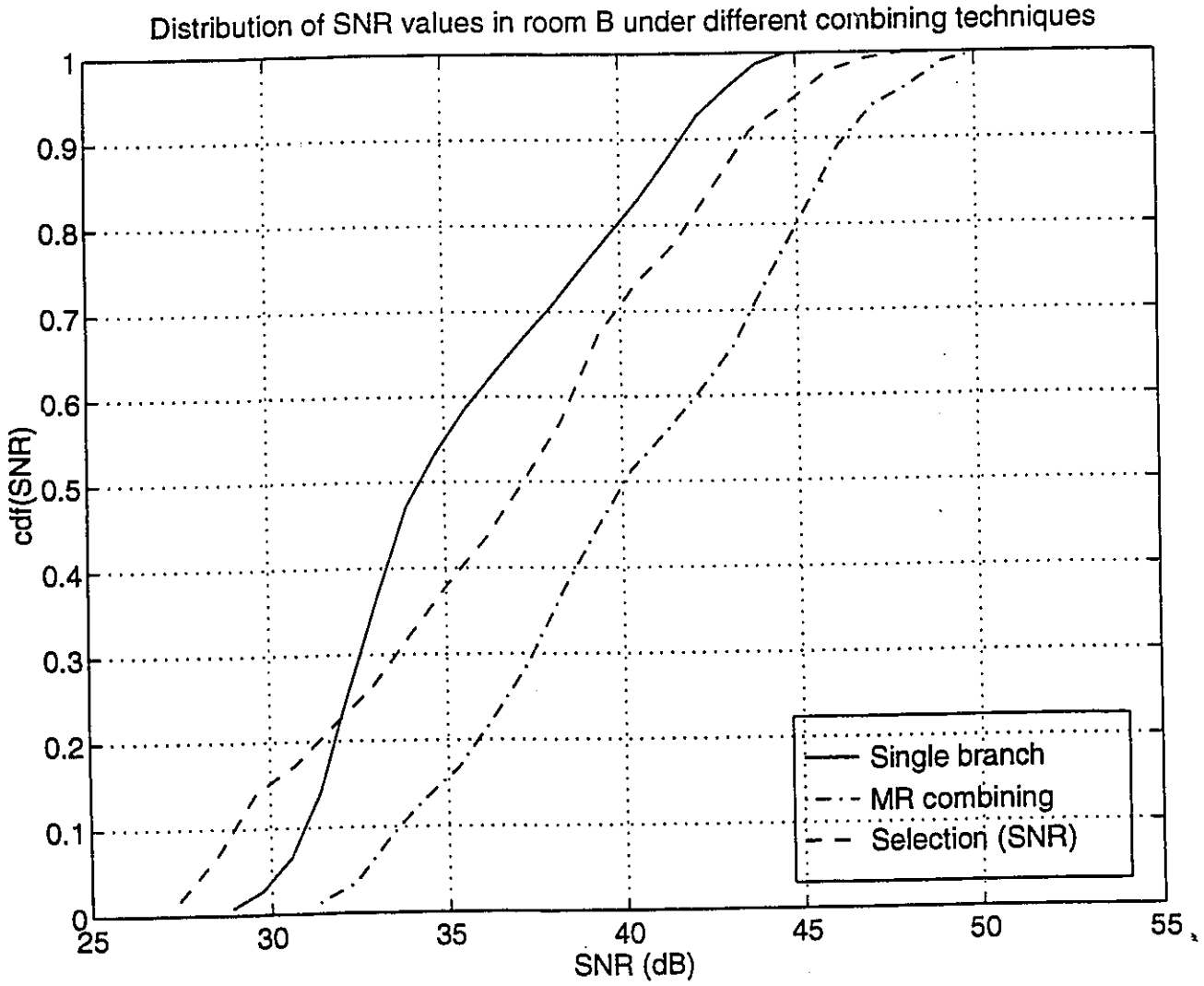

Figure 4.18 CDF of SNR values for a single-branch receiver, a seven branch diversity receiver using maximum ratio combining or selection combining.

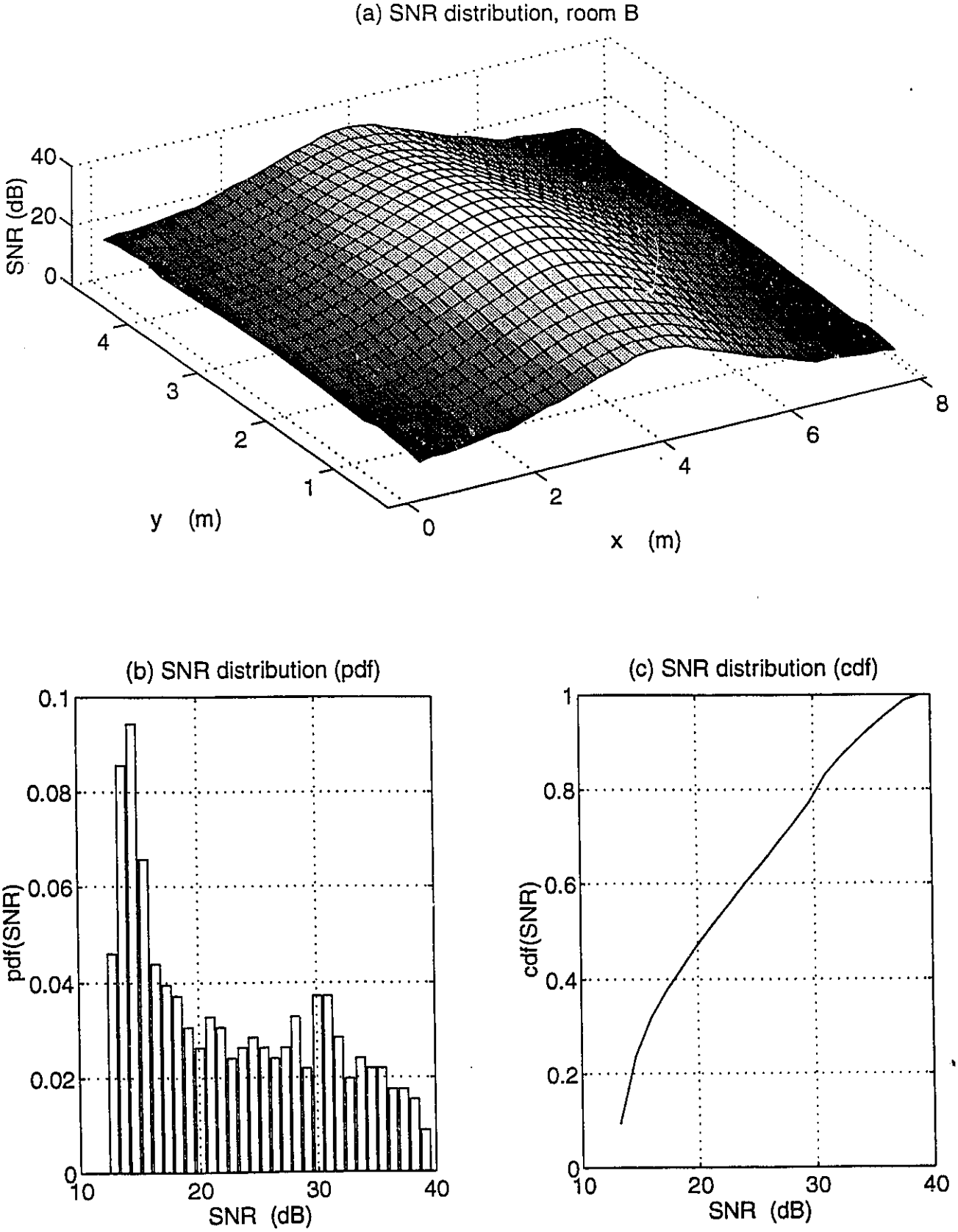

Figure 4.19 Spatial and numerical distribution of the SNR for the diversity receiver when selection combining based on the delay spread is used.

4.5.3. Selection diversity based on delay spread

For the same configuration, we calculated the delay spread on each branch at each location. The interesting point is that at all the locations in this room, the lowest delay spread is on branch No. 7 with the photodiode looking directly toward the ceiling. In other words, the highest power branch is not always detecting the lowest delay spread in each location. This can be explained by noting that photodiode No. 7 receives its major power from the ceiling reflection at first bounce (powerful bounce) and receives much less reflected lights from walls (in the first bounce) and therefore its impulse response has a lower delay spread. The SNR distribution of this selection method is shown in Fig. 4.19. It is clear that SNR value is smaller in this configuration because the receiver does not avoid noise sources by selection or weighting and also because of its limited FOV receives less amount of signal power. From plot (c), we see that only 15% of the room has a SNR value of more than 35 dB. This is less than a quarter of the covered area with the MRC method. Therefore, we see this technique suitable only when noise problem is solved by other means like narrow-band optical filters.

Chapter 5

Summary and Conclusions

In this thesis, we discussed issues related to Indoor non-directed channel characteristics. We presented a baseband channel model for this channel and compared it to RF channels. Space fading due to multipath and random behavior of channel characteristics are not seen in this type of the channel, while they are very common in RF channels. Multipath dispersion causes ISI in this channel, as it does in RF channels and proper antimultipath techniques should be used to compensate for this distortion. The major source of noise in IR receivers is shot noise induced by ambient light. To prevent this noise from decreasing the SNR in a receiver, optical filters should be used at the receiver. To achieve a high SNR, one would like to transmit as much optical power as possible. On the other hand, there are safety limits for the amount of radiation at each wavelength and under different viewing and radiation conditions. We discussed the related issues in detail and gave some numerical examples. Results indicate that portable transmitters can safely transmit up to about 500 mW of IR power from a properly diffused source.
To have more useful information about channel behavior under different configurations, use of a simulation software seems necessary. Models used for radiation and reflection as well as the software algorithm were presented. Some important implementation issues were also discussed. This software was used to calculate the impulse response under different channel configurations. From impulse response we are able to extract some channel information such as frequency response, r.m.s delay spread, maximum delay spread, received power and the 3-dB channel bandwidth. Using these results, we were able to derive power, and delay distribution of a specific configuration over indoor offices. These results show us how we should design the optical configuration of these systems for the best performance. Comparison between non-directed LOS and diffuse configurations in these simulations show us that in general, we expect a higher received power and less distortion due to multipath in non-directed LOS configuration. The advantage of diffuse systems are in their tolerance to shadowing and flat distribution of received power in indoor environment. We

show that coverage area should be considered in designing the optical configuration because designing for worst case makes the system too complex, expensive and impractical . Effects of room size, reflection coefficient of walls were also discussed. We also presented a novel technique to achieve advantages of LOS configuration while making the system more tolerant to shadowing by using optical passive reflectors in different locations of the ceiling. Simulation results showed distribution of power and delay spread for this configuration to be in between LOS and diffuse.

We presented the idea of diversity in general. Angular diversity is a good candidate for optical receivers. We discussed different aspects of this technique and gave some examples on how to design a diversity combining receiver. We discussed effects of FOV and rotation on the received power and the delay spread. The results are helpful as a guideline for choosing the number of diversity branches in an angular diversity receiver. A comparison between several different combining methods based on simulation were also presented. Noise sources are directional in this channel and therefore angular diversity receivers with a limited FOV can avoid strong noise sources by employing proper combining techniques. A design example along with simulation of noise sources plus signal sources was performed and results were combined under different combining techniques. We saw that maximum ratio combining is the best combining technique yielding the highest SNR and the best distribution. Selection diversity based on the highest SNR on each branch ranks second and as far as SNR is concerned, we shall not use selection diversity based on the delay spread.

Simulation shows that in diffuse configuration, there is no guarantee that if a receiver receives the highest value of the optical power in a location, it also shows the lowest delay spread in its impulse response. There is such a strong relationship between power and delay spread in different locations for LOS configuration. It was also shown that for diffuse configuration, there is not even a guarantee that if the receiver direction is such that it receives the maximum possible light in a direction, it receives the minimum delay spread in that direction. Although this was shown for some typical configurations, we expect this to be valid generally for diffuse configuration. As a practical example in an angular diversity receiver, in diffused configuration, a branch with the highest detected power does not necessarily corresponds to a branch with the lowest delay spread. This is helpful for future works on combining techniques aiming at reducing the delay spread. .

Overall, this work was aimed at presenting some details on an indoor IR channel based on software simulation. We believe that using IR for broadband indoor wireless communications is a promising techniques. There are still many problems to be solved before practical cost effective implementation of these systems. We hope to advance the state of the arts in this field.

References

[1] D. R. Pauluzzi, P. R. H. McConnell, and R. L. Poulin, "Free-space, undirected infrared (IR) voice and data communications with a comparison to RF systems," *Proc. IEEE Int. Conf. Sel. Topics wireless Comm.*, pp. 279-285, 1992.

[2] K. Pahlavan, "Wireless communications for office information networks," *IEEE Comm. Mag.*, Vol. 23, No. 6, pp. 19-27, June 1985.

[3] K. Pahlavan, "Wireless data communication techniques for indoor applications", *Proc. of IEEE Int. Conf. on Comm. 85*, pp.372-378, 1985.

[4] K. Pahlavan, "A review of wireless in-house data communication systems," *Proc. Comp. Networking Symp.*, pp. 129-136, 1984.

[5] A. Lessard, M. Gerla, "Wireless Communications in the automated factory environment," *IEEE Network*, Vol. 2, No. 3, pp.64-69, May 1988.

[6] J. M. Cour, M. Misson, T. Val, "Using infrared impulse to transfer data asynchronously," *Proc. of 16th Conf. on Local Computer Networks*, Minneapolis USA, pp. 282-287, Oct. 1992.

[7] A. Paepcke, R. Jamp, R. Crawford, C. Freeman, F. Lee, and R. Paull, "Chipnet- an optical network of terminals and workstations,"

[8] A. Paepcke, R. Crawford, C. Freeman, F. Lee, and R. Paull, "An optical local area network," *Conf. Karlsruhe*, W. Germany, Mar. 1985

[9] I. A. Parkin and J. Zic, "An application of Infra-red Communication," *J. of Electrical and Electronic Eng.*, Australia, Vol. 4, No. 4, pp.331-336, Dec. 1984.

[10] V. C. Georgopoulos, C. J. Gerorgopolous," A multiple IR/ RF wireless transmission system for indoor and outdoor communications," *Proc. of IEEE Int. Conf. on Comm. 86,* pp. 955-959, 1986.

[11] D. Liu and J. H. Herzog, "OptoNet- an omnidirectional optical data communication system," *IEEE Pacific Rim Conf. on Communication, Computer, and Signal Processing*, May 9-10, pp. 95-97, 1991.

[12] M J. Betancor, F. J. Gabiola, F. J. Lopez-Hernandez, "IR Wireless system on ARCNet Local Area Network," *Proc. of 15th Conference on Local Computer Networks*, pp. 183-187, Oct. 1990.

[13] F. J. Gabiola, N. J. Betancor, A. Santamaria, A. Polo and F. J. Lopez-Hernandez, "Optical-Electrical interface for IR wireless Ethernet local area network," *Proc. 16th LCN '92*, pp. 273-275, 1992

[14] A. Santamaria, J. L. Munoz, F. J. Gabiola, and F. J. Lopez-Hernandez, "IR wireless system for Ethernet local area network," *Proc. of the 9th annual European Fiber Opt. comm. and LAN Conf.*, Vol:LAN, pp. 126-130, June 1991.

[15] M. J. Betancor, A. Santamaria, F. J. Gabiola, A. Polo, J. Martin-bernardo, V. M. Melian, F. J. Lopez-Herandez, "Infrared wireless system for local area network and data communications," pp. 51-55, 1992.

[16] R. Valadas, A. Moreira, and A. Durate, "Hybrid (wireless infrared/coaxial) Ethernet local area networks," *Proc. of the IEEE Int. Conf. on wireless LAN implementation*, pp. 21-29, Sept. 1992.

[17] D. P. Johnson, D. J. Cowan, "Free space local area network (FIRLAN), " SPIE, Vol. 32, No. 9, pp.2114-2117, 1993

[18] "Wireless networking," *BYTE Magazine*, pp. 291-294, April 1992

[19] G. Berline and E. Perratore, "Wireless LANs," *PC Magazine*, pp. 291-314, Feb. 1992.

[20] A. Gunn, "Connecting over the airwaves," *PC Magazine*, pp. 359-384, Aug. 1993.

[21] M J. Betancor, J. Martin-Bernardo, A. Santamaria, V. M. Melian, F. J. Lopez-Hernandez, "Infrared wireless system for high speed RS-232/RS-423/RS-422 communications," IEEE, pp.505-510, 1992

[22] M J. Betancor, J. Martin, J. Rivero, V. M. Melian, F. J. Gabiola, F. J. Lopez-Hernandez, "IEEE-488.2 communications by infrared wireless link," IEEE, pp. 500-504, 1992

[23] H. A. Ankerman, "Transmission of audio signals by infrared light carrier," *SMPTE journal*, Vol. 89, pp. 834-837, Nov. 1980

[24] R. L. Poulin, D. R. Pauluzzi, and M. R. Walker, "A multi-channel infrared telephony demonstration system for public access applications," *Proc. IEEE Int. Conf. Sel. Topics wireless Comm.*, pp. 286-291, 1992.

[25] M. D. Kotzin, A. P. van den Heuvel, "A duplex infrared system for in-building communications," *Proc. IEEE Vehic. Tech. Conf. '86*, pp. 179-185, 1986.

[26] E. Braun and S. Schon, "A cordless infrared telephone," *Telcom. report 3*, No. 2, pp. 83-86, 1980.

[27] M.Ishida, E. Toide, "A spatial optical transmission system for digital audio," *Mitsubishi electronic advances*, Vol. 58, pp. 36-38, 1992.

[28] R. Citta, "An infrared wireless speaker system utilizing a super wide-band FM carrier," *IEEE Trans. on Consumer Elect.*, CE-21 , pp. 115-119, 1975.

[29] J. M. Kahn, J. R. Barry, M. D. Audeh, E. A. Lee, and D. G. Messerschmitt, "Design of high-speed wireless link using non-directional infrared radiation," *in Proc. of Third WINLAB Workshop on Third Generation Wireless Information Networks,* East Brunswick, N. J., April 28-29, 1992.

[30] J. R. Barry, J. M. Kahn, E. A. Lee, and D. G. Messerschmitt, "High speed nondirective optical communication for wireless networks," *IEEE Network Mag.*, pp. 44-54, Nov. 1991.

[31] M. J. McCullagh, D. R. Wisely, P. L. Eardley, P. P. Smyth, "A 50 Mb/s optical wireless LAN link using novel optical and electronic enabling technologies," *Proc.Int. Zurich Seminar on Dig. Comm.*, Switzerland, pp. 298-309, 1994.

[32] D. Hash, J. Hillery, and J. White, "IR roomnet: Model and measurment," *IBM Commun. ITL Conf.*, June 1986.

[33] P. Hortensius, "Research and development plan of the infrared portable data link," internal report, IBM T. J. Watson Res. Cent., Yorktown Heights, New York, 1990.

[34] J. R. Barry, J. M. Kahn, J. Krause, E. A. Lee, and D. G. Messerschmitt, "Simulation of multipath impulse response for indoor wireless optical channels'" *IEEE J. on Sel. Areas in Comm.*, Vol. 11, No. 3, pp. 367-379, April 1993

[35] H. Hashemi, G. Yun, M. Kavehrad, F. Behbahani, P. Galko, "Frequency Response Measurement of the Wireless Indoor Channel at Infrared Optics," *Proc. Int. Zurich Seminar on Dig. Comm.*, Switzerland, pp. 273-284, 1994.

[36] W. Krause, "Experimental characterization of Non-directive Indoor infrared channels," Master's report, University of California at Berkeley, Dec. 1992.

[37] J. M. Kahn and W. J. Krause, "Experimental characterization of multipath free-space infrared channels for wireless in-building networks," *Proc. 19th European Conf. on Optical Communications*, Montreux, Switzerland, Sept. 1993.

[38] M. D. Kotzin, "Short-range communications using diffusely scattered infrared radiation," Ph.D. Dissertation, Northwestern University, June 1981.

[39] F. J. Gabiola and K. L. Prentzas, "Signal power requirements for indoor directive and diffuse infrared communications channels," *Microwave and Opt. Tech. J.*, Vol. 5, No. 3, pp. 148-152, 1992.

[40] F. J. Gabiola, N. J. Betancor, A. Santamaria, A. Polo and F. J. Lopez-Hernandez, "Irradiance analysis for indoor point-to-point and quasi-diffuse infrared channels," *Microwave and Opt. Tech. J.*, Vol. 6, No. 9, pp. 557-560, July 1993.

[41] Y. Yamauchi, M. Sato, T. Namekawa, "In-house wireless optical digital SSMA," *Electronics and communications in Japan*, Part 1, Vol. 70, No. 6, 1987.

[42] J. R. Barry, "Wireless communication using non-directed infrared light," Ph.D. dissertation, University of California at Berkeley, Dec. 1992.

[43] K. Chen, "On-Off keying optical transmission and channel capacity for indoor high rate wireless data networks," *Proc. GLOBECOM '91*, pp. 0418-0422,1991.

[44] M. D. Audeh, J. M. Kahn, "Performance evaluation of L-Pulse Position modulation on Non-directed indoor infrared channels," *Proc. ICC '94*, pp. 660-664, 1994.

[45] M. D. Audeh, and J. M. Kahn, " Performance evaluation of L-Pulse Position Modulation on non-directed indoor infrared channels," *Subm. to IEEE J. Sel. Areas in Comm., Nov. 1993.*

[46] M. D. Audeh and J. M. Kahn, "Performance simulation of baseband OOK modulation for wireless infrared LAN at 100 Mb/s," *Proc. of the IEEE Int. Conf. on Selected Topics in Wireless Comm.*, Vancouver, B. C., Canada, pp. 271-274, June 25-26, 1992.

[47] M. D. Audeh and J. M. Kahn, "Performance evaluation of baseband OOK for wireless indoor infrared LANs operating at 100 Mb/s," *Submitted to IEEE Trans. on Comm.*

[48] M. D. Audeh, "Performance evaluation of baseband OOK for wireless indoor infrared LANs operating at 100 Mb/s ," Master's report, University of California at Berkeley, Nov. 1992.

[49] C. S. Yen and R. D. Crawford, "The use of directed optical beams in wireless computer communications," *Proc. of the IEEE GLOBECOM '85 Conf.*, New Orleans, pp. 1181-1184, Dec. 2-5, 1985.

[50] T. S. Chu and M. J. Gans, "High speed infrared local wireless communication," *IEEE Comm. Mag.*, Vol. 25, No. 8, pp. 4-10, Aug. 1987.

[51] J. M. Kahn, J. R. Barry, M. D. Audeh, J. B. Carruthers, W. J. Krause and G. W. Marsh, "Non-directed Infrared links for High-capacity wireless LANs," *Submitted Jan. 94 to IEEE personal Comm. Mag.*

[52] M. J. McCullagh, I. Neild, D. R. Wisely, "A 1 Gb/s Optical Wireless LAN Supporting Mobile Transceivers, " pp. 468-480, Wireless '94, Calgary, Canada, July 94.

[53] T. Minami, K. Yano, T. Touge, H. Morikawa and O. Takahashi, "Optical wireless modem for office communications," *Proc. AFIPS National Comp. Conf.*, Vol. 52, pp. 721-728, May 1983.

[54] G. Yun, and M. Kavehrad, "Spot diffusing and fly-eye receivers for indoor infrared wireless communications," in *Proc. of the IEEE intern. Conf. on Selected Topics in Wireless Comm.*, Vancouver, B. C., Canada, pp. 262-265, 1992.

[55] Y. Nakata, J. Kashio, T. Kojima, and T. Nouguchi, "In-house wireless communication system using infrared radiation," *Proc. Int. Conf. Comp. Comm.*, pp. 333-337, 1984.

[56] F. R. Gfeller and U. Bapst, "Wireless in-house data communication via diffuse infrared radiation," *Proc. IEEE*, Vol. 67, No. 11, pp. 1474-1486, Nov. 1979.

[57] M. R. Pakravan, M. Kavehrad, "A Solution to Multipath Problem in Indoor Infrared Wireless Broadband Communications," *17th Biennial Symp. on Comm.*, Kingston, Canada, pp. 341-345, 1994.

[58] W. R. Leeb, "Degradation to signal to noise ratio in optical free space data links due to background illumination," *Applied optics*, Vol. 28, No. 15, pp. 3443-3449, 15 Aug. 1989.

[59] M. Marhic, M. Kotzin, van den Heuvel, "Reflectors and immersion lenses for detectors of diffuse radiation," *J. Opt. Soc. Am.*, Vol. 72, No. 3, pp. 352-355, Mar. 1982.

[60] W. L. Casey, et al., "Design considerations for air-to-air laser communications", *SPIE*, Vol. 1417, pp. 89-98, 1991.

[61] Georgopoulos, "Suppressing background-light interference in an in-house infrared communications system by optical filtering," *Int. J. of Opt.*, Vol. 3, No. 3, pp. 247-256, 1988.

[62] Cotton and Casey, "Narrowband optical interference filters," *Proc. O. E. Laser '91*, Los Angles, CA, Jan. 1992.

[63] IEC 825: "Radiation safety of Laser Products," equipment classification and user's guide

[64] "American National Standard for the Safe Use of Lasers," ANSI/Z136.1-1986, American National Standard Institute, New York.

[65] P. McKee, D. Wood, P. P. Smyth, "Applications of computer generated, free space diffracted optics from interconnections and packaging to optical wireless antennas," *Fourth Int. Conf. on Holographic Systems, Components and Applications*, Sept. 1993.

[66] M. P. Dames, R. J. Dowling, P. McKee, D. Wood, "Efficient optical elements to generate intensity weighted spot arrays: design and fabrication," *Applied Optics*, Vol. 30, No. 19, pp. 2685-2691.

[67] P. P. Smyth, M. McCullage, D. Wisely, S. Ritchie, P. Eardley and Cassidy, "Optical wireless Local Area Networks-enabling technologies," *B.T. Technol. J.*, Vol. 11, No. 2, Apr. 1993.

[68] P.P. Smyth, D. Wood, S. Ritchie and S. Cassidy, "Optical wireless: New enabling technologies," *Proc. of ICC '93*, Vol. 1, pp. 562-566, 1993.

[69] F. R. Gfeller, P. Bernasconi, W. Hirt, C. Elisii, and B. Weiss, "Dynamic cell planning for wireless infrared in-house data transmission," *Proc.Int. Zurich Seminar on Dig. Comm.*, Switzerland, pp. 261-272, 1994.

[70] C. R. A. T. Lomba, R. T. Vladas and A. M. de Oliveria Durate, "Propagation losses and impulse response of the indoor optical channel: a simulation package," *Proc.Int. Zurich Seminar on Dig. Comm.*, Switzerland, pp. 285-297, 1994.

[71] D. D. Falconer, M. Abdulrahman, N. W. K. Lo, B. R. Peterson, A. U. Sheikh, "Advances in Equalization and diversity for portable wireless systems," *Digital Signal Processing* 3, pp.148-162, 1993.

[72] J. H. Winters, "Optimum Combining in Digital Mobile Radio with Cochannel Interference," *IEEE J. on Sel. area in Comm.*, Vol. SAC-2, No. 4, July 1984.

[73] M. Kavehrad, G. Yun, "Optical taper for increasing the effective area of a photodiode in atmospheric free space communications applications," Patent Number 5,192,863, United states patent, 09 March 1993.